

OPTIMAL SPEED PLANNING TO MINIMIZE
ENERGY USE OF AUTONOMOUS BATTERY
ELECTRIC AND FUEL CELL HYBRID
ELECTRIC VEHICLES

OPTIMAL SPEED PLANNING TO MINIMIZE ENERGY USE OF AUTONOMOUS BATTERY ELECTRIC AND FUEL CELL HYBRID ELECTRIC VEHICLES

By

ATA MESHGINQALAM

A Thesis Submitted to the School of Graduate Studies in Partial Fulfilment of the
Requirements for the Degree of Doctor of Philosophy in Electrical and Computer
Engineering

Hamilton, Ontario, Canada, 2022

McMaster University © Ata Meshginqalam 2022

Descriptive Note

Doctor of Philosophy (2022)

McMaster University

Electrical and Computer Engineering

Hamilton, Ontario

Title: OPTIMAL SPEED PLANNING TO MINIMIZE ENERGY USE OF
AUTONOMOUS BATTERY ELECTRIC AND FUEL CELL HYBRID
ELECTRIC VEHICLES

Author: Ata Meshginqalam, M. Sc. Electrical Engineering (Iran University of
Science and Technology)

Supervisor: Dr. Jennifer Bauman, P. Eng.

Number of Pages: xv, 155

Lay Abstract

Autonomous vehicles are expected to be the future of transportation, however, the high continuous electrical accessory power needed for control and perception is a challenge. Fortunately, there is an inherent property of speed planning for autonomous vehicles that can help deal with this problem. This thesis focuses on optimal speed planning to minimize energy use, proposing convex methods considering detailed internal and external losses for battery electric vehicles (BEVs), and optimal speed planning integrated with optimal energy management for fuel cell hybrid electric vehicles (FCHEVs). The proposed framework in this thesis is accurate while maintaining a low computational effort, which are the desired criteria for real-time algorithms.

Abstract

Electric vehicles with autonomous driving are the future of transportation, as they are sustainable, efficient, environmentally friendly, and can provide collision-free congestion-free driving. However, the sensing and control technology adds new accessory loads which increase the vehicle energy use. Thus, it is critical to minimize energy use where possible, and optimal speed planning is a promising way to achieve this goal and is thus the topic of study for this thesis.

First, a low-computation framework for the onboard calculation of energy-optimal cruising speed of battery electric vehicles is proposed. The framework is used to investigate the critical parameters for energy-optimal cruising speed determination, and it includes major internal and external vehicle losses, uses accurate motor-inverter efficiency maps as look-up tables, and does not require knowledge of the future route. This framework is validated using three electric vehicle models in MATLAB/SIMULINK.

Secondly, a novel two-level model predictive control (MPC) speed control algorithm for battery electric autonomous vehicles as a successive convex optimization problem is proposed. The proposed successive convex approach produces a highly accurate optimal speed profile while also being solvable in real-time with the vehicle's onboard computing resources. This algorithm is used to perform a variety of simulated test cases, which show an energy savings potential of about 1% to 20% for different driving conditions, compared to a non-energy-optimal driving profile.

Lastly, the research is expanded to consider fuel cell hybrid electric vehicles (FCHEVs), which have the added need for an optimal energy management strategy in

addition to optimal speed planning. Novel successive and integrated convex speed planning and energy management algorithms are proposed to solve the minimum hydrogen consumption problem for autonomous FCHEVs. The simulation results show that the proposed integrated method, which considers fuel cell system efficiency in the optimization objective function for speed planning, leads to 0.19% to 2.37% less hydrogen consumption compared to the successive method on short drive cycles with varying accessory loads. On the same test cycles, the integrated method uses 10.12% to 21.62% less hydrogen than an arbitrary constant-speed profile.

Acknowledgment

I would like to express my deepest appreciation to my academic supervisor, Dr. Jennifer Bauman, for her continued support through my Ph.D. and related research, and for her valuable guidance, patience, motivation, and immense knowledge. She has always been a supportive and caring mentor.

I would like to extend my sincere thanks to my supervisory committee members, Dr. Ali Emadi, and Dr. Mehdi Narimani, for their insightful comments and helpful feedback during my studies.

Many thanks should also go to all my friends in Bauman Lab for their unceasing help and sympathy through my research. It was fantastic to have the opportunity to work on multiple projects with them.

Last but not least, I would like to genuinely thank my wife Sanaz, my parents, my sisters, and all my family and friends for the endless encouragement, support, and attention.

Table of Contents

Lay Abstract	iii
Abstract.....	iv
Acknowledgment.....	vi
Table of Contents	vii
List of Figures.....	xi
List of Tables	xv
1. Introduction.....	1
1.1 Background and Motivations.....	2
1.2 Review of Autonomous Driving and Speed Optimization for AVs	5
1.3 Contributions.....	8
1.3.1 Optimal Cruising Speed Selection Framework	8
1.3.2 Real-Time Determination of Near-Optimal Transition Rate.....	8
1.3.3 Energy-Optimal Speed Problem in a Two-Level MPC Platform	9
1.3.4 Integrated Convex Speed Planning and Energy Management for FCHEVs	9
1.4 Publications	10
1.4.1 Journal Publications	10
1.4.2 Conference Publications.....	11

1.5	Outline of the Thesis.....	11
1.6	Chapter 1 References.....	13
2.	Investigation of Critical Parameters for Selecting Energy-Optimal Cruising Speed Using a Low-Computation Framework.....	15
2.1	Introduction	16
2.2	Proposed Framework.....	20
2.2.1	System Architecture	20
2.2.2	Steady-State Loss Equations	22
2.2.3	Optimal Speed Transition Determination.....	29
2.3	Vehicle Model Creation and Validation.....	33
2.4	Simulation Results.....	40
2.4.1	Steady-State Optimal Cruising Speed	40
2.4.2	Steady-State Cruising Speed Sensitivity Analysis	48
2.4.3	Optimal Speed Transition.....	49
2.5	Flexible Implementation Option.....	52
2.6	Conclusion.....	54
2.7	Chapter 2 References.....	56
3.	Two-level MPC Speed Profile Optimization of Autonomous Electric Vehicles Considering Detailed Internal and External Losses	59

3.1	Introduction	60
3.2	Convex Problem Formulation.....	63
3.2.1	Vehicle Dynamics	64
3.2.2	Losses Formulation	66
3.2.3	Physical Limitations	71
3.2.4	Optimization Formulation	72
3.3	Vehicle Modeling	80
3.4	Simulation Results.....	84
3.4.1	Energy Focused Optimization	85
3.4.2	Time and Mixed Time-Energy Optimization	91
3.4.3	Computational Effort.....	93
3.5	Conclusion.....	95
3.6	Chapter 3 References.....	97

4. Integrated Convex Speed Planning and Energy Management for Autonomous Fuel Cell Hybrid Electric Vehicles100

4.1	Introduction	101
4.2	Convex Problem Modeling and Formulation	106
4.2.1	General Overview	106
4.2.2	Convex Vehicle Model.....	108
4.2.3	Convex Optimization Formulation.....	119
4.3	Convex Simulation Results and Discussion	128

4.3.1	Short Test Cycle Results	128
4.3.2	Electric Accessory Sensitivity Analysis	130
4.3.3	Logged Driving Cycle Results	133
4.3.4	Road Speed Limit Changes	137
4.3.5	Computational Effort Analysis.....	138
4.4	Convex Comparison to Dynamic programming.....	140
4.4.1	Dynamic Programming Formulation.....	141
4.4.2	Dynamic Programming Results.....	143
4.5	Conclusions and Future Work.....	144
4.6	Chapter 4 References.....	146
5.	Conclusions and Future Work.....	151
5.1	Summary	152
5.2	Recommendations for Future Work	154

List of Figures

Figure 1-1 Effect of electrical accessories on vehicle energy usage in different cruising speeds	3
Figure 2-1 The proposed inner structure of EOVG block	22
Figure 2-2 Wind in an arbitrary direction	24
Figure 2-3 Block diagram of vehicle model	26
Figure 2-4 Acceleration trajectory in distance domain from 75km/h to 80km/h	32
Figure 2-5 Acceleration trajectory in distance domain from 50km/h to 80km/h	32
Figure 2-6 Acceleration results from DP analysis and proposed equation	33
Figure 2-7 Scheduled and simulated speed profile for nine test cycles	37
Figure 2-8 Simulated battery SOC vs logged SOC of Spark EV (S3 cycle)	38
Figure 2-9 Simulated battery current vs logged current of Spark EV (S3 cycle)	38
Figure 2-10 Simulated battery voltage vs logged voltage of Spark EV (S3 cycle)	39
Figure 2-11 Vehicle energy consumption for different accessory usage levels	42
Figure 2-12 Vehicle energy consumption for different wind speeds	43
Figure 2-13 Equation validation using energy consumption of Tesla Model S	46
Figure 2-14 Equation validation using energy consumption of Chevrolet Bolt	46
Figure 2-15 Equation validation using energy consumption of Chevrolet Spark EV	47
Figure 2-16 Optimal speed in different study cases	47
Figure 2-17 Energy usage with curb mass +100 kg and + 600kg for Cases 1-6	49
Figure 2-18 Energy usage with standard rolling resistance and 20% higher values for Cases 1-6	50

Figure 2-19 Sensitivity analysis of optimal speed selection	50
Figure 2-20 Velocity trajectory in the time domain.....	51
Figure 2-21 SOC comparison between DP and suggested trajectory	52
Figure 2-22 Energy-based flexible implementation approach.....	54
Figure 3-1 EV block diagram.....	66
Figure 3-2 Wind in an arbitrary direction	67
Figure 3-3 2010 Prius combined motor-inverter efficiency contours at 650 Vdc [27].....	70
Figure 3-4 Illustration of proposed method for optimization	73
Figure 3-5 Efficiency data vs fitted second order approximation from Chevy Bolt EV [12]	75
Figure 3-6 Error between efficiency data and fitted polynomial from Chevy Bolt EV [12]	75
Figure 3-7 Flowchart of the successive convex optimization approach	77
Figure 3-8 Proposed two-level control platform.....	78
Figure 3-9 Block diagram of vehicle model	81
Figure 3-10 Logged vs simulated drive cycle data of a Tesla Model S.....	82
Figure 3-11 a) Time-speed profile b) Distance-speed profile c) Time-SOC d) Energy consumption of the Tesla model S with constant efficiency	84
Figure 3-12 a) Time-speed profile b) Distance-speed profile for five different cases.....	87
Figure 3-13 a) Time-speed profile b) Distance-speed profile c) Time-SOC d) Energy consumption of the Tesla model S at 3 kW accessory usage	88

Figure 3-14 a) Time-speed profile b) Distance-speed profile c) Time-SOC d) Energy consumption of the Tesla model S at 8 kW accessory usage	88
Figure 3-15 a) Time-speed profile b) Distance-speed profile c) Time-SOC d) Energy consumption of the Tesla model S at 11 kW accessory usage	89
Figure 3-16 Energy consumption vs. trip duration for two different cases with three different optimization objectives (Energy optimal, Time optimal, Mixed time-energy)...	92
Figure 3-17 Speed profiles for two different cases with three different optimization objectives (Energy focused, Time focused, Mixed Time-Energy) a) speed vs time b) speed vs distance	93
Figure 3-18 Execution time vs. vehicle energy usage for different horizon length.....	95
Figure 4-1 a) Successive optimization method b) Integrated optimization method using η_{FC} feedback	107
Figure 4-2 Toyota Mirai 2017 block diagram.....	108
Figure 4-3 FC system efficiency as a function of FC output power, as extracted from [43]	111
Figure 4-4 UDDS test cycle for fuel cell system validation (Test ID 61712033)	112
Figure 4-5 Battery model validation a) battery input current b) battery terminal voltage c) battery SOC.....	115
Figure 4-6 Combined PM motor and inverter efficiency map based on [48].....	117
Figure 4-7 . Effect of fuel cell efficiency on energy consumption and optimal speed selection.	119

Figure 4-8 Integrated optimization algorithm flowchart (the successive method does not contain the orange-encircled part).....	127
Figure 4-9 Comparison of arbitrary speed profile with optimal results from successive and integrated methods	130
Figure 4-10 Sensitivity analysis optimal speed trajectories for different values of electric accessory power	132
Figure 4-11 Optimal vs logged driving for Trip 1: a) time-speed trajectory b) distance-speed trajectory c) cumulative H2 consumption d) time-SOC curve e) optimal power split based on optimal speed planning	134
Figure 4-12 . Optimal vs logged driving for Trip 2: a) time-speed trajectory b) distance-speed trajectory c) cumulative H2 consumption d) time-SOC curve e) optimal power split based on optimal speed planning	135
Figure 4-13 Optimal vs logged driving for Trip 3: a) time-speed trajectory b) distance-speed trajectory c) cumulative H2 consumption d) time-SOC curve e) optimal power split based on optimal speed planning	136
Figure 4-14 Optimal speed trajectory with addition of desired velocity to the objective by (a) time, and (b) distance.....	138
Figure 4-15 Optimal speed trajectory with addition of desired velocity to the objective	140
Figure 4-16 Comparison between three speed trajectories generated using the integrated method, successive method, and DP method.....	144

List of Tables

Table 2-1 Baseline Values of Vehicle Parameters.....	34
Table 2-2 Vehicle Model Energy Usage Validation.....	40
Table 2-3 Baseline Values of Vehicle Parameters for Test Cases.....	43
Table 2-4 Test Case Specifications.....	44
Table 3-1 Baseline values of Tesla Model S vehicle parameters	83
Table 3-2 Vehicle Model Energy Usage Validation.....	83
Table 3-3 Study cases for different cases.....	87
Table 3-4 Simulated energy use of cases over 585m trip	90
Table 4-1 Validation of Fuel Cell Model.....	113
Table 4-2 Validation of Battery Model.....	116
Table 4-3 Vehicle Specifications based on Toyota Mirai.....	118
Table 4-4 Optimization Results for Short Test Cycles	130
Table 4-5 Optimization Results for Sensitivity Analysis of Pacc.....	132
Table 4-6 Summary of Results for Optimal speed vs logged speed (both using optimal EMS).....	137
Table 4-7 Equivalent Hydrogen Consumption Comparison for DP Method.....	144

Chapter **1**

1. Introduction

1.1 Background and Motivations

The transportation industry is currently undergoing two radical transformations: electrification, to reduce the harmful environmental effects of internal combustion engines, and autonomous driving, to reduce traffic fatalities and transform the way society moves. However, the computational and perceptual burden of autonomous vehicles and the continuous demand for extra energy to run these systems is in disagreement with one of the main environmental objectives of transportation electrification. Thus, it is vital to use every opportunity available to reduce the energy use of autonomous electric vehicles.

Much work in the area of autonomous vehicles focuses on sensors, signal processing, computations, security, and safety, which are critical areas of research in the transition to fully autonomous vehicles. Other work has demonstrated the clear potential for reductions in energy consumption due to optimal route selection [1], smoother driving [2][3], and more optimal energy management in hybrid vehicles [4]-[6]. For fully connected autonomous vehicles, further energy usage reductions can be made through ridesharing [7], improved traffic flow at intersections [8][9], and platooning [10].

The standard method of quantifying vehicle energy consumption involves driving a test vehicle on a dynamometer at speeds specified by standard drive cycles. Automotive engineers design and control powertrain components to minimize losses on these cycles. To build a mathematical method to calculate detailed losses for electric vehicles (internal and external), [11] proposes a framework, where all the internal and external losses of the vehicle are converted into per distance unit (J/m) and the sum of these losses is used as an objective function to find the optimal cruising speed.

This study shows different parameters such as electrical accessory power level, ambient temperature, grade, vehicle mass, wind speed, and battery SOC level can affect optimal speed selection. This study shows that some of these parameters such as electrical accessory power level, and grade are more dominant in comparison to other variables.

Figure 1-1 shows the effect of electrical accessories on BEVs energy usage at different cruising speeds. This figure can summarize the main motivation for this research, as it shows having a higher electrical accessory power level encourages the vehicle to go at a faster speed.

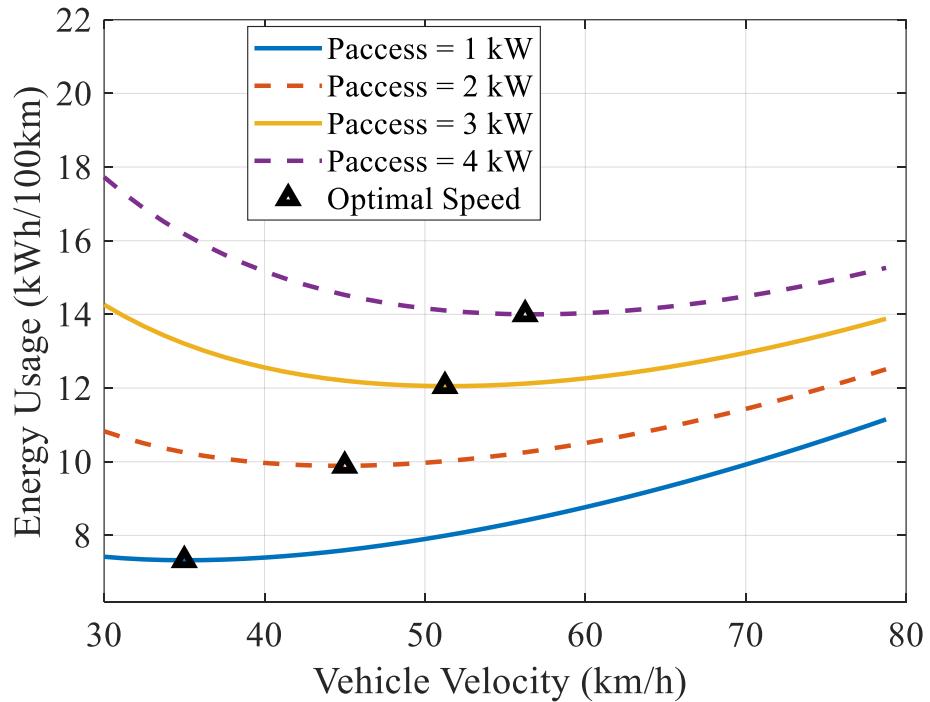


Figure 1-1 Effect of electrical accessories on vehicle energy usage in different cruising speeds

Autonomous vehicles (AVs) offer many advantages and features such as collision avoidance, passenger convenience, and mobility for groups with driving challenges, however, perception of the vehicle’s environment, and autonomous driving control systems

contain many sensors and computational hardware, which results in higher accessory power loads. Even though the exact values of this power consumption are not well-published and differ among different vehicles, [11] estimates it to be around a few kilowatts of continuous power. Luckily, autonomous driving essentially presents two exclusive opportunities for energy reduction: determination of optimal speed trajectory at vehicle level and optimal energy management if it is a hybrid vehicle.

Now that the importance of optimal speed selection is established, this research tackles this challenging problem in three ways. First, optimal cruising speed for battery electric vehicles (BEVs) is studied to point out what are the main parameters influencing optimal speed selection, then an optimal transition between these optimal cruising speeds are explored using the dynamic programming method and the findings are fitted into a fitting function to maintain the real-time performance of the framework. This algorithm could be used by a not-fully-autonomous vehicle, and it also can be used by an autonomous vehicle during cruising on a highway to reduce the computational burden compared to city driving. Secondly, an optimal speed planning in an MPC platform for BEVs is proposed to generate the whole speed trajectory from the starting point to the end point of the trip. Thirdly, optimal speed planning, as well as optimal energy management is proposed for a fuel cell hybrid electric vehicle (FCHEV), to better highlight challenges and advantages of having additional energy storage (usually a battery) on the optimal speed planning algorithm.

1.2 Review of Autonomous Driving and Speed Optimization for AVs

It was in 1926 that the first attempts for experimental AV were done, and it wasn't before 1986 that the first modern AVs were created[12][13]. Most major automotive manufacturers are working on the development of AVs since 2010 [14], and Google's AV traveled over one million kilometers in 2016 which was a major milestone in the field. The complexity of the task in addition to safety and reliability concerns are the main reasons for slightly slow progress in the development [15].

According to the Society of Automotive Engineers (SAE) [16], there are six levels of automation in the AV area (0-5). Level 0 is the "no automation" level, where all driving aspects are performed by human drivers. Level 1 is "driver assistance" (hands-on), where automation shares some performance tasks with the driver. Level 2 automation is "partial automation" (hands-off), where all driving aspects are automated, but the human driver should supervise the system. Level 3 automation is "conditional automation" (eyes-off), where the driver intervention may be requested and all driving aspects are automated. Level 4 is "high automation" (mind-off), which is similar to level 3, however, the automatic system continues to control even if the human driver does not respond to a request. The last stage is level 5 "full automation", where the steering wheel is optional and human intervention is never requested.

According to [17], autonomous driving consists of three layers, the perception layer, the reference generation layer, and the control layer. The perception layer is responsible for recognizing the vehicle's environmental settings, such as obstacles, road signs, and so on. The reference generation layer is responsible for generating reference

instructions based on data gathered by the perception layer, and path planning is an example of this layer's duties. The control layer is responsible for tasks such as steering, acceleration, and braking to guarantee that the vehicle follows the desired trajectory.

The main objective of eco-driving is to determine the optimal speed profile for a vehicle to minimize its energy usage over a given distance with a constraint on its desired arrival time. There are some prior works focused specifically on vehicle energy minimization by optimization of speed profile. A variety of techniques are proposed to obtain the optimal solution for this problem. A summary of these techniques is listed below.

Dynamic Programming (DP) is a common approach to finding a globally optimal speed profile, which is critical to truly minimize energy use over a trip, is to use dynamic programming (DP) [18]-[21]. However, this approach is computationally expensive and does not align well with the fast real-time needs of a driving vehicle, yet it can be used as benchmark method for evaluation purposes.

Evolutionary Optimization algorithms are algorithms inspired by nature and attempt to solve problems using behavioral actions of living organisms. Reference [22] uses an off-line evolutionary optimization approach to solve the speed optimization problem, and in [23] the ant colony algorithm is used to solve speed profile optimization for a train, but it is not applicable for real-time implementation.

Model Predictive Control (MPC) has also been used to solve various formulations of the energy-optimal speed selection problem. The idea of eco-driving with consideration of safety is studied in [24] for connected autonomous vehicles. It uses MPC to solve the optimization problem with the objective of minimizing energy consumption while avoiding

collision with nearby connected vehicles. However, in order to get real-time results, motor losses are approximated with a simple expression and other internal vehicle losses are ignored. Similarly, MPC is used to optimize the speed trajectory for heavy-duty urban vehicles in [25], but a simplified vehicle model is used which ignores the vehicle internal losses.

Convex Optimization uses convex formulation, and it is an attractive alternative for energy-optimal speed determination because it can generally find the globally optimal solution in a computationally efficient way, which is well suited to the quickly-changing driving conditions in urban settings. However, to make the problem convex, many simplifications are often made, which can alter the accuracy of the results. For example, [26] and [27] use a convex formulation in a MPC platform to solve the speed optimization problem, but only simple external vehicle losses are considered, and internal losses such as the motor losses and accessories are ignored. An innovative approach for the real-time calculation of the optimal speed trajectory for a commuter train is proposed in [28]. The second-order cone programming method is used to formulate the optimization problem in a convex way. However, simplifications have again been made to create the convex formulation: the motor efficiency is assumed constant for the trip and other internal losses are not considered.

1.3 Contributions

1.3.1 Optimal Cruising Speed Selection Framework

The first contribution of this thesis is the proposal of a framework to generate optimal cruising speed considering detailed internal and external losses. Parameters are divided into three types; fixed parameters (frontal area, drag coefficient, ...), slowly changing parameters (ambient temperature, vehicle mass, ...), and fast-changing parameters (road grade, electrical accessory power, ...). All the considered losses are converted into per distance unit (J/m) and the algorithm evaluates total internal and external losses at velocity samples between minimum and maximum allowed speed and chooses the best option to minimize the objective function (total losses). This algorithm is suitable for vehicles that are not fully autonomous, and it is also useful for fully autonomous vehicles when driving on a highway to reduce the computational burden.

1.3.2 Real-Time Determination of Near-Optimal Transition Rate

The second contribution of this thesis is a real-time determination of the near-optimal transition rate between the previous and new optimal cruising speed when a vehicle state change is added. Criteria for real-time implementation in this work is to keep code run time under one second for computation effort. Initially, DP is used to find the best transition rate between two optimal cruising speeds, and the findings are used to generate a fitting polynomial approximation based on ΔE and V_{orig} .

1.3.3 Energy-Optimal Speed Problem in a Two-Level MPC Platform

The third contribution of this thesis is the proposal of a new convex formulation of the energy-optimal speed problem in a two-level MPC platform which considers detailed internal and external losses of an electric vehicle (EV), to generate a highly accurate result. The proposed algorithm uses the successive convex approach to obtain a real-time means of solving the optimization problem with a mixed objective of time and energy. Successive convex optimization is an iterative method: at each iteration, it uses the efficiency data calculated from the last iteration. By repeating the algorithm, the speed profile starts to converge, resulting in the final answer. The optimal solution can be updated periodically by using new data so it can re-evaluate and adjust to new conditions. Using a convex formulation ensures a fast run-time, making it suitable for on-board implementation on autonomous vehicles. This convex optimal speed planning with consideration of detailed internal and external losses is novel in this area of research.

1.3.4 Integrated Convex Speed Planning and Energy Management for FCHEVs

The last contribution of this thesis is the development of a framework for energy use minimization of a FCHEV through optimal speed planning and energy management using convex optimization. The convex formulation allows the algorithm to run in real-time, and detailed loss modeling is used to ensure a highly accurate result. Thus, the first novel contribution in this area is the proposed successive method, where convex optimization is first used to generate the optimal speed trajectory, then convex optimization is used to solve the EMS problem using the optimal speed trajectory. The second novel contribution of this work is the proposed integrated method, which uses the knowledge of the EMS

(instantaneous fuel cell power) to affect the optimal speed trajectory, such that the speed planning and EMS problems are solved in an integrated way using convex optimization. The consecutive convex optimal speed planning and integrated method using fuel cell system efficiency are novel compared to prior work in the literature.

1.4 Publications

This thesis is written in the “Sandwich Thesis” format, where each following chapter is based on a journal paper. These papers keep the main content intact but have a slightly modified structure to comply with the format of the thesis. Chapters 2, 3, and 4 have been prepared based on publications shown in Section 1.4.1 respectively.

1.4.1 Journal Publications

- [1] Meshginqalam and J. Bauman, "Investigation of Critical Parameters for Selecting Energy-Optimal Cruising Speed Using a Low-Computation Framework," in *IEEE Transactions on Industry Applications*, vol. 57, no. 3, pp. 2825-2837, May-June 2021, doi: 10.1109/TIA.2021.3057037.

- [2] A. Meshginqalam and J. Bauman, "Two-Level MPC Speed Profile Optimization of Autonomous Electric Vehicles Considering Detailed Internal and External Losses," in *IEEE Access*, vol. 8, pp. 206559-206570, 2020, doi: 10.1109/ACCESS.2020.3038050.

- [3] A. Meshginqalam and J. Bauman, " Integrated Convex Speed Planning and Energy Management for Autonomous Fuel Cell Hybrid Electric Vehicles," accepted for publication in IEEE Transaction on Transportation Electrification, June 2022.

1.4.2 Conference Publications

- [1] Meshginqalam and J. Bauman, "An Onboard Real-Time-Implementable Framework for Calculating the Optimal Cruising Speed of Electric Autonomous Vehicles," 2019 IEEE Transportation Electrification Conference and Expo (ITEC), 2019, pp. 1-6, doi: 10.1109/ITEC.2019.8790538.

1.5 Outline of the Thesis

This thesis is organized into five chapters. Chapter 1 has given the background and motivation for the speed optimization in electric autonomous vehicles and this research's contributions. Chapter 2 discusses the proposed algorithm to find optimal cruising speed for an autonomous BEV and optimal transition between two optimal speed choices. This method is computationally efficient and can also be used in not fully autonomous vehicles. Chapter 3 discusses the design process for the algorithm to generate optimal speed trajectory for autonomous BEVs using MPC. The simulation results for different study cases are presented and computational effort analyses are conducted to show the ability to implement it in real-time. This method is more suitable for autonomous vehicles driving in a city where multiple stop-and-go scenarios should be performed. Chapter 4 discusses the optimal speed planning for FCHEVs, and two frameworks are proposed for the optimization problem, successive and integrated methods. Simulation scenarios for these

studies show that the integrated method can outperform the successive method. Also, computational effort evaluations are shown to verify the real-world implementation ability of the framework. Chapter 5 gives the conclusion and future work.

1.6 Chapter 1 References

- [1] A. Cela et al., "Energy optimal real-time navigation system," *IEEE Intelligent Transportation Systems Magazine*, vol. 6, no. 3, pp. 66-79, Fall 2014.
- [2] K. P. Divakarla, A. Emadi, and S. Razavi, "A cognitive advanced driver assistance systems (ADAS) architecture for autonomous-capable electrified vehicles," *IEEE Transactions on Transportation Electrification*, pp. 1–1, 2018.
- [3] P. Michel, D. Karbowski, and A. Rousseau, "Impact of connectivity and automation on vehicle energy use," *SAE Technical Paper Series*, May 2016.
- [4] Y.-C. Lin and H. Nguyen, "Development of an eco-cruise control system based on digital topographical data," *Inventions*, vol. 1, no. 3, p. 19, Dec. 2016
- [5] V. Larsson, L. Johannesson Mårdh, B. Egardt and S. Karlsson, "Commuter route optimized energy management of hybrid electric vehicles," *IEEE Transactions on Intelligent Transportation Systems*, vol. 15, no. 3, pp. 1145-1154, June 2014.
- [6] G. Ma, M. Ghasemi and X. Song, "Integrated powertrain energy management and vehicle coordination for multiple connected hybrid electric vehicles," *IEEE Transactions on Vehicular Technology*, vol. 67, no. 4, pp. 2893-2899, April 2018.
- [7] L. Tate, S. Hochgreb, J. Hall, and M. Bassett, "Energy efficiency of autonomous car powertrain," *SAE Technical Paper Series*, Mar. 2018.
- [8] S. I. Guler, M. Menendez, and L. Meier, "Using connected vehicle technology to improve the efficiency of intersections," *Transportation Research Part C: Emerging Technologies*, vol. 46, pp. 121–131, 2014.
- [9] G. Bucsan, A. Goupilleau, P. Frene, M. Ishigaki, A. Iwai, J. S. Lee, M. Pokhrel, M. Balchanos, and D. Mavris, "Mobility analysis of electric autonomous vehicle networks driven by energy-efficient rerouting," 2017 *IEEE 85th Vehicular Technology Conference (VTC Spring)*, 2017.
- [10] V. Turri, B. Besselink and K. H. Johansson, "Cooperative look-ahead control for fuel-efficient and safe heavy-duty vehicle platooning," *IEEE Transactions on Control Systems Technology*, vol. 25, no. 1, pp. 12-28, Jan. 2017.
- [11] A. Meshginqalam and J. Bauman, "An Onboard Real-Time-Implementable Framework for Calculating the Optimal Cruising Speed of Electric Autonomous Vehicles," 2019 *IEEE Transportation Electrification Conference and Expo (ITEC)*, 2019, pp. 1-6, doi: 10.1109/ITEC.2019.8790538.
- [12] M. Sentinel, "Phantom auto'll tour city," *Milwaukee Sentinel*, vol. 4, Dec. 1926.
- [13] T. Kanade, C. Thorpe, and W. Whittaker, "Autonomous land vehicle project at CMU," in *Proc. ACM 14th Annu. Conf. Comput. Sci.*, 1986, pp. 71–80.
- [14] D. Neil, "Who's behind the wheel? nobody. the driverless car is coming. and we all should be glad it is," *Wall Street J.*, Sep. 2012. [Online]. Available: <https://www.proquest.com/newspapers/whos-behindwheel-nobody-driverless-car-is-coming/docview/1064085009/se-2?accountid=40023>
- [15] S. Hacohen, O. Medina and S. Shoval, "Autonomous Driving: A Survey of Technological Gaps Using Google Scholar and Web of Science Trend Analysis," in *IEEE Transactions on Intelligent Transportation Systems*, doi: 10.1109/TITS.2022.3172442.

- [16] Taxonomy and Definitions for Terms Related to Driving Automation Systems for on-Road Motor Vehicles (J3016), Society for Automotive Engineering, Warrendale, PA, USA, 2016
- [17] AE On-Road Automated Vehicle Standards Committee, "Taxonomy and definitions for terms related to on-road motor vehicle automated driving systems," SAE Standard J., vol. 3016, pp. 1–16, Jan. 2014.
- [18] K. Kim, H. Lee, C. Song, C. Kang and S. W. Cha, "Optimization of speed trajectory for eco-driving considering road characteristics," 2018 IEEE Vehicle Power and Propulsion Conference (VPPC), Chicago, IL, 2018, pp. 1-5.
- [19] E. Ozatay et al., "Cloud-based velocity profile optimization for everyday driving: a dynamic-programming-based solution," IEEE Transactions on Intelligent Transportation Systems, vol. 15, no. 6, pp. 2491-2505, Dec. 2014.
- [20] S. Akhegaonkar, L. Nouvelière, S. Glaser and F. Holzmann, "Smart and green ACC: energy and safety optimization strategies for EVs," in IEEE Transactions on Systems, Man, and Cybernetics: Systems, vol. 48, no. 1, pp. 142-153, Jan. 2018, doi: 10.1109/TSMC.2016.2600273.
- [21] P. Themann, J. Bock, and L. Eckstein, "Optimisation of energy efficiency based on average driving behaviour and driver's preferences for automated driving," IET Intell. Transport Syst., vol. 9, no. 1, pp. 50–58, 2015.
- [22] W. ShangGuan, X. Yan, B. Cai and J. Wang, "Multiobjective optimization for train speed trajectory in CTCS high-speed railway with hybrid evolutionary algorithm," IEEE Transactions on Intelligent Transportation Systems, vol. 16, no. 4, pp. 2215-2225, Aug. 2015.
- [23] L. Fan, F. Cao, B. Ke and T. Tang, "Speed profile optimization for train operation based on ant colony algorithm," 2015 IEEE Advanced Information Technology, Electronic and Automation Control Conference (IAEAC), 2015, pp. 48-53, doi: 10.1109/IAEAC.2015.7428516
- [24] J. Han, A. Sciarretta, L. L. Ojeda, G. De Nunzio and L. Thibault, "Safe- and eco-driving control for connected and automated electric vehicles using analytical state-constrained optimal solution," in IEEE Transactions on Intelligent Vehicles, vol. 3, no. 2, pp. 163-172, June 2018.
- [25] M. Held, O. Flärdh and J. Mårtensson, "Optimal speed control of a heavy-duty vehicle in urban driving," IEEE Trans. on Intelligent Transportation Systems, vol. 20, no. 4, pp. 1562-1573, April 2019.
- [26] Y. Shao and Z. Sun, "Eco-approach with traffic prediction and experimental validation for connected and autonomous vehicles," in IEEE Transactions on Intelligent Transportation Systems, Feb. 2020.
- [27] M. A. S. Kamal, M. Mukai, J. Murata, and T. Kawabe, "Model predictive control of vehicles on urban roads for improved fuel economy," IEEE Trans. Control Syst. Technol., vol. 21, no. 3, pp. 831–841, May 2013.
- [28] D. Yazhensky, M. Rashid and S. Sirouspour, "An on-line optimal controller for a commuter train," in IEEE Transactions on Intelligent Transportation Systems, vol. 20, no. 3, pp. 1112-1125, March 2019

Chapter 2

2. Investigation of Critical Parameters for Selecting Energy-Optimal Cruising Speed Using a Low-Computation Framework

2.1 Introduction

In autonomous vehicles or vehicles with eco-cruise control, it is important to minimize cruising energy use while adhering to driver trip time constraints so that advanced vehicle deployment is aligned with the vision of clean and efficient transportation. However, there is one major vehicle parameter that has not been focused on by previous research in this area: vehicle accessory loads. It is commonly assumed that for an electric vehicle (EV) there is always a trade-off between vehicle energy use and trip time while cruising (i.e., on a highway or backroad drive). The usual assumption is that since a higher travel speed equates to more aerodynamic losses, lower speeds should be selected for eco-driving. However, when considering higher vehicle accessory loads, among other vehicle parameters, this trade-off can change and may no longer apply.

This is an important area of research because autonomous vehicles inherently have a large amount of sensors and computation required, which increases the vehicle's accessory power load. Reports of this load increase are not yet widely available, but [1] estimates that at least a few kilowatts of continuous power is required in fully autonomous vehicles, meaning the extra load is in the same range as heating and air conditioning loads, which are already a major concern for EVs [1]. Further, even non-autonomous EVs with cruise control can have a high accessory load up to 8 kW due to heating, ventilation, and air conditioning (HVAC), which will greatly affect the energy-optimal cruising speed.

Prior work in eco-driving has demonstrated the clear potential for reductions in energy consumption due to optimal route selection [2], smoother driving [3][4], and more optimal energy management in hybrid vehicles [5][6]. For fully connected autonomous

vehicles, further energy usage reductions can be made through ride-sharing [7], improved traffic flow at intersections [8][9], and platooning [10]. References [11]-[13] present detailed algorithms to determine vehicle speed with the goal of minimizing jerk, thus ensuring a smooth and comfortable ride.

With a focus on minimizing energy consumption, [14] assumes full knowledge of the future route, divides the route into segments based on constant road grade, and then generates an optimal speed for each segment to minimize energy use for a specified travel time. Reference [14] considers only the aerodynamic, rolling, and grade losses, and does not consider losses within the vehicle. In [15], additional internal vehicle losses for a hybrid electric vehicle are considered, yet the models are very simplified so that the resulting nonlinear optimization problem can be solved offline by MATLAB's *fmincon* function. For example, the motor efficiency is assumed constant and the inverter losses are ignored, both of which are poor approximations [16]-[21]. Furthermore, the engine losses are not speed-dependent, and the battery losses are calculated for a fixed battery state-of-charge (SOC) of 50%. In [22], optimal velocity for a route with varying grade is determined by considering aerodynamic, rolling, and grade losses, as well as engine losses, where the engine losses are approximated by a simple polynomial equation. Reference [23] assumes future knowledge of the grade of the route, and includes aerodynamic, rolling, grade, motor, and inverter losses, but does not specify the level of detail of the motor and inverter models, and does not consider accessory losses. It uses a look-ahead window and dynamic programming to consider many hundreds of possible speed trajectory paths. Reference [24] uses dynamic programming in a cloud-based system, which is needed to handle the high

computational burden, to calculate the optimal speed profile for a known route considering aerodynamic, rolling, grade, and engine losses using an analytical engine model. The most detailed loss models are considered for an EV in [25]-[27], where an analytical vehicle model is used to generate a speed profile that minimizes energy consumption during acceleration and deceleration events, for a given cruising velocity, but it does not calculate the energy-optimal cruising velocity. They consider grade losses, aerodynamic losses, rolling losses, and the copper and iron losses in the motor. However, in order to make their motor model tractable, they neglect spinning losses in the motor and inverter losses. Furthermore, they do not consider battery losses nor accessory power use.

In order to address gaps in the prior work of determining energy-optimal cruising speeds, this chapter develops and investigates a framework with the following contributions:

- 1) All major vehicle losses, both internal and external to the vehicle, are considered in the optimization to attain very high accuracy. These losses depend on the current state of the vehicle parameters (SOC, temperature, etc.). The investigation particularly focuses on the high accessory vehicle loads that can greatly affect optimal cruising speed and have not been considered previously.
- 2) Loss maps for motors and inverters, in the form of look-up-tables (LUTs) are used directly in the framework, as opposed to prior work that approximates constant efficiency or uses simple polynomials to approximate efficiency. The use of test-based LUTs is more accurate than simple polynomial modeling: [28] finds that in order to achieve high accuracy motor loss accuracy, the constant torque region must be modeled

separately from the constant power region, where the constant torque region requires 11 terms of torque (τ) and speed (ω), up to τ^4 and ω^4 , and the constant power region requires 15 terms that combine orders of τ and ω . This level of complexity for non-LUT approaches is not suitable for analytical solutions.

- 3) No future route or traffic information is required, as the framework simply finds the optimal cruising speed for the current vehicle state. While future connected vehicles will ideally have vast knowledge of the future route, there is an immediate need for non-connected autonomous vehicles and vehicles using eco-cruise control to be able to calculate the local optimal cruising speed with minimal connected/external information. Thus, the proposed framework has a low number of computations and is easily implemented in real time without the requirement of connectivity or cloud-based computations.

The proposed framework can be applied in any cruising situation such as: low-traffic semi-urban roads which may have speed limits between 50 km/h and 60 km/h, regional roads at the outskirts of cities and between cities that may have speed limits between 60 km/h and 90 km/h, and major highways. The speed optimization of stop-and-go urban driving considering accessory losses and accurate motor/inverter losses will be addressed in future work, and will likely require a higher computational burden.

In [29] the core concept of the framework was proposed and investigated using vehicle parameters for the Chevrolet Spark EV. This study expands on [29] by: (i) validating the framework using multiple vehicle models created from real-world driving data, (ii) adding a real-time determination of near-optimal transition rate between the

previous and new optimal cruising speed when a vehicle state changes, (iii) investigating higher accessory loads which better represent the loads of autonomous vehicles, (iv) performing a sensitivity analysis for two vehicle parameters that are difficult to estimate in real time, and (v) proposing a flexible implementation option for when a driver wants to drive faster than the energy-optimal speed. Section 2.2 presents the proposed framework and derives the associated equations, Section 2.3 describes the vehicle model creation and validation process, Section 2.4 presents the simulation results, and Section 2.5 presents the flexible option for implementing the proposed algorithm. Section 2.6 discusses the conclusions and future work.

2.2 Proposed Framework

2.2.1 System Architecture

The main goal of the framework is to find the cruising speed that minimizes the energy use per unit distance for any particular vehicle state. Figure 2-1 shows the proposed system architecture. It is assumed that the *Autonomous Safety System* gathers and processes all the sensor and driver data in order to produce both a minimum and maximum cruising velocity bound (v_{min}, v_{max}), which limits the optimal velocity, v_{opt} . In an autonomous vehicle, these bounds would be calculated as a result of many factors (e.g., speed of the vehicle in front, road speed limit, etc.). Also, any driver trip time constraint would bound the lower limit, v_{min} . For example, if the cruising speed bounds are 50 km/h and 80 km/h, the Energy-Optimal Velocity Generation (EOVG) block uses vehicle internal and external data to calculate the optimal cruising velocity, v_{opt} , between 50 km/h and 80 km/h, for that point

in time.

Inside the EOVG block, there are four main parts. The first part is the parameter block, which accepts fixed and changing parameters from a variety of sources: vehicle internal sensors, external sensors, and optional connected data such as wind speed. These parameters are sent to the next set of blocks, LUTs and loss equations, which populate the equations derived in this study with the specific operating parameters and motor-inverter efficiency at that point in time. The result of the second part is a fully-specified equation summing all of the relevant vehicle losses as a function of motor speed, ω_{mot} , for the current state of the vehicle and the vehicle's environment (equation (11) below). The third part simply evaluates (11) at various values of ω_{mot} , since once a value of ω_{mot} is selected, the total loss is directly calculable using (11). The selection of ω_{mot} values to evaluate can be β evenly spaced velocities between v_{max} and v_{min} , where β is fixed to a reasonable value like 10 or 20 evaluation points, or can vary to achieve a fixed resolution, such as evaluating every 1 km/h or 2 km/h. Out of the β evaluation points, the vehicle velocity with the least losses per unit distance (J/m) is selected as v_{opt} . The fourth part calculates the near-optimal speed transition between the previous optimal speed and the new optimal speed, whenever internal or external parameters change to alter the optimal cruising speed. The resulting signal, v_{ref} , is then sent into the closed-loop vehicle speed controller as a reference speed, and the appropriate motor torque command is generated to achieve this vehicle velocity. The entire EOVG block would run on a loop, such as every 2 or 5 seconds, and/or be triggered when input parameters change.

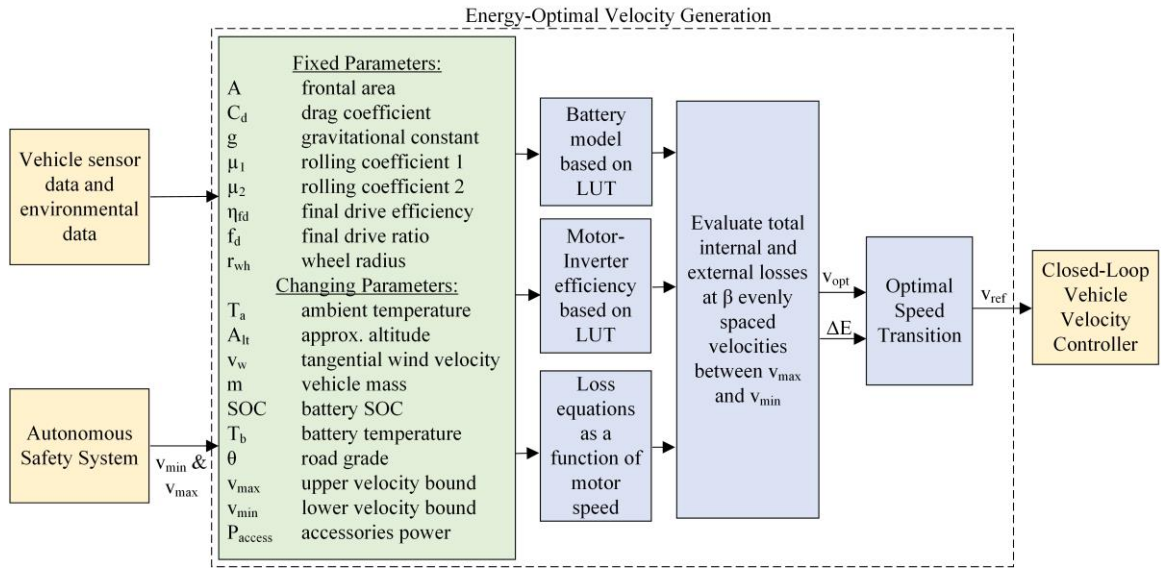


Figure 2-1 The proposed inner structure of EOVG block

2.2.2 Steady-State Loss Equations

The framework uses low-computations because it relies on well-known vehicle modeling equations that have been reduced into loss equations that only depend on motor speed. Thus, while the baseline equations are not new, the use of the final equation formulations to find the optimal cruising speed is unique. In order to consider the losses for a certain trip distance, and not for a certain trip driving time, the loss equations are formulated in units of J/m, instead of the more usual watts (J/s). It is a cornerstone of the proposed framework that the losses can be calculated simply for any vehicle cruising speed, and thus all loss equations are formatted as a function of motor speed, ω_{mot} .

External resisting forces against the vehicle are presented in (1)-(4). Equation (1) shows the aerodynamic drag, F_{aero} , where ρ is the air density, A is the vehicle effective frontal area, C_d is the drag coefficient, v_{chass} is the chassis speed (in m/s), and $v_{w,tangential}$ is the

tangential wind speed (defined as being in the same direction as the vehicle is driving). For operation in different regions, the GPS altitude measurement and the vehicle ambient temperature measurement can be used to accurately estimate the local air density. Equation (2) shows the rolling resistance, where F_{roll} is the rolling resistance force, m is vehicle mass, g is the gravitational constant, θ is the road grade in radians, and μ_1 and μ_2 are rolling resistance coefficients. The resisting force of grade, F_{grade} , is shown in (3). The wheel output force, F_{out_wh} , is shown in (4), where τ_{in_wh} is the input torque to the wheel and r_{wh} is the wheel radius in m. Equation (5) is Newton's second law of motion applied to (1)-(4), where the vehicle will have zero net force, F_{net} , applied for a constant cruising speed.

$$F_{aero} = \frac{1}{2} \rho A C_d (v_{chass} - v_{w,tangential})^2 \quad (1)$$

$$F_{roll} = mg \cos \theta (\mu_1 + \mu_2 v_{chass}) \quad (2)$$

$$F_{grade} = mg \sin \theta \quad (3)$$

$$F_{out_wh} = \frac{\tau_{in_wh}}{r_{wh}} - F_{roll} \quad (4)$$

$$F_{net} = F_{out_wh} - F_{aero} - F_{grade} = 0 \quad (5)$$

The connected wind data is optional, but if available, it would yield a more accurate result on a windy day. If desired, the vehicle communication system can be setup to obtain real-time wind data from weather service providers using an application programming interface (API). For example, in the U.S.A, the National Weather Service provides an API service that allows developers to access current and forecasted wind speed and direction (in degrees), as well as other weather data [30], for any specified location. This wind data can be obtained periodically over the course of a trip, perhaps at 1 or 5 minute intervals. Since

the direction of vehicle movement is known by the vehicle through GPS coordinates, the effective wind speed in the direction of vehicle movement, $v_{w,tangential}$, can be found based on (6), as shown in Figure 2-2.

$$V_{w,tangential} = V_w \cos(\phi) \quad (6)$$

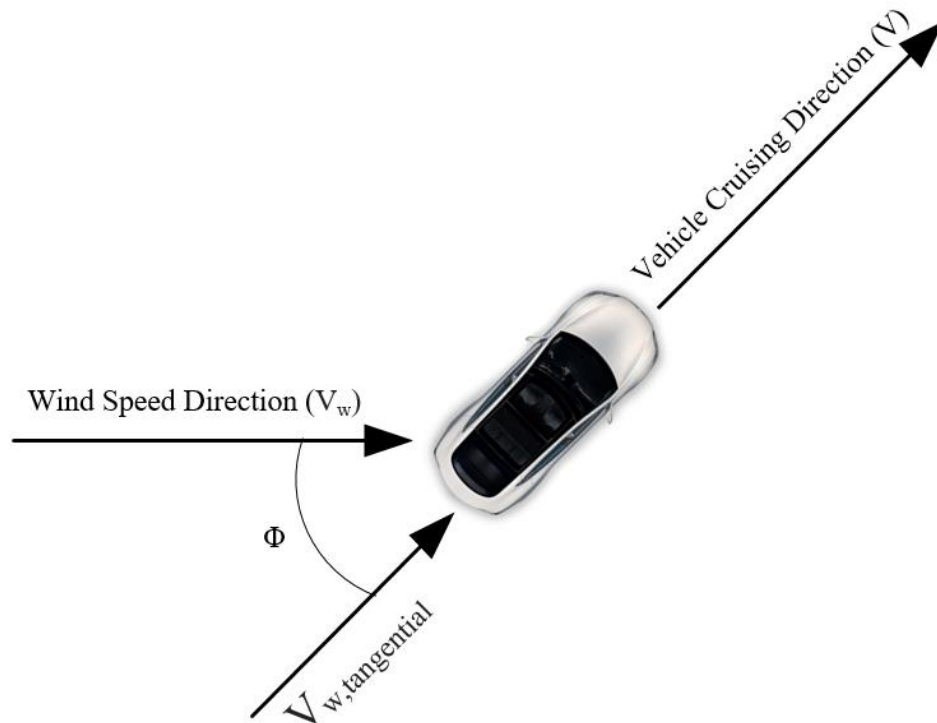


Figure 2-2 Wind in an arbitrary direction

The relationship among different parts of the vehicle is presented in (7) and (8). ω_{mot} is the motor speed, f_d is the final drive ratio, and ω_{wh} is wheel speed in rad/s. Equation (9) shows how the wheel torque is related to motor torque. Though final drive efficiency is often represented by a 2-D map dependent on speed and torque, this formulation simplifies it to a constant efficiency η_{fd} to increase the simplicity of the algorithm. This is a reasonable

approximation since a gear efficiency map is quite flat in the cruising speed areas, and only dips lower at low speed or low torque.

$$v_{chass} = \frac{\omega_{mot} r_{wh}}{f_d} \quad (7)$$

$$\omega_{wh} = \frac{\omega_{mot}}{f_d} \quad (8)$$

$$\tau_{in_wh} = \tau_{mot} f_d \eta_{fd} \quad (9)$$

An expression for motor torque is obtained using (1)-(9), as shown in (10). Equation (10) expresses the motor torque, τ_{mot} , as a function of ω_{mot} , which is crucial because it makes the search for the optimal vehicle speed one dimensional, based only on the selection of ω_{mot} .

$$\tau_{mot} = \frac{r_{wh}}{f_d \eta_{fd}} \left[mg \cos \theta (\mu_1 + \mu_2 \frac{\omega_{mot} r_{wh}}{f_d}) + \frac{1}{2} \rho A C_d (\frac{\omega_{mot} r_{wh}}{f_d} - v_{w,tangential})^2 + mg \sin \theta \right] \quad (10)$$

The summation of the vehicle losses is described by (11), where the *Total Loss* is the function to be minimized. These losses occur in the plant blocks of the vehicle model shown in Figure 2-3. These losses must all be given in J/m to minimize the losses for a certain trip distance. In the EOVG block, this function is tested at β evenly spaced options of v_{chass} between v_{min} and v_{max} . These v_{chass} options correlate to ω_{mot} using (7), where ω_{mot} is the actual parameter varied in (11). The calculations can run on a fast loop, which re-evaluates (11) when a parameter changes.

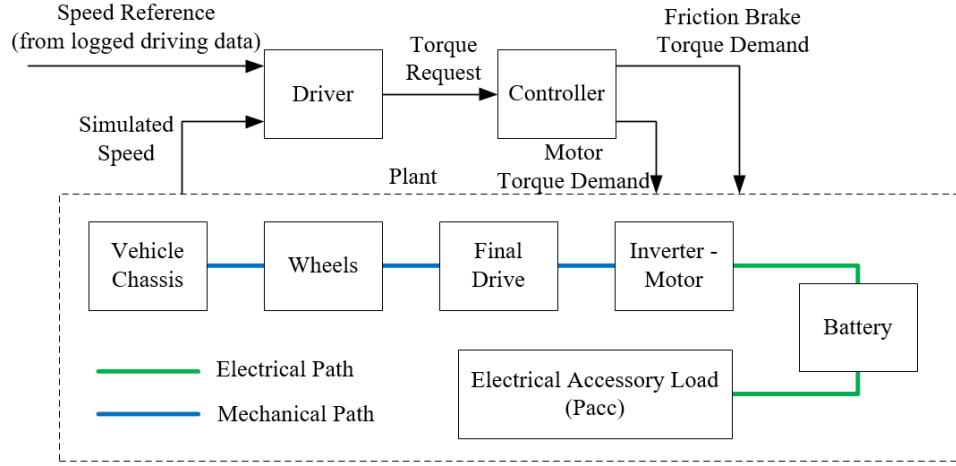


Figure 2-3 Block diagram of vehicle model

$$Total\ Loss = \left[\begin{array}{l} Aero\ Loss + Rolling\ Loss + \\ Grade\ Loss + Final\ Drive\ Loss + \\ Motor\ Inverter\ Loss + \\ Accessory\ Loss + Battery\ Loss \end{array} \right] \quad (11)$$

The motor and inverter loss can be combined into one LUT; hence, the total loss of the vehicle consists of seven speed-dependent losses that are considered to determine optimal cruising speed. The first three losses are the aerodynamic losses from (1), the rolling resistance losses from (2), and the grade losses from (3), which are all already expressed in J/m. The fourth loss is in the final drive as shown in (12). To convert this power (J/s) to J/m, P_{loss_fd} must be divided by the vehicle chassis speed, v_{chass} (from (7)). The result is shown in (13).

$$P_{loss_fd} = \omega_{mot} \tau_{mot} (1 - \eta_{fd}) \quad (12)$$

$$Final\ Drive\ Loss(J / m) = \frac{\tau_{mot} f_d (1 - \eta_{fd})}{r_{wh}} \quad (13)$$

The fifth loss is the combined motor and inverter loss, and a two-dimensional LUT (with ω_{mot} and τ_{mot} as inputs) is used to find the combined efficiency, η_{motinv} , at any ω_{mot} selected. Though the LUT is two-dimensional, this is reduced to a one-dimensional problem using (10) since τ_{mot} is dependent on ω_{mot} . Once this efficiency is determined, (14)-(15) calculate the total motor and inverter losses in J/m.

$$P_{loss_mot_inv} = \omega_{mot} \tau_{mot} (1 - \eta_{motinv}) \quad (14)$$

$$Motor\ Inverter\ Loss(J / m) = \frac{\tau_{mot} f_d (1 - \eta_{motinv})}{r_{wh}} \quad (15)$$

The sixth loss is expressed in (16) as the energy used by the electrical accessories, which can be large since autonomous vehicles can use multiple kilowatts of continuous power for sensing and computation [1]; also, if HVAC is set to high, it will add to this amount, meaning very high total accessory power draws are possible, which will affect the optimal cruising speed greatly. P_{acc} is the accessory power usage, which is measured by the vehicle.

$$Accessory\ Loss(J / m) = \frac{P_{acc} f_d}{\omega_{mot} r_{wh}} \quad (16)$$

The seventh loss is the battery loss, which is a function of SOC-dependent parameters such as battery resistance R_b , open-circuit voltage V_{oc} , and battery current I_b , where the positive direction of I_b is defined as leaving the battery. To make the solution tractable, R_b and V_{oc} are determined from one-dimensional LUTs based on battery SOC as the input. Terminal voltage is calculated in (17), which is used to show battery power in (18). Combining (17) and (18) yields (19).

$$V_{oc} - R_b I_b = V_{term} \quad (17)$$

$$P_b = V_{term} I_b \quad (18)$$

$$V_{oc} - R_b I_b = \frac{P_b}{I_b} \quad (19)$$

Battery power consumption, P_b , is comprised of both vehicle demand and accessory usage, which is shown in (20).

$$P_b = \frac{\omega_{mot} \tau_{mot}}{\eta_{mot_inv}} + P_{acc} \quad (20)$$

Equations (19) and (20) can be combined to generate (21), which describes the battery current as a function of ω_{mot} and P_{acc} . The lowest positive quadratic solution to (21) will give the correct battery current.

$$I_b = \frac{V_{oc} \pm \sqrt{V_{oc}^2 - 4R_b P_b}}{2R_b} \quad (21)$$

Once battery current is determined, battery loss power is calculated in (22), and is converted to energy per distance using (23). By using the battery current calculated in (21), battery loss can be calculated as (24), which is given in J/m.

$$P_{loss_batt} = R_b I_b^2 \quad (22)$$

$$E_{loss_batt} (J / m) = \frac{P_{loss_batt}}{v_{chass}} \quad (23)$$

$$Battery\ Loss(J / m) = \frac{I_b^2 R_b f_d}{\omega_{mot} r_{wh}} \quad (24)$$

The battery state-of-health (SOH) over time can also be considered if the vehicle has an on-board SOH estimation algorithm. Internal battery resistance, R_b , is the main SOH-dependent parameter that will affect battery loss. Thus, if an SOH algorithm is available, it's estimated R_b for the given SOC can be used, rather than the battery beginning-of-life

R_b value.

Equations (1) to (24) describe the proposed framework and require specific parameters that are unique to each vehicle. In this study, these parameters are estimated based on models validated to logged driving data for three vehicles. In a real implementation, these parameters, such as vehicle frontal area, drag coefficient, wheel radius, motor/inverter efficiency map, final drive efficiency, etc., will be known by the vehicle manufacturer and thus easily programmable.

2.2.3 Optimal Speed Transition Determination

Though constant cruising speed is the main focus of the algorithm, the optimal cruising speed will change as vehicle and/or environmental parameters change during the drive. Thus, to complete the framework, this section proposes a real-time low-computational method to find near-optimal transition rates between optimal speeds. Previous work has tackled this transient speed rate problem offline using dynamic programming (DP) [23]. The proposed method is to use offline dynamic programming to find parameters for the proposed equation, and then use this vehicle-specific equation for the real-time implementation. Thus, a DP algorithm is created to (i) fit the parameters in the proposed equation and (ii) validate the overall energy use including speed transitions of the proposed algorithm compared to the optimal DP results (Section IV-C).

When the optimal cruising speed changes, the new optimal speed may be higher or lower than the original optimal speed. When the new optimal speed is lower, and the vehicle should slow down, the optimal transition will be the one that moves to the new optimal

speed as quickly as possible but does not generate any additional losses in any powertrain components. Whenever regenerative braking occurs, one portion of the kinetic energy of the vehicle is transferred back to the battery and the other portion is lost in the pathway to the battery (final drive, motor/inverter, battery internal resistance). Thus, the optimal braking transition is to set the motor torque to zero (similar to the driver taking their foot off the gas pedal), and let the aerodynamic and rolling resistance forces slow the vehicle down to the new optimal speed, so that no additional losses are generated in the powertrain components. Thus, the proposed algorithm focuses only on finding the optimal acceleration transition rate.

The DP algorithm is set up with a fixed acceleration distance (60 m) divided into four equal segments, where each segment can have a different constant acceleration rate. The fixed distance of 60 m is chosen based on the average acceleration distance found in the Tesla Model S logged data. Other distances can be used, but the resulting coefficients below will be different. In each segment, one of six acceleration rates is possible, ranging from zero acceleration to the upper limit of 4.5 m/s^2 , which is recommended in [31] as an upper comfort limit for the driver. Or, a lower limit such as 2 m/s^2 can be used for even better driver comfort. For a single test case, the offline DP algorithm searches all of the resulting 56 acceptable combinations (either positive or zero acceleration in each segment) by running the validated vehicle model on the 56 unique acceleration profiles, and then calculating the energy usage of each profile. For example, Figure 2-4 shows four of the 56 results for the test case of the optimal speed changing from 75 km/h to 80 km/h. Figure 2-5 shows the same for a different test case, where the optimal speed changes from 50 km/h

to 80 km/h.

Twenty-one different test cases are considered (original optimal speeds to new optimal speeds) that cover various values for vehicle mass, wind, accessory power use, etc., in order to represent the full case of possible scenarios. It is found that often, the optimal acceleration profile is equal or close to a constant acceleration rate, and this rate varies based on the change in energy consumption at the original and new optimal speed, ΔE , and the vehicle starting speed, V_{orig} . Also, as expected, it is found that it is always better to start accelerating as soon as the optimal speed changes, rather than to stay at the original optimal speed any longer. Based on these findings, (25) is proposed to calculate the near-optimal constant acceleration rate, a_{opt} , in real time, which is a fifth order equation of ΔE and V_{orig} . The weighting coefficients, α_i and γ_i , are found offline using the DP results across the 21 test cases – thus, these weighting coefficients will change vehicle-to-vehicle. For example, for the Chevrolet Spark EV, the curve-fitted weighting coefficients are found to be $\alpha_1=16.2604$, $\alpha_2=0.0045$, $\alpha_3=0.0135$, $\alpha_4=0.0499$, $\alpha_5=0.2184$, $\gamma_1=6.81 \times 10^{-5}$, $\gamma_2=-2.75 \times 10^{-5}$, $\gamma_3=-2.48 \times 10^{-5}$, $\gamma_4=8.92 \times 10^{-7}$, $\gamma_5=-6.91 \times 10^{-9}$.

$$a_{opt} = \sum_{i=1}^5 (\alpha_i \Delta E^i + \gamma_i V_{orig}^i) \quad (25)$$

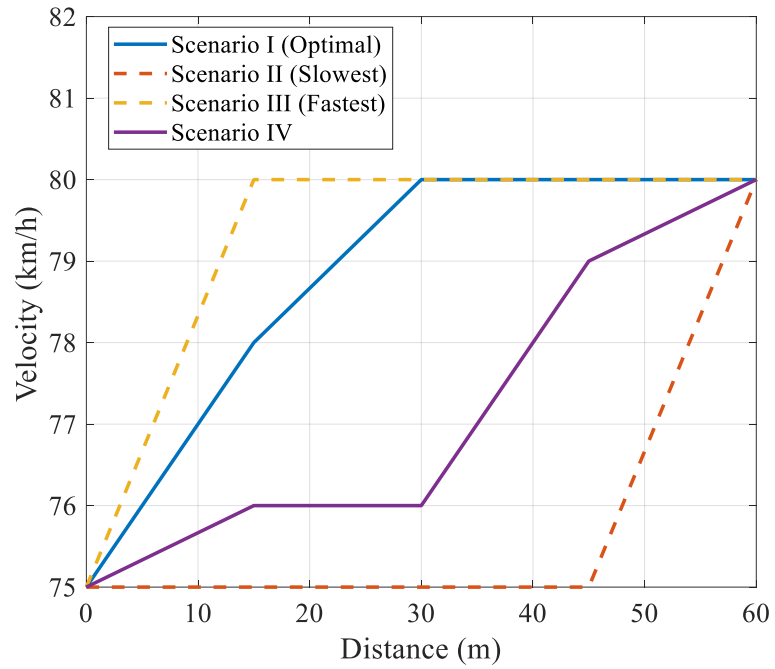


Figure 2-4 Acceleration trajectory in distance domain from 75km/h to 80km/h

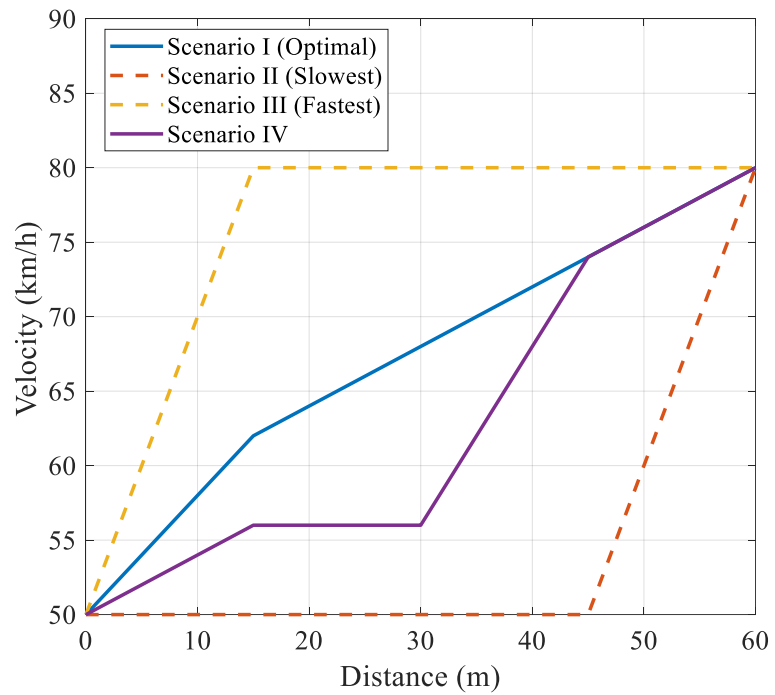


Figure 2-5 Acceleration trajectory in distance domain from 50km/h to 80km/h

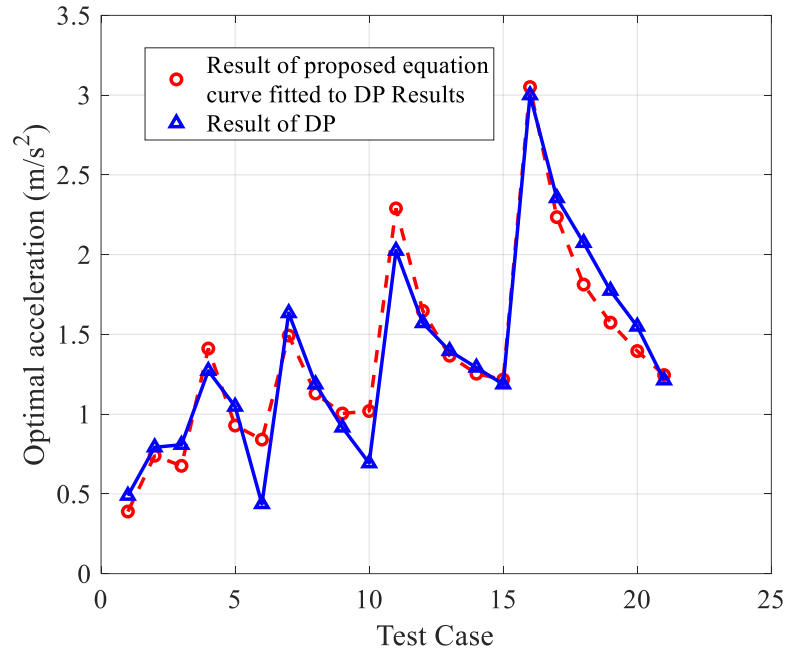


Figure 2-6 Acceleration results from DP analysis and proposed equation

Figure 2-6 compares the determined acceleration rates from (25) for the 21 test cases to the optimal acceleration rates from the offline DP algorithm which relies on running the vehicle model to calculate energy consumption during accelerations. The results show that (25) can closely match the DP results. The simulation results in Section IV-C quantify the small error that results in the difference between the rate found by (25) (red) and the DP optimal rate (blue).

2.3 Vehicle Model Creation and Validation

Using logged driving data, dynamic models for three different vehicles were created in MATLAB/Simulink: Chevrolet Bolt EV, Chevrolet Spark EV, and Tesla Model S with 85kWh battery. Selected vehicle parameters are shown in Table 2-1. The Bolt and Model S driving data were obtained from real-world driving in the Toronto, Canada area.

The Spark EV data is obtained from dynamometer testing [32]. Three logged cycles for each vehicle are used to validate the accuracy of the models. The goal is to compare cruising energy use between the validated models and the proposed framework, to show the accuracy of the proposed equations for calculating optimal cruising speed.

Table 2-1 Baseline Values of Vehicle Parameters

	Mass m_c (kg)	C_d	Frontal Area (m^2)	Battery Size (kWh)	Wheel Radius (mm)
Model S	2108	0.24	2.43	85	352
Bolt	1616	0.32	2.41	60	292
Spark EV	1300	0.35	1.90	20	324

The top-level block diagram of the vehicle models is shown in Figure 2-3. In this structure, a PI feedback loop represents the driver behavior; there is a logged speed reference from the drive cycle feeding into this loop as the reference speed, and considering the current simulated speed, the driver requests motor/brake torque to follow the speed profile as closely as possible. In the controller block, the requested torque is an input and the controller generates the motor torque demand or brake torque demand subject to limitations of the vehicle components. In the plant model, the next simulated speed sample is calculated using the force applied to the wheels and resisting forces, as shown in (26).

$$v_{chas}(t+1) = v_{chas}(t) + \left(\frac{1}{m} \int_t^{t+1} \left(F_{out_wh} - \frac{1}{2} \rho A C_d v_{chas}^2(t) dt \right) \right) \quad (26)$$

In (26), m is the vehicle mass in kg, ρ is the air density, A is the vehicle frontal area in m^2 , and C_d is the coefficient of drag. The force out of the wheel block is calculated from the torque into the wheel block, the friction braking torque, and the rolling resistance losses, as shown in (4).

With inputs of motor speed and motor torque, the motor/inverter block calculates the DC input current required from the battery using (27).

$$I_{in_motor} = \frac{\omega_{mot} \tau_{mot} \times \eta_{motinv}(\omega_{mot}, \tau_{mot})}{V_{term}} \quad (27)$$

The total battery current (I_b) is the sum of the required motor current (I_{in_motor}) and the required electrical accessory current, as shown in (28).

$$I_b = I_{in_motor} + \frac{P_{access}}{V_{term}} \quad (28)$$

The battery model uses the battery current and an initial SOC value to determine the SOC and battery terminal voltage at the next simulation step. The SOC at the next simulation step is the integral of the battery current divided by the total battery capacity (C_{batt}), as shown in (29). The same R_b -SOC and V_{oc} -SOC LUTs are used in the Simulink models as are used in the equations of the proposed algorithm.

$$SOC(t+1) = SOC(t) + \frac{1}{C_{batt}} \int_t^{t+1} -I_b dt \quad (29)$$

For creating the vehicle models, the main available logged signals are: time and date of trip, battery voltage, battery current, battery SOC, vehicle speed, outside ambient temperature, altitude (for real-world driving of Bolt and Model S), and grade (for dynamometer testing of Spark EV). For the Bolt, air conditioning power and heater power data are also logged. In the model, tire rolling resistance is estimated as $\mu_1 = 0.008$ and $\mu_2 = 0.00012$ for driving on dry asphalt, based on Autonomie approximations from Argonne National Laboratory [33]. The final drive efficiency is represented by a 2-D lookup table based on torque and speed, which was obtained for the *Aisin AW AF33 5-Speed*

Transmission from [33]. For the motor/inverter efficiency, multiple sources are used. For the Chevrolet Spark EV, the combined motor-inverter efficiency map of the Toyota Prius [34] is used as a baseline, and the torque and speed indices are scaled according to the specific size of the Spark motor. For the Chevrolet Bolt, the motor efficiency map is available in [35]. This is combined with a scaled version of the Toyota Prius inverter efficiency map [34] to create a combined motor-inverter efficiency map based on motor torque and speed. Since there was no specific data available for the Tesla Model S motor, the created motor-inverter efficiency map for the Bolt is scaled according to the maximum torque and speed of the Tesla Model S motor. The logged heater power of the Bolt can reach 8 kW, thus the maximum accessory power considered is 11 kW, including the autonomous vehicle continuous load.

Considering the real implementation of the proposed framework, the tire rolling resistance and vehicle mass would not be known by the manufacturer for future drives. For example, winter tires may be installed and cargo load can change. One suggested approach is to always use the original estimate of stock tires on the most common road surface, asphalt, and curb mass plus one passenger. This approach is shown to be reasonable by a sensitivity analysis in Section IV-B. Another approach is to perform online parameter estimation [36]-[39].

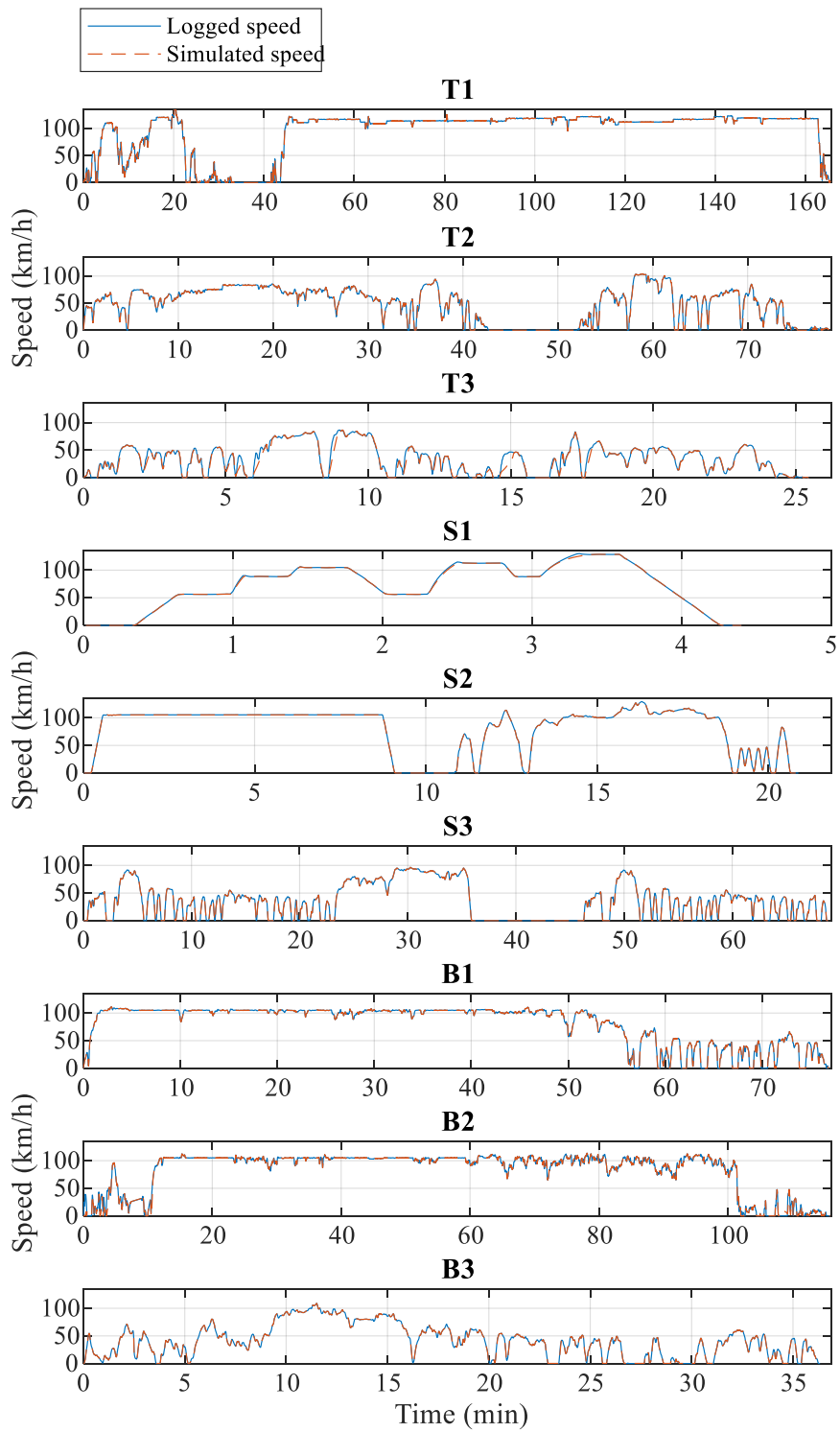


Figure 2-7 Scheduled and simulated speed profile for nine test cycles

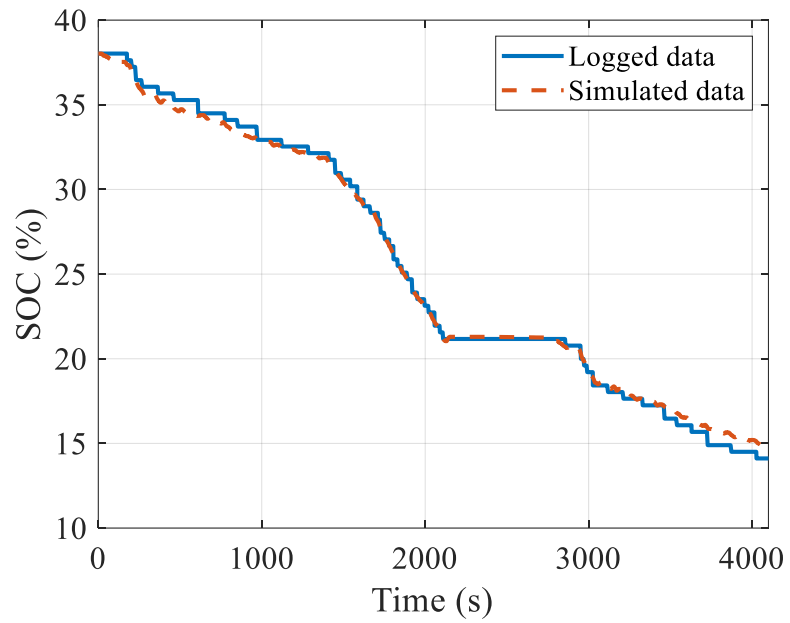


Figure 2-8 Simulated battery SOC vs logged SOC of Spark EV (S3 cycle)

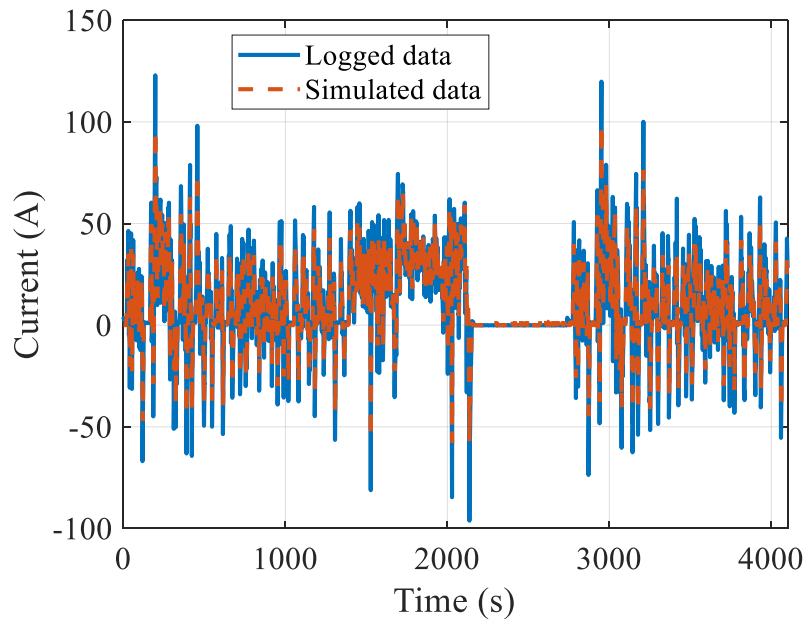


Figure 2-9 Simulated battery current vs logged current of Spark EV (S3 cycle)

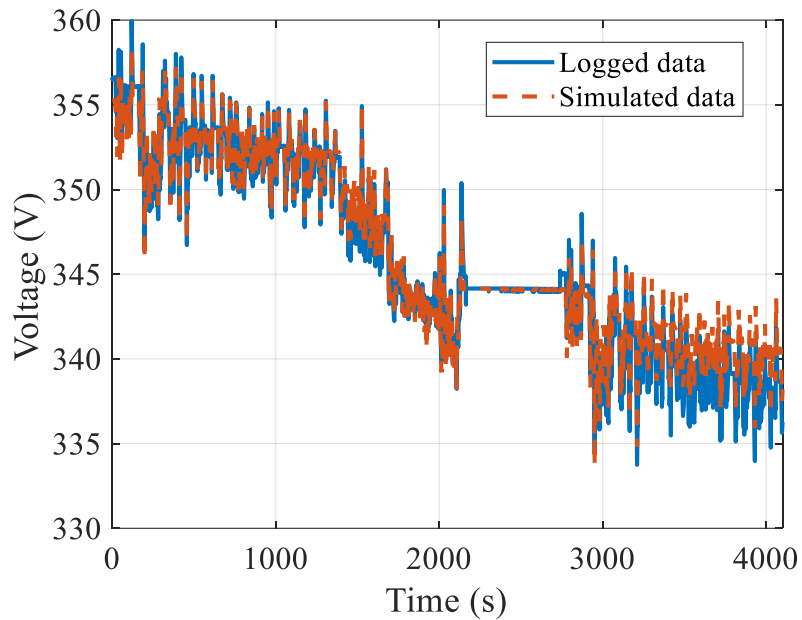


Figure 2-10 Simulated battery voltage vs logged voltage of Spark EV (S3 cycle)

Logged speed data and simulated speed data for three drive cycles for each of the three vehicles are shown in Figure 2-7. The cycles are labeled as “T#” for Tesla cycles, “S#” for Spark EV cycles, and “B#” for Bolt cycles. Figs. 2-8 to 2-10 shows the validation plots for the Spark EV. The results show that the created models have very similar behavior to the actual logged vehicles. Figure 2-8 shows that the simulated Spark EV has an ending SOC value within 1% of the logged data. When the simulated battery voltage follows the logged voltage data well, as shown in Figure 2-10, it means that the R_b -SOC LUT data points are well determined for the battery model, since the R_b value at any point in time determines the voltage rise or drop at the battery terminal voltage from the OCV. Table 2-2 compares the simulated vehicle energy consumption to the logged energy consumption for each of the nine validation trips. The results show that all models are within 5% of real

energy use, which is quite close considering some driving factors were unknown (e.g., wind and mass).

Table 2-2 Vehicle Model Energy Usage Validation

Vehicle Model	Cycle	Logged Energy (kWh/cycle)	Simulated Energy (kWh/cycle)	Error (%)
Tesla Model S	T1	22.95	23.17	0.97
	T2	21.29	21.99	3.30
	T3	41.16	40.40	-1.85
Chevrolet Bolt EV	B1	20.77	20.11	-3.14
	B2	19.95	20.94	4.48
	B3	15.81	15.99	1.13
Chevrolet Spark EV	S1	41.39	39.53	-4.48
	S2	14.63	15.19	3.85
	S3	10.57	10.21	-3.43

2.4 Simulation Results

2.4.1 Steady-State Optimal Cruising Speed

The related prior work [29] showed that wind speed, road grade, and accessory power usage are the most influential factors for determining optimal cruising speed, based on the Spark EV vehicle parameters. However, the consideration of all relevant variables, as shown in (11), is important as the less significant factors, such as vehicle mass and ambient temperature, are still useful for fine-tuning the optimal speed. To expand the investigation, this section studies the effects of all factors for the three vehicles analyzed, and considers even higher accessory load values, up to 11 kW. Since a high accessory load significantly moves the optimal speed to higher speeds to reduce the travel time for a fixed trip distance, it is important to consider the impact of these high accessory loads.

Figure 2-11 shows the calculated vehicle energy consumption, using the proposed algorithm, for each vehicle across a range of speeds when the accessory power is set to 3 kW, 7 kW, and 11 kW. The baseline values for other parameters are as shown in Table 2-3. The energy consumption is calculated using (11), because the sum of all losses equals the total energy consumption for a cruising state. The results show that, as expected, optimal speeds are higher when accessory power is higher, so as to shorten the trip time. Also, when comparing the three vehicles at a constant accessory power, such as 11 kW (blue traces), it is clear that the specific vehicle parameters of each EV model have a large influence on the optimal speed. For example, when $P_{acc} = 11$ kW, the Spark EV has an optimal speed of 80 km/h whereas the Model S has an optimal speed of 71.2 km/h and the Bolt has an optimal speed of 68.7 km/h. When comparing within the same vehicle type, say the Model S (solid lines), it is clear that significant energy savings can be realized by following the optimal speed. For example, if $P_{acc} = 11$ kW, and the Model S is cruising at 50 km/h instead of the optimal 71.2 km/h, the vehicle energy consumption will be 38.8 kWh/100km instead of the optimal 35.6 kWh/100km, an 8.9% increase. Tesla Model S energy consumption is higher than that of the other vehicles during cruising mainly due to its higher mass compared to the other vehicles studied.

Figure 2-12 shows the optimal velocity selection for the vehicles at three different wind speeds. The baseline values for other parameters are given in Table 2-3. Using (11), the total energy usage for each vehicle is calculated. When the wind speed is in the same direction as vehicle cruising, it pushes the optimal speed to higher values, while an opposing wind direction lowers the optimal speed. The optimal speed for different vehicles

are different for the same condition. For example, when wind speed is 20 km/h, the optimal speed for the Spark EV and Bolt EV is 62.5 km/h, and for the Model S it is 60 km/h. In this case, the Spark EV cruising at 50 km/h instead of the optimal 62.5 km/h yields 3.95% higher energy usage.

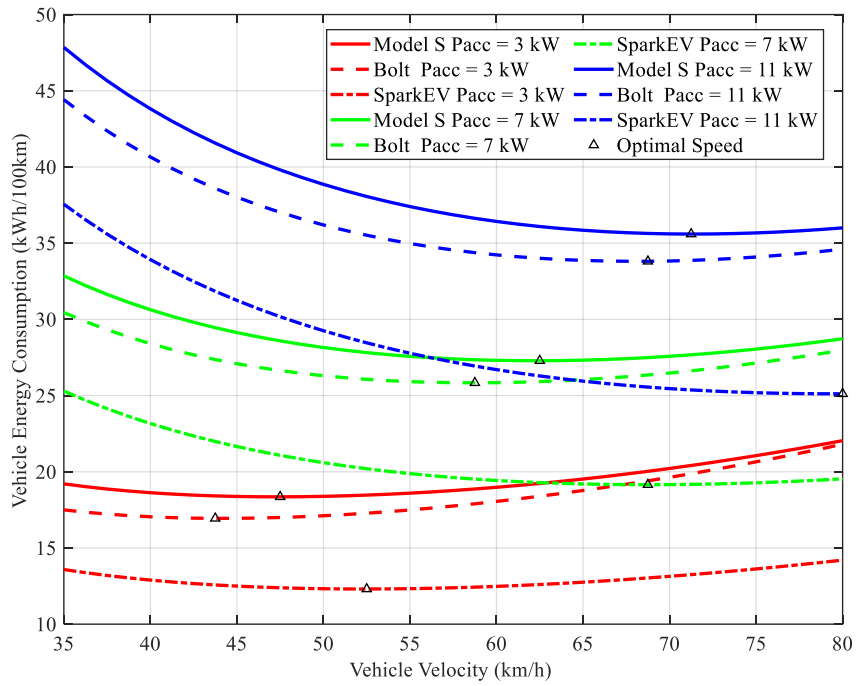


Figure 2-11 Vehicle energy consumption for different accessory usage levels

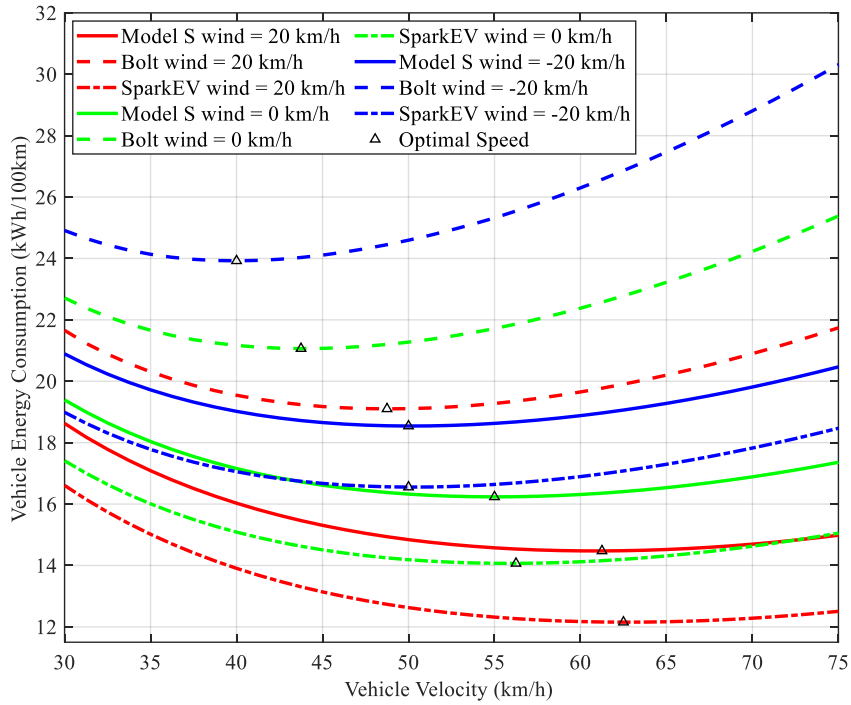


Figure 2-12 Vehicle energy consumption for different wind speeds

Table 2-3 Baseline Values of Vehicle Parameters for Test Cases

	Mass (kg)	SOC (%)	Wind speed (km/h)	Grade (%)	Temp (°C)	P _{acc} (kW)
P _{acc} changing	Curb mass + 80	50	0	0	25	Changing
Wind speed changing	Curb mass + 80	50	Changing	0	25	4

In addition to varying one parameter at a time, it is useful to consider a set of realistic test cases, as shown in Table 2-4. The minimum accessory power is set to 2 kW in Case 1 as the very lower potential limit of autonomous power needs with no HVAC load. Numerous additional parameters are varied in the cases, including different road grades, battery SOCs, vehicle mass (where m_c is the curb mass of the vehicle and the additional 400 kg represents a vehicle loaded with multiple passengers or cargo). The six

cases are used as a base for validating the proposed equation-based algorithm to the dynamic MATLAB/Simulink vehicle models, which themselves have been validated to actual driving data, as per Table 2-2. The goal is to connect the accuracy of the proposed equations back to real driving data, using the verified vehicle models as an intermediate link.

Table 2-4 Test Case Specifications

	P_{acc} (kw)	Mass (kg)	Wind speed (km/h)	Grade (%)	SOC (%)	Temp (°C)
Case 1	2	m_c	-10	0	60	20
Case 2	4	m_c+400	-20	0	70	20
Case 3	4	m_c	0	-1	90	15
Case 4	8	$m_c +400$	0	+1	80	30
Case 5	8	m_c	+10	0	80	-10
Case 6	11	$m_c +400$	+15	0	55	-20

Figure 2-13 shows the results for different cases of the Tesla Model S. Figure 2-13 shows that in varying conditions, optimal speed choice can change over a large interval. For example, in Case 4, the energy usage can change by 5.5% between driving at the optimal speed (70 km/h) and 50 km/h. A comparison of the “Equation” (solid) and “Model” (dashed) lines shows that the equation-based algorithm is extremely accurate in energy prediction when compared to the full dynamic Simulink-based vehicle model. This conclusion holds for the Model S, as well as for the Bolt and Spark EV as shown in Figure 2-14 and 2-15, respectively. Figure 2-14 presents the energy consumption for the Chevrolet Bolt EV for the six cases. Optimal cruising speed selection can have a vast range depending on the internal and external vehicle conditions. For example, in Case 2, choosing optimal speed (48 km/h) over a higher speed such as 70 km/h can save 8.7% of battery energy. The energy usage results of the Chevrolet Spark EV are shown in Figure 2-15. Note that for

high accessory power usage (Case 6), optimal speed is 81.6 km/h. In this particular case cruising at 50 km/h instead of the optimal speed can result in 18.4% higher energy consumption.

The optimal speed choice for all the vehicles in different study cases are summarized in Figure 2-16. It can be seen that the behavior of changes in different cases is similar for all vehicles; nevertheless, the value of the optimal velocity is different for each vehicle even in the same case, which shows that internal parameters of the vehicles are as important as the environmental factors. Specifically, this study has uniquely proven that the high accessory power loss expected in fully autonomous vehicles will have a large effect on optimal speed selection and will generally make the optimal cruising speed higher than for that of a non-autonomous vehicle with lower accessory power losses. For example, from low accessory power use to high ($P_{acc} = 3\text{kW}$ to 11kW) in the Tesla Model S, with other parameters constant, v_{opt} can change from 47.5 km/h to 71.2 km/h.

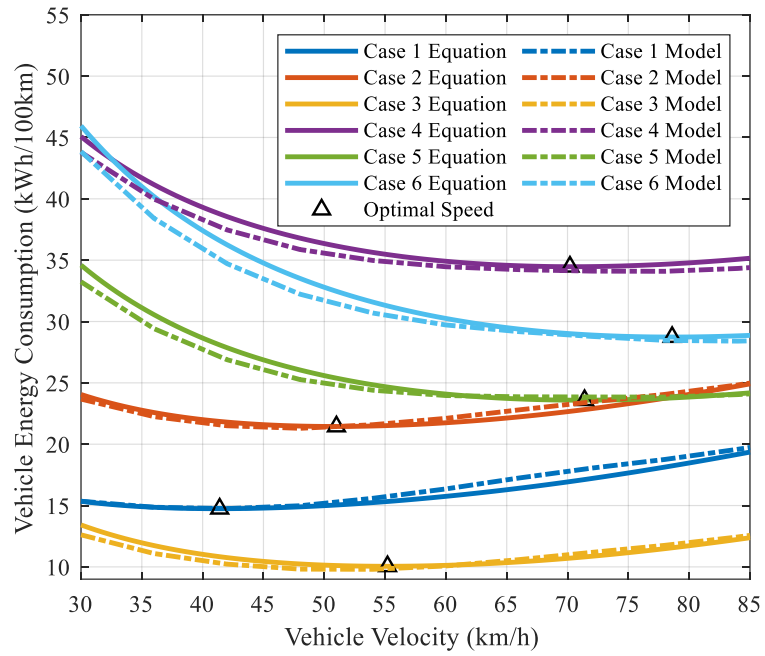


Figure 2-13 Equation validation using energy consumption of Tesla Model S

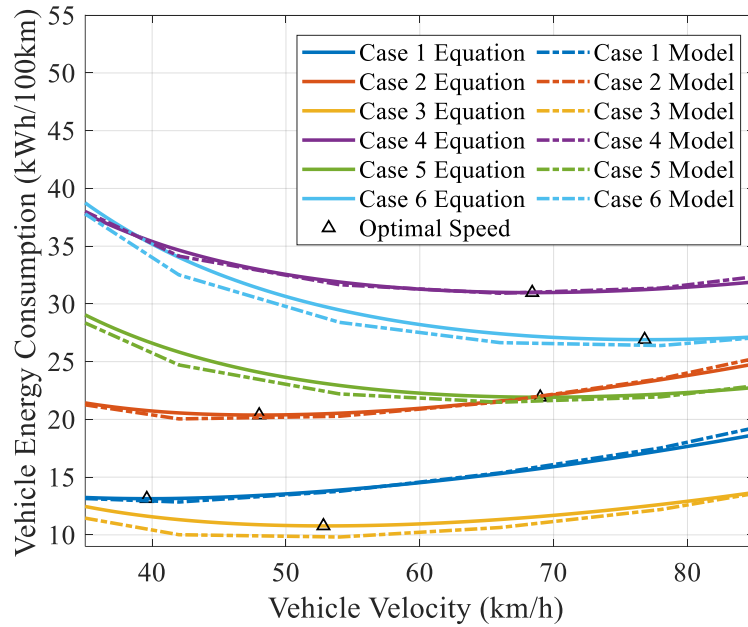


Figure 2-14 Equation validation using energy consumption of Chevrolet Bolt

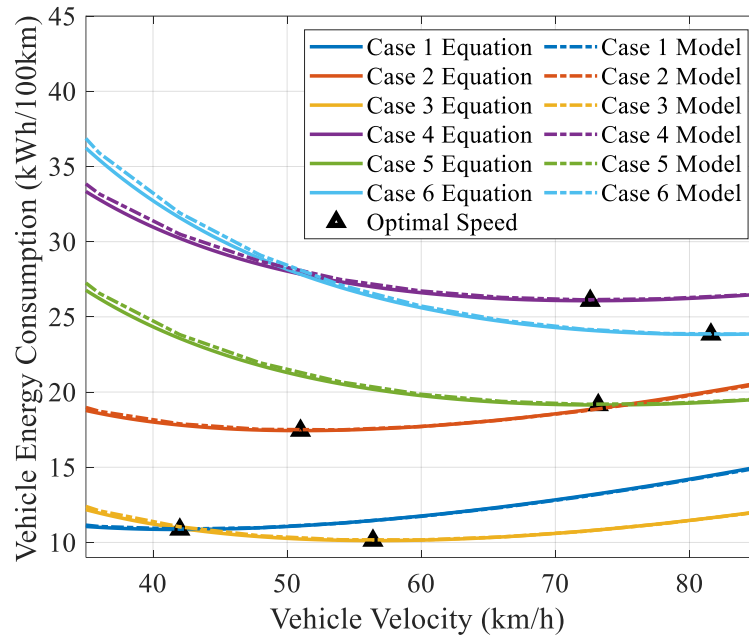


Figure 2-15 Equation validation using energy consumption of Chevrolet Spark EV

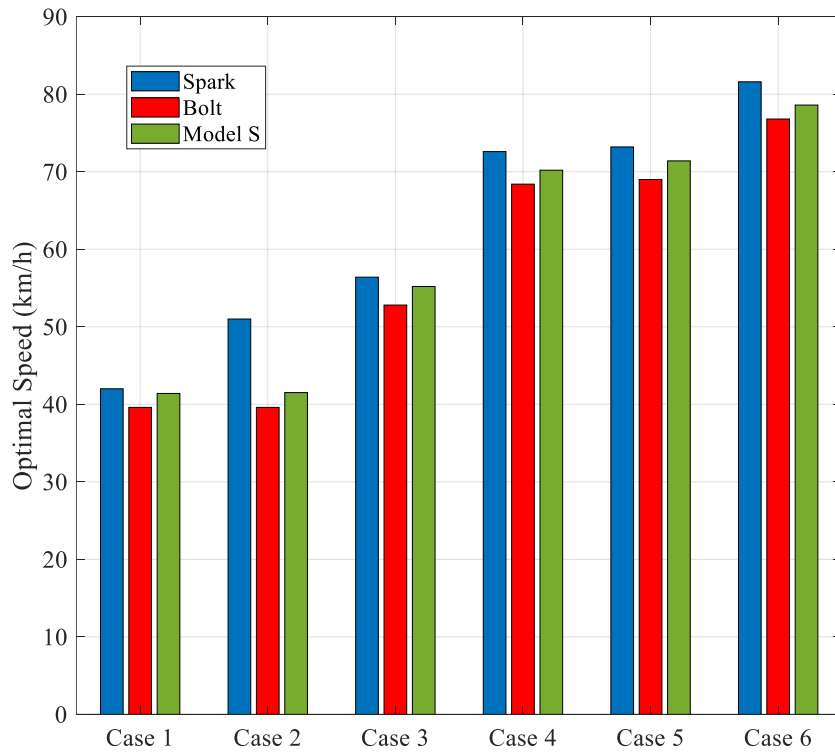


Figure 2-16 Optimal speed in different study cases

2.4.2 Steady-State Cruising Speed Sensitivity Analysis

The vehicle manufacturer will have detailed data for the powertrain components for use in the proposed framework, but vehicle mass and rolling resistance may change frequently in an unknown manner. Thus, it is important to study the effects that can these factors have on the optimal speed selection. Figure 2-17 shows vehicle energy consumption curves for the six cases described in Table 2-4 for both the scenario of the vehicle mass being curb mass + 100 kg and curb mass + 600 kg. Although the vehicle mass does make a significant change in the energy consumption, the optimal speed changes only slightly because losses due to vehicle mass are not highly speed-dependent, i.e., the loss curve maintains a very similar shape for different masses.

Figure 2-18 shows a similar study of changing rolling resistance, where standard values are $\mu_1 = 0.008$ and $\mu_2 = 0.00012$, and 20% higher values are compared. Similar to the mass study, the results show that the energy use curve shape does not change significantly, and thus small changes in rolling resistance will not greatly affect the optimal cruising speed. Figure 2-19 summarizes these results, which show that these two parameters have only a small effect on optimal cruising speed, meaning approximation or online parameter estimation may be used to determine them in the proposed framework. This result can be understood by the fact that rolling resistance losses (either from higher vehicle mass or higher resistance coefficients) do not change significantly with speed, in contrast to losses that are highly speed-dependent, such as wind and accessory losses.

2.4.3 Optimal Speed Transition

While in some cruising cases, parameters may not change for a large portion of the drive, the proposed method for determining optimal dynamic speed transition between an old optimal speed and a new optimal speed is best tested on the case of quickly changing parameters – otherwise, the cruising speed energy use would overshadow any differences in energy use

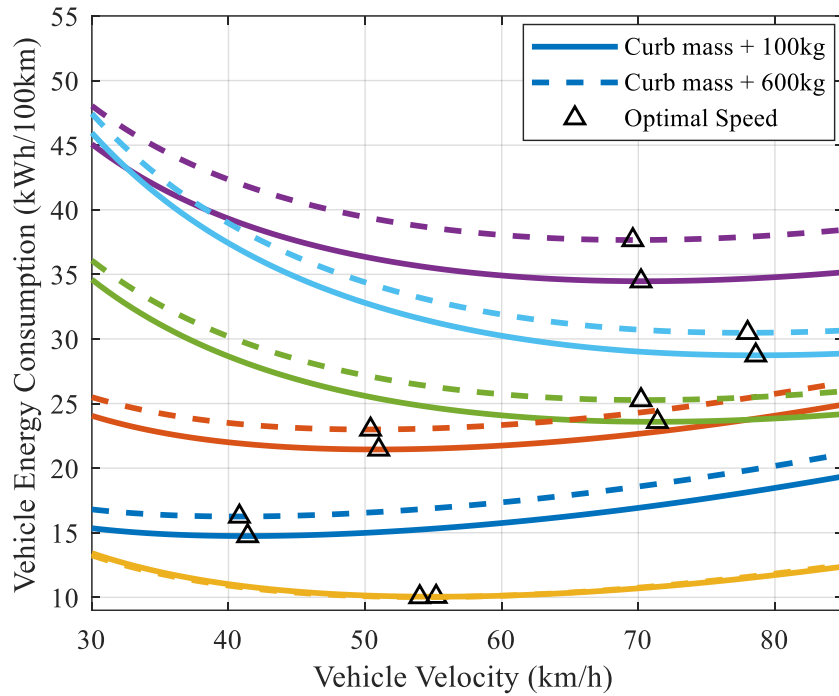


Figure 2-17 Energy usage with curbside mass +100 kg and + 600kg for Cases 1-6

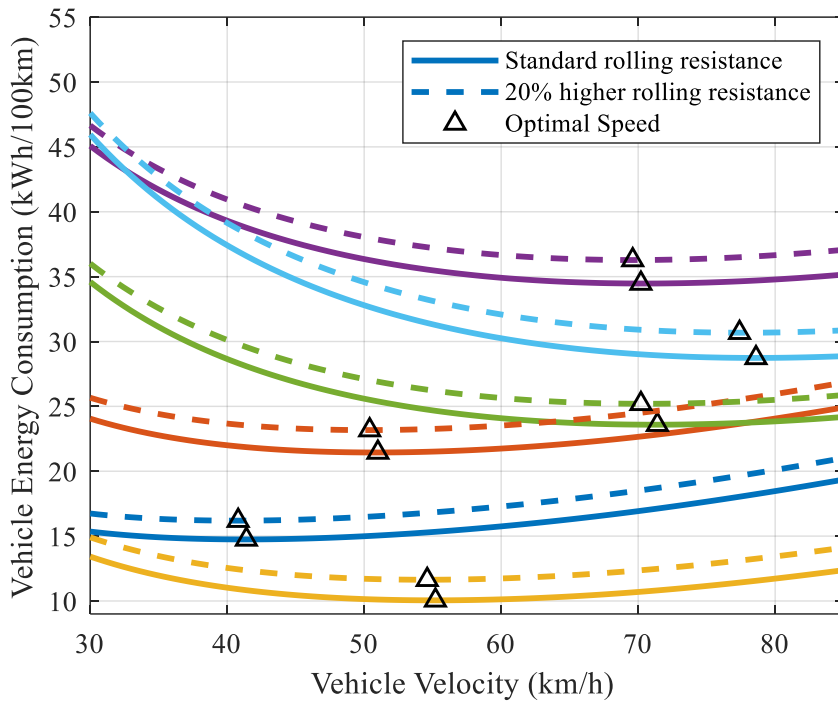


Figure 2-18 Energy usage with standard rolling resistance and 20% higher values for Cases 1-6

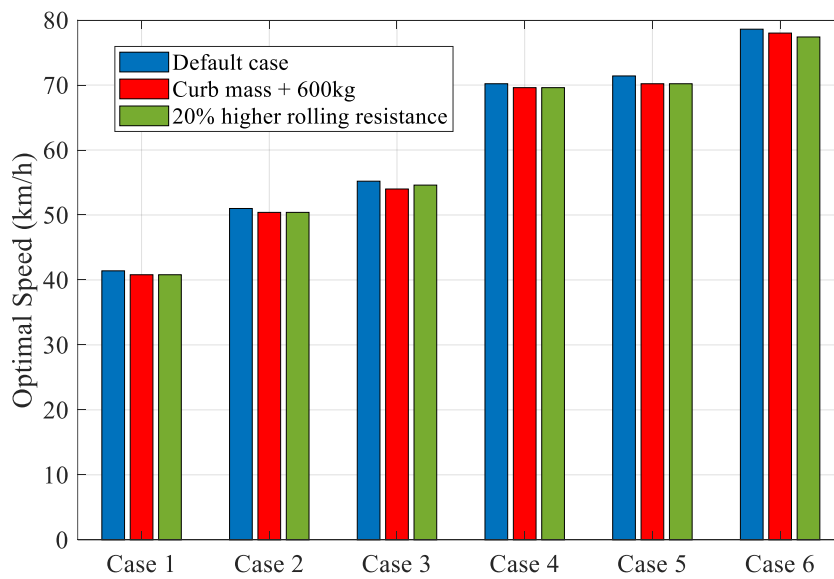


Figure 2-19 Sensitivity analysis of optimal speed selection

during speed transitions. Thus, a test case has been formulated where three changes occur in the environment and/or vehicle over a 2 km distance to simulate the performance of the optimal speed transition algorithm. Each new optimal speed is calculated from the steady state loss calculations and the speed rate change is set according to (25) with the DP-fitted α and γ parameters. Figure 2-20 shows the resulting speed compared to the optimal offline DP results and Figure 2-21 shows the resulting battery SOC compared to the optimal offline DP results. The proposed constant rate acceleration in (25) results in a 0.45% higher energy use compared to the ideal offline-calculated DP speed transitions over the 2 km test case. These results show that the proposed fast online approximation of the optimal speed transition is very close to the performance of the computationally-expensive offline DP method.

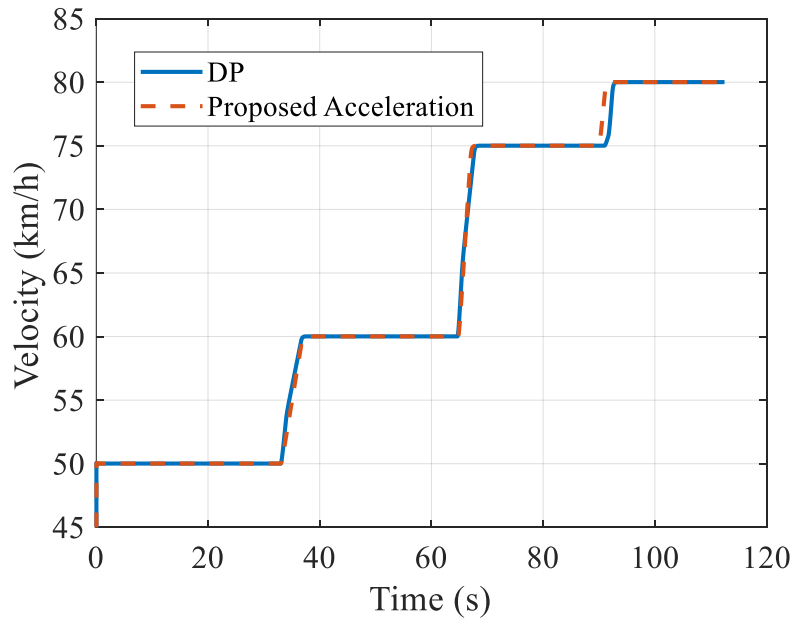


Figure 2-20 Velocity trajectory in the time domain

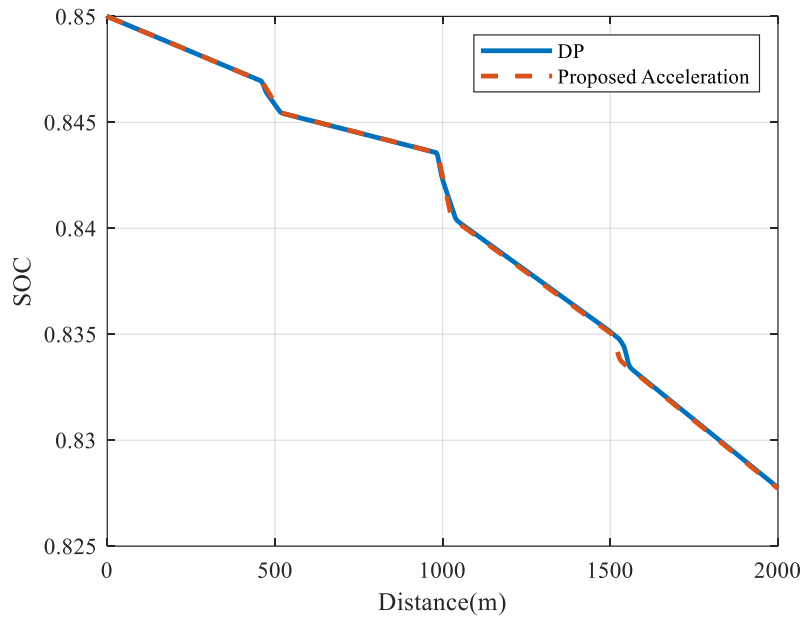


Figure 2-21 SOC comparison between DP and suggested trajectory

2.5 Flexible Implementation Option

The main proposed algorithm is ideal for optimizing cruising speed for minimal energy usage between the allowable v_{min} and v_{max} at any instant in time. The algorithm offers two main benefits to the driver: (i) reduced charging costs due to lowered energy use, and (ii) higher driving range due to lowered energy use. At times, the driver may prefer to cruise at the lowest-energy speed to maximize these benefits, and at other times, trip time may be the most important factor. This section presents a flexible implementation option based on energy usage that allows the driver to stay close to energy optimal, but decrease the trip time if needed. This energy-based approach allows the driver to stay within a selected energy use percentage of the optimal speed energy use. This is a straightforward way to encompass the effect on both charging costs and electric range. For

example, if the driver specifies to stay within 5% of optimal energy use, they are accepting 5% higher charging costs and 5% lower driving range.

Since the proposed algorithm calculates energy use curves at β test points between allowable v_{min} and v_{max} , the algorithm innately finds the relationship between increased energy usage and higher speeds that may be desirable for some drivers at some times. The main concept of the proposed energy-based approach is to limit the selected driven speed to a percentage of energy over the energy use at the optimal speed. Having the calculated energy use curve is insightful here, because for a certain percentage more energy consumption, α , the vehicle may be able to drive much faster for only a small increase in energy if the energy use curve is relatively flat to the right of the optimal point. If $E(v_{opt})$ is the energy use (in kWh/100km) of the vehicle cruising at v_{opt} , then the new energy use limit, E_{lim} , is calculated by (30).

$$E_{lim} = (1 + \alpha) \times E(v_{opt}) \quad (30)$$

Then, the selected vehicle speed, v_{sel} , is chosen from the β already-calculated points on the curve to select the vehicle velocity that correlates to the energy use closest to, but not over, E_{lim} . This concept is illustrated in Figure 2-22, which shows energy usage curves for two arbitrary cases, X and Y, and α values of 1%, 10%, and 20%. For Case Y, the curve is relatively flat to the right of the optimal point. If the energy use is limited to 1% over optimal, v_{sel} is 88km/h. However, for Case X, the curve increases to much higher values at high speeds, and thus even a 10% increase in energy use would make v_{sel} equal to 70 km/h. It is proposed that the α parameter is user-definable by the driver, and could be set once

based on the driver's general preference, or could be set for each trip based on the driver's needs at that time.

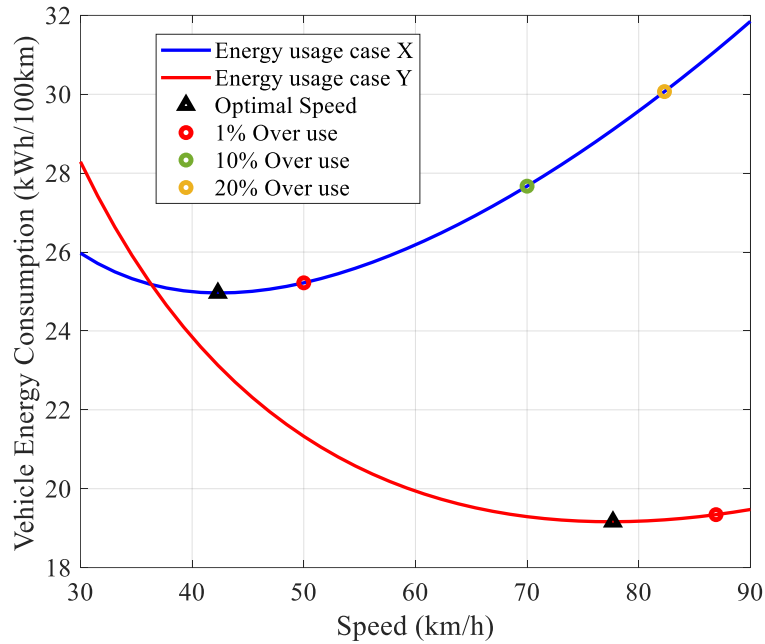


Figure 2-22 Energy-based flexible implementation approach

2.6 Conclusion

This work has shown that it is critical to consider detailed internal and external vehicle parameters to determine energy-optimal cruising speed at any given time. In particular, the high accessory loads of EVs and especially autonomous EVs change the normally-assumed relation that higher speeds use more energy, because when a fixed trip distance is considered, and accessory loads are high, higher vehicle speeds can indeed be optimal. A simple framework is proposed to quickly calculate the energy-optimal cruising speed and determine near-optimal transition rates when parameters change that lead to a new energy-optimal cruising speed. Future work will address the high-traffic urban driving

scenario, while considering all the essential vehicle internal and external parameters identified in this research

2.7 Chapter 2 References

- [1] J. A. Baxter, D. A. Merced, D. J. Costinett, L. M. Tolbert and B. Ozipineci, "Review of Electrical Architectures and Power Requirements for Automated Vehicles," *IEEE Transportation Electrification Conference and Expo (ITEC)*, Long Beach, CA, pp. 944-949, 2018.
- [2] A. Cela et al., "Energy optimal real-time navigation system," *IEEE Intelligent Transportation Systems Magazine*, vol. 6, no. 3, pp. 66-79, Fall 2014.
- [3] K. P. Divakarla, A. Emadi, and S. Razavi, "A cognitive advanced driver assistance systems (ADAS) architecture for autonomous-capable electrified vehicles," *IEEE Transactions on Transportation Electrification*, vol. 5, no. 1, pp. 48-58, March 2019.
- [4] P. Michel, D. Karbowski, and A. Rousseau, "Impact of connectivity and automation on vehicle energy use," *SAE Technical Paper Series*, No. 2016-01-0152, May 2016.
- [5] V. Larsson, L. Johannesson Mårdh, B. Egardt and S. Karlsson, "Commuter route optimized energy management of hybrid electric vehicles," *IEEE Transactions on Intelligent Transportation Systems*, vol. 15, no. 3, pp. 1145-1154, June 2014.
- [6] G. Ma, M. Ghasemi and X. Song, "Integrated powertrain energy management and vehicle coordination for multiple connected hybrid electric vehicles," *IEEE Transactions on Vehicular Technology*, vol. 67, no. 4, pp. 2893-2899, April 2018.
- [7] L. Tate, S. Hochgreb, J. Hall, and M. Bassett, "Energy efficiency of autonomous car powertrain," *SAE Technical Paper Series*, No. 2018-01-1092, Mar. 2018.
- [8] S. I. Guler, M. Menendez, and L. Meier, "Using connected vehicle technology to improve the efficiency of intersections," *Transportation Research Part C: Emerging Technologies*, vol. 46, pp. 121–131, 2014.
- [9] G. Bucsan, A. Goupilleau, P. Frene, M. Ishigaki, A. Iwai, J. S. Lee, M. Pokhrel, M. Balchanos, and D. Mavris, "Mobility analysis of electric autonomous vehicle networks driven by energy-efficient rerouting," *IEEE 85th Vehicular Technology Conference (VTC Spring)*, pp 1-5, 2017.
- [10] V. Turri, B. Besselink and K. H. Johansson, "Cooperative look-ahead control for fuel-efficient and safe heavy-duty vehicle platooning," *IEEE Transactions on Control Systems Technology*, vol. 25, no. 1, pp. 12-28, Jan. 2017.
- [11] C. G. L. Bianco and M. Romano, "Optimal velocity planning for autonomous vehicles considering curvature constraints," *Proceedings 2007 IEEE International Conference on Robotics and Automation*, pp. 2706-2711, 2007.
- [12] C. G. L. Bianco, A. Plazzi, and M. Romano, "Velocity planning for autonomous vehicles," *IEEE Intelligent Vehicles Symposium*, pp. 413-418, 2004.
- [13] J. Villagra, V. Milanés, J. P. Rastelli, J. Godoy, E. Onieva,"Path and speed planning for smooth autonomous navigation," *IEEE Intelligent Vehicles Symposium*, June 2012.

- [14] C. Flores, V. Milanés, J. Pérez, D. González, and F. Nashashibi, "Optimal energy consumption algorithm based on speed reference generation for urban electric vehicles," *IEEE Intelligent Vehicles Symposium (IV)*, pp. 730-735, 2015.
- [15] T. V. Keulen, B. D. Jager, D. Foster, and M. Steinbuch, "Velocity trajectory optimization in hybrid electric trucks," *Proceedings of the 2010 American Control Conference*, pp. 5074-5079, 2010.
- [16] F. Momen, K. Rahman, Y. Son and P. Savagian, "Electric Motor Design of General Motors' Chevrolet Bolt Electric Vehicle," in *SAE International Journal of Alternative Powertrains*, vol. 5, pp. 286-293, 2016
- [17] S. Zhu, Y. Hu, C. Liu, K. Wang and W. Chen, "Reduction of Stator Core Loss in Interior PM Machines for Electric Vehicle Applications," in *IEEE Transactions on Magnetics*, vol. 54, no. 11, pp. 1-5, Nov. 2018, Art no. 8700405, doi: 10.1109/TMAG.2018.2856750.
- [18] Y. Hu, S. Zhu and C. Liu, "Magnet Eddy-Current Loss Analysis of Interior PM Machines for Electric Vehicle Application," in *IEEE Transactions on Magnetics*, vol. 53, no. 11, pp. 1-4, Nov. 2017, Art no. 7402904, doi: 10.1109/TMAG.2017.2700850.
- [19] V. Ruuskanen, J. Nerg, M. Rilla and J. Pyrhönen, "Iron Loss Analysis of the Permanent-Magnet Synchronous Machine Based on Finite-Element Analysis Over the Electrical Vehicle Drive Cycle," in *IEEE Transactions on Industrial Electronics*, vol. 63, no. 7, pp. 4129-4136, July 2016, doi: 10.1109/TIE.2016.2549005.
- [20] A. Frias, A. Kedous-Lebouc, C. Chillet, L. Albert, L. Calegari and O. Messal, "Loss Minimization of an Electrical Vehicle Machine Considering Its Control and Iron Losses," in *IEEE Transactions on Magnetics*, vol. 52, no. 5, pp. 1-4, May 2016, Art no. 8102904, doi: 10.1109/TMAG.2016.2517657.
- [21] S. Jahdi, O. Alatise, C. Fisher, L. Ran and P. Mawby, "An Evaluation of Silicon Carbide Unipolar Technologies for Electric Vehicle Drive-Trains," in *IEEE Journal of Emerging and Selected Topics in Power Electronics*, vol. 2, no. 3, pp. 517-528, Sept. 2014, doi: 10.1109/JESTPE.2014.2307492.
- [22] Y.-C. Lin and H. Nguyen, "Development of an eco-cruise control system based on digital topographical data," *Inventions*, vol. 1, no. 3, 19 pages, Dec. 2016.
- [23] A. Freuer and H.-C. Reuss, "Consumption optimization in battery electric vehicles by autonomous cruise control using predictive route data and a radar system," *SAE International Journal of Alternative Powertrains*, vol. 2, no. 2, pp. 304–313, Aug. 2013.
- [24] E. Ozatay et al., "Cloud-based velocity profile optimization for everyday driving: a dynamic-programming-based solution," *IEEE Transactions on Intelligent Transportation Systems*, vol. 15, no. 6, pp. 2491-2505, Dec. 2014.
- [25] Y. Ikezawa, H. Fujimoto, D. Kawano, Y. Goto, and M. Tsuchimoto, "Bench test of minimum time autonomous driving for electric vehicle based on optimization of velocity profile considering energy constraint," *IECON 2015 - 41st Annual Conference of the IEEE Industrial Electronics Society*, 2015.
- [26] H. Yoshida, H. Fujimoto, D. Kawano, Y. Goto, and M. Tsuchimoto, "Range extension autonomous driving for electric vehicles based on optimal velocity trajectory and driving braking force distribution considering road gradient

- information,” *IECON 2015 - 41st Annual Conference of the IEEE Industrial Electronics Society*, 2015.
- [27] Y. Ikezawa, H. Fujimoto, Y. Hori, D. Kawano, Y. Goto, M. Tsuchimoto, and K. Sato, “Range extension autonomous driving for electric vehicles based on optimal velocity trajectory generation and front-rear driving-braking force distribution,” *IEEE Journal of Industry Applications*, vol. 5, no. 3, pp. 228–235, 2016.
- [28] A. Mahmoudi, W. L. Soong, G. Pellegrino and E. Armando, "Loss function modeling of efficiency maps of electrical machines," *IEEE Transactions on Industry Applications*, vol. 53, no. 5, pp. 4221-4231, April 2017.
- [29] A. Meshginqalam and J. Bauman, "An Onboard Real-Time-Implementable Framework for Calculating the Optimal Cruising Speed of Electric Autonomous Vehicles," *2019 IEEE Transportation Electrification Conference and Expo (ITEC)*, Detroit, MI, USA, pp. 1-6, 2019.
- [30] National Weather Service, Oceanic and Atmospheric Administration, <https://www.weather.gov/documentation/services-web-api>
- [31] A. A. Malikopoulos, S. Hong, B. B. Park, J. Lee and S. Ryu, "Optimal control for speed harmonization of automated vehicles," *IEEE Transactions on Intelligent Transportation Systems*, vol. 20, no. 7, pp. 2405-2417, July 2019.
- [32] Downloadable Dynamometer Database for 2015 Chevrolet SparkEV, <https://www.anl.gov/es/energy-systems-d3-2015-chevrolet-spark-ev>
- [33] Argonne National Laboratory, Vehicle System Simulation Tool Development (Autonomie), <https://www.autonomie.net/>
- [34] A. T. Burrell, S. L. Campbell, C. Coomer, C. W. Ayers, A. A. Wereszczak, J. Ph. Cunningham, L. D. Marlino, L. E. Seiber, and H. T. Lin, "Evaluation of the 2010 Toyota Prius Hybrid Synergy Drive System". United States, March 2011, <https://www.osti.gov/servlets/purl/1007833>.
- [35] F. Momen, K. Rahman and Y. Son, "Electrical propulsion system design of Chevrolet Bolt battery electric vehicle," *IEEE Transactions on Industry Applications*, vol. 55, no. 1, pp. 376-384, Jan.-Feb. 2019.
- [36] D. Zhang, A. Ivanco, and Z. Filipi, "Model-based estimation of vehicle aerodynamic drag and rolling resistance," *SAE Int. J. Commer. Veh.* Vol. 8, pp. 433-439, 2015
- [37] C. E. Tannoury, S. Moussaoui, F. Plestan, N. Romani and G. Pita-Gil, "Synthesis and application of nonlinear observers for the estimation of tire effective radius and rolling resistance of an automotive vehicle," *IEEE Transactions on Control Systems Technology*, vol. 21, no. 6, pp. 2408-2416, Nov. 2013.
- [38] V. Winstead and I. V. Kolmanovsky, "Estimation of road grade and vehicle mass via model predictive control," *Proceedings of 2005 IEEE Conference on Control Applications, 2005. CCA 2005.*, Toronto, Ont., 2005, pp. 1588-1593.
- [39] H. K. Fathy, Dongsoo Kang and J. L. Stein, "Online vehicle mass estimation using recursive least squares and supervisory data extraction," *2008 American Control Conference*, Seattle, WA, 2008, pp. 1842-1848.

Chapter 3

3. Two-level MPC Speed Profile Optimization of Autonomous Electric Vehicles Considering Detailed Internal and External Losses

3.1 Introduction

The transportation industry is currently undergoing two radical transformations: electrification, to reduce the harmful environmental effects of internal combustion engines, and autonomous driving, to reduce traffic fatalities and transform the way society moves. Unfortunately, the addition of large amounts of sensors and computing resources on board autonomous vehicles increases the continuous vehicle load by at least a few kilowatts [1]. This increase in energy use is in clear opposition to the environmental goals of transportation electrification. Thus, it is imperative to use every opportunity available to reduce the energy use of autonomous electric vehicles, since by their very nature, they consume more energy than baseline electric vehicles. Fortunately, autonomous vehicles provide a new degree of freedom in this quest to minimize losses: energy-optimal determination of second-by-second vehicle speed.

Much autonomous vehicle research focuses on the sensors, signal processing, algorithms, and computations required to assure the safe operation of a fully driverless vehicle. Once safety is assured, algorithms to minimize energy consumption while driving can be implemented. Some prior research has focused on reducing energy consumption through optimal route selection [2], path planning [3], smoothing the driving speed profile [4], [5] and optimizing energy management in hybrid vehicles [6], [7]. Furthermore, [8] seeks to determine both the optimal hybrid energy management and the energy-optimal local speed profile, but to make the problem tractable it uses a simple vehicle model considering only vehicle external losses (aerodynamic, rolling resistance, and grade).

Some prior work focuses specifically on vehicle energy reduction by optimizing the speed profile. Reference [9] reduces energy use by dividing the trip into road segments of constant grade and generating an optimal speed for each segment, but considers only vehicle external losses and does not consider losses within the vehicle. Similarly, [10] and [11] do not consider inverter loss, motor mechanical loss, battery loss, or accessory loss, and seek to find the local optimum speed rather than the global optimum for a trip segment. Reference [12] has developed a simple and fast framework for determining the energy-optimal cruising speed while considering all major vehicle internal and external losses, but as this algorithm is focused on cruising, it is not suitable for urban stop-and-go driving patterns. However, [12] does uniquely show the importance of considering vehicle internal losses, especially accessory losses, in the determination of energy-optimal speed.

A common approach to finding a globally optimal speed profile, which is critical to truly minimize energy use over a trip, is to use dynamic programming (DP) [13]-[16]. However, this approach is computationally expensive and does not align well with the fast real-time needs of a driving vehicle. For example, [14] has implemented the DP algorithm in the cloud as the computational requirement was too high for on-board implementation, and although fuel consumption was improved on the highway, much less improvement was obtained for urban driving due to rapid changes in the driving conditions. Reference [17] uses an off-line evolutionary optimization approach to solve the speed optimization problem, but it is not applicable for real-time implementation. Reference [16] seeks to replace the offline-calculated DP results with approximated look-up tables for use on board the vehicle, but does not consider detailed internal vehicle losses.

Model predictive control (MPC) has also been used to solve various formulations of the energy-optimal speed selection problem. The idea of eco-driving with consideration of safety is studied in [18] for connected autonomous vehicles. It uses MPC to solve the optimization problem with the objective of minimizing energy consumption while avoiding collision with nearby connected vehicles. However, in order to get real-time results, motor losses are approximated with a simple expression and other internal vehicle losses are ignored. Similarly, MPC is used to optimize the speed trajectory for heavy-duty urban vehicles in [19], but a simplified vehicle model is used which ignores the vehicle internal losses. In general, MPC will only produce the optimal speed profile for the prediction horizon length considered.

Using a convex formulation is an attractive alternative for energy-optimal speed determination because it can generally find the globally optimal solution in a computationally efficient way, which is well suited to the quickly-changing driving conditions in urban settings. However, to make the problem convex, many simplifications are often made, which can alter the accuracy of the results. For example, [20] and [21] use a convex formulation in a MPC platform to solve the speed optimization problem, but only simple external vehicle losses are considered, and internal losses such as the motor losses and accessories are ignored. An innovative approach for the real-time calculation of the optimal speed trajectory for a commuter train is proposed in [22]. The second-order cone programming method is used to formulate the optimization problem in a convex way. However, simplifications have again been made to create the convex formulation: the

motor efficiency is assumed constant for the trip and other internal losses are not considered.

The contribution of this study is the development of a new convex formulation of the energy-optimal speed problem in a two-level MPC platform which considers detailed internal and external losses of an electric vehicle (EV), in order to generate a highly accurate result. The proposed algorithm uses the successive convex approach to obtain a real-time means of solving the optimization problem with a mixed objective of time and energy. Successive convex optimization is an iterative method: at each iteration, it uses the efficiency data calculated from the last iteration. By repeating the algorithm, the speed profile starts to converge, resulting in the final answer. The optimal solution can be updated periodically by using new data so it can re-evaluate and adjust to new conditions. Using a convex formulation ensures a fast run-time, making it suitable for on-board implementation on autonomous vehicles.

The rest of the chapter is organized as follows: Section 3.2 presents the convex problem formulation and the associated equations, Section 3.3 explains the vehicle modeling, Section 3.4 presents the simulation results, and Section 3.5 presents the conclusions of this work

3.2 Convex Problem Formulation

By definition, a convex optimization problem is an optimization problem where the objective function is a convex function, and its constraints are convex as well [23]. Convex optimization problems have desirable features such as globally optimal solutions and fast convergence times with linear programming. Although non-convex problems can have

more complex and precise modeling, there is no assurance of convergence to a feasible globally optimal solution [24]. Non-linear convex problems can be solved using interior-point method. MOSEK is a software package capable of solving large-scale optimization problems using the interior-point method which is used in this work [25].

The proposed model formulation consists of four parts: (A) vehicle dynamics, (B) losses, (C) physical limitations and essential constraints, and (D) optimization objective.

3.2.1 Vehicle Dynamics

As shown in [22], formulating vehicle dynamics in the position domain regardless of its more complicated formulation will result in less non-linearity, which is an essential characteristic when it comes to convex optimization. The vehicle dynamics are modeled as a discrete position point-mass system. In this system, the dynamics are modeled using the basic kinematic rule in (1)-(2),

$$\Delta x_i = v_i \Delta t_i \quad (1)$$

$$\Delta t_i = \Delta x_i / v_i \quad (2)$$

where Δx_i is the traveled distance (m) in the i^{th} segment, Δt_i is the amount of time (s) required to travel Δx_i , and v_i is the velocity (m/s) in that segment, where each segment is assumed to have a constant velocity. From (1) and (2), the time at each segment can be calculated using (3),

$$t_{i+1} = t_i + \Delta x_i / v_i \quad (3)$$

where t_i represents the time at the end of the i^{th} segment. Acceleration is the result of net applied force, as shown in (4) where ΣF is the net applied force (N), m is the vehicle mass (kg), and a is the acceleration (m/s^2). It is reasonable to assume a constant acceleration in each segment if the segments are small enough. The acceleration in segment i (a_i) will affect the speed of the next segment (v_{i+1}). With constant segment acceleration assumed, the relationship between velocity, time, and acceleration is shown in (5). To calculate the speed of each segment, acceleration in position domain is defined as γ_i , which is the change of speed over the change of position as shown in (6), and thus the velocity in each segment can be calculated by (7). Using (6) and (7), the velocity calculation during each segment can be expressed as (8).

$$\Sigma F = ma \quad (4)$$

$$\Delta v = a\Delta t \quad (5)$$

$$\gamma_i = \frac{\partial v_i}{\partial x} = \frac{a_i}{v_i} = \frac{F_{net,i}/m}{v_i} \quad (6)$$

$$v_{i+1} = v_i + \gamma_i \Delta x \quad (7)$$

$$v_{i+1} = v_i + \frac{(\Sigma F_i / m) \Delta x_i}{v_i} \quad (8)$$

3.2.2 Losses Formulation

A basic block diagram of an EV powertrain is shown in Figure 3-1. The inverter-motor block generates the torque required and applies it to the wheels through the final drive. The torque at the wheels is applied to the chassis, considering the external losses such as aerodynamic losses, grade losses, and rolling resistance losses. The vehicle speed is calculated based on the net force applied to the chassis. The battery supplies power to both the inverter and the electrical accessories, which includes controllers, lights, steering, etc., as well as heating, ventilation, and air conditioning (HVAC).

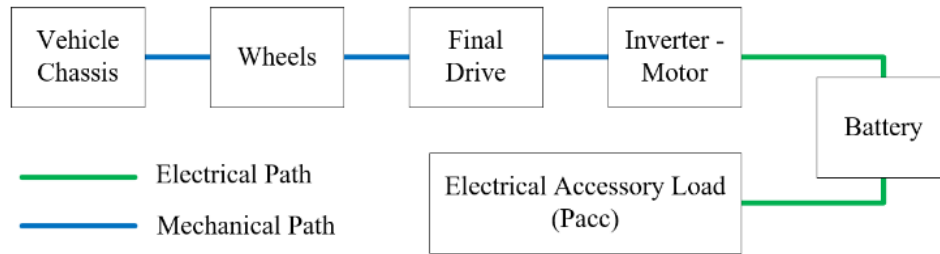


Figure 3-1 EV block diagram

As shown in (8), in order to calculate velocity at each segment, the net force in that segment is calculated first. The net force equals the driveshaft output force minus the external resisting forces, as shown in (9).

$$F_{net,i} = \sum F_i = F_{driveshaft} - F_{roll} - F_{aero} - F_{grade} \quad (9)$$

Equation (10) shows the aerodynamic drag where ρ is the air density, A is the vehicle effective frontal area, C_d is the drag coefficient, v is the vehicle speed (in m/s), and

$v_{w,tangential}$ is the tangential wind speed (defined as being in the same direction as the vehicle is driving in).

$$F_{aero} = \frac{1}{2} \rho A C_d (v - v_{w,tangential})^2 \quad (10)$$

The real-time wind data can be estimated from weather service providers using an application programming interface (API). For example, the National Weather Service in the U.S.A provides the current and forecasted wind speed and direction, in addition to other data [26]. The vehicle direction of motion is known using GPS, thus the effective wind speed can be calculated using (11) as shown in Figure 3-2.

$$V_{w,tangential} = V_w \cos(\Phi) \quad (11)$$

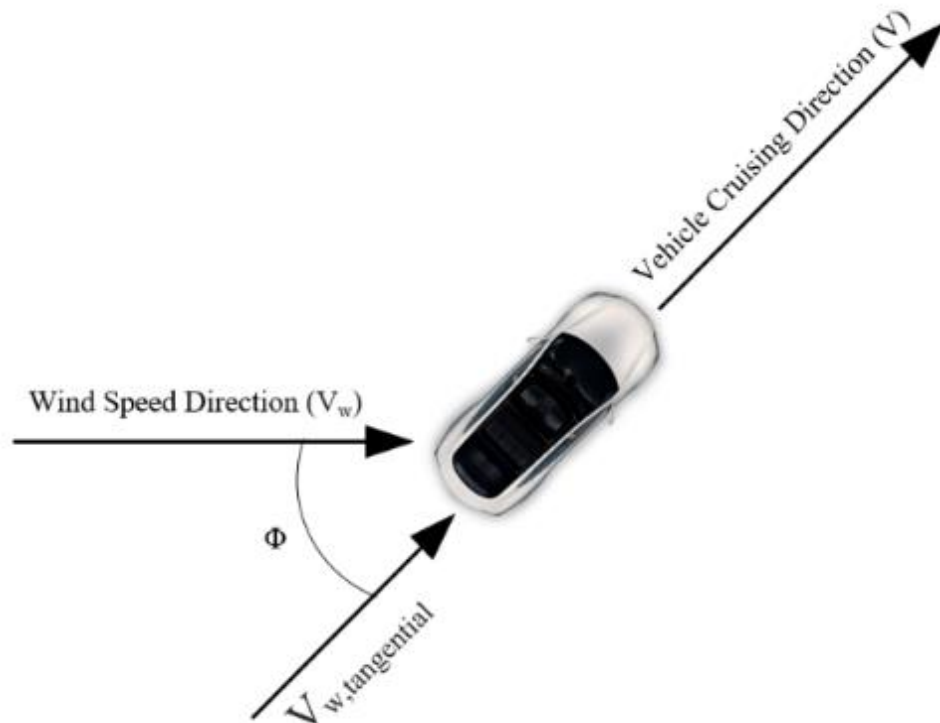


Figure 3-2 Wind in an arbitrary direction

Equation (12) shows the rolling resistance where m is vehicle mass, g is the gravitational constant, θ is the road grade in radians, and μ_1 and μ_2 are rolling coefficients. The resisting force of grade is shown in (13).

$$F_{roll} = mg \cos \theta (\mu_1 + \mu_2 \nu) \quad (12)$$

$$F_{grade} = mg \sin \theta \quad (13)$$

The force at the output of the final drive is represented by $F_{driveshaft}$ which is the motor output torque applied through the final drive to the wheels, as calculated in (14),

$$\begin{cases} F_{driveshaft} = \frac{\tau_{mot} f_d \eta_{fd}}{r_{wh}} & \tau_{mot} > 0 \\ F_{driveshaft} = \frac{\tau_{mot} f_d}{r_{wh} \eta_{fd}} & \tau_{mot} < 0 \end{cases} \quad (14)$$

where f_d is the final drive ratio, η_{fd} is the final drive efficiency, r_{wh} is the wheel radius, and τ_{mot} is the motor output torque.

The force required to accelerate the vehicle is not strictly considered a loss because this energy is converted to kinetic energy as the vehicle drives at a higher speed. The actual loss associated with acceleration stems from the fact that the motor and inverter operate at different operating points than during cruising, where the high torque and low speed operating points during acceleration are generally less efficient than cruising operating points. Thus, because this work uniquely considers a detailed motor/inverter efficiency

map, it is better able to capture these acceleration losses. During regenerative braking, the vehicle's kinetic energy is converted back to mechanical then electrical energy for storage in the battery, and the loss formulations also account for these losses when the torque is negative. Thus, the internal vehicle losses are formulated in (15)-(18) based on prior work of the authors in [12]. These losses are formatted in Joules per meter so that they become suitable to use in a distance domain formulation.

$$Loss_{Final\ Drive} (J / m) = \frac{\tau_{mot} f_d (1 - \eta_{fd})}{r_{wh}} \quad (15)$$

$$Loss_{Motor\ Inverter} (J / m) = \frac{\tau_{mot} f_d (1 - \eta_{motinv})}{r_{wh}} \quad (16)$$

$$Loss_{Battery} (J / m) = \frac{I_b^2 R_b}{v} \quad (17)$$

$$I_b = \frac{V_{oc} - \sqrt{V_{oc}^2 - 4R_b \left(f_d \frac{v}{r_{wh}} \tau_{mot} + P_{accessory} \right)}}{2R_b} \quad (18)$$

η_{motinv} is the motor-inverter efficiency at the given speed-torque operating point, R_b is the internal battery resistance, I_b is the battery current, V_{oc} is the open circuit voltage, and $P_{accessory}$ is the power consumption of the accessories in the vehicle.

One of the crucial aspects to consider in EV modeling is the electrical motor and inverter's efficiency. In most prior work on speed profile optimization, motor/inverter efficiency is not considered or is assumed to be a constant value, but it can actually vary dramatically at different operating points. As shown in Figure 3-3, the combined motor-inverter efficiency for the Toyota Prius can change from 65% to 96%.

The accessory power draw has a significant effect on the resulting optimal speed profile, and yet it is ignored in all prior work on this subject. Large accessory loads can result from the autonomous sensors and computations in autonomous vehicles and HVAC loads in any electric vehicle. Smaller loads include controllers, battery management systems, lights, windshield wipers, power steering, etc. Since these loads manifest as a constant or near-constant power consumption, the longer the vehicle drives, the more accessory energy will be used on a trip. Thus, although aerodynamic losses increase with increased vehicle speed, total trip accessory losses decrease with increased vehicle speed. Due to this opposing effect on optimal speed of these significant losses, it is critical to consider the accessory losses, as in some cases, driving faster may be more energy optimal despite the higher aerodynamic losses. This usage is usually presented in the form of power; thus, the energy consumption is as shown in (19) where $P_{accessory,i}$ is the constant accessory power in segment i :

$$Accessory\ Loss_i(J) = P_{accessory,i} \times \Delta t_i \quad (19)$$

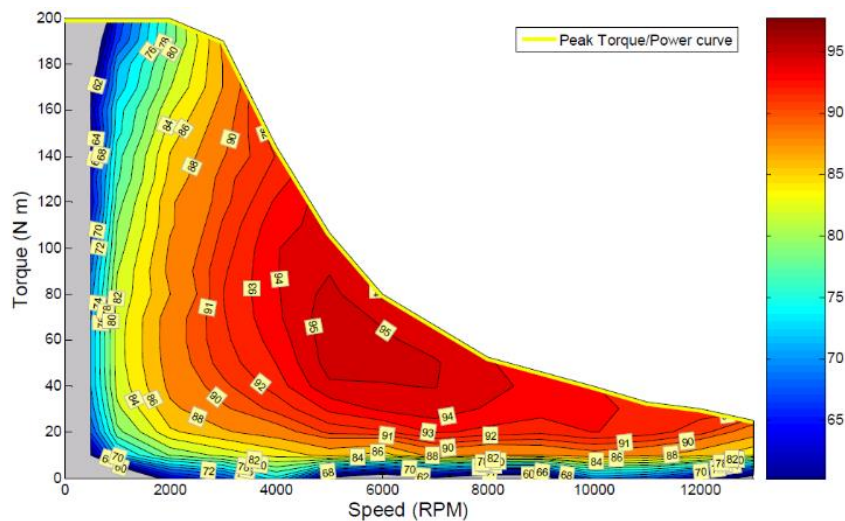


Figure 3-3 2010 Prius combined motor-inverter efficiency contours at 650 Vdc [27]

3.2.3 Physical Limitations

One main physical limitation of the vehicle is that the maximum output torque of the electric motor depends on the motor's rotational speed. The yellow line on the top of the efficiency map (upper boundary) in Figure 3-3 shows the maximum torque curve. This curve can be broken into two sections: in the low speed region, the motor can supply a high constant torque, and in the higher speed region, the motor operates in constant power mode and the maximum output torque decreases as the motor speed increases. It is suggested in [22] to model this maximum torque curve as a minimum of a maximum constant torque portion (first part) and a second order polynomial (second part), as shown in (20),

$$\tau_{mot} = \min(\tau_{maximum}, r_0 + r_1 v_i + r_2 v_i^2) \quad (20)$$

where r_0 , r_1 , and r_2 are polynomial coefficients which can be curve-fitted to match the experimental or manufacturer data [23], and $\tau_{maximum}$ is the maximum torque the motor can provide.

The second physical limitation to consider is driver comfort. To maintain the comfort of the passengers during the trip, the vehicle velocity trajectory should have a smooth shape, without hard acceleration or deceleration events (unless it is necessary for safety). It is suggested in [28] to keep acceleration and deceleration rates below 4.5 m/s^2 for this purpose.

3.2.4 Optimization Formulation

The optimization problem in this work is a mixed-objective optimization problem considering both vehicle energy use and travel time. Thus, the proposed objective function seeks to minimize energy consumed ($E_{consumption}$) and trip time (T_{trip}), as shown in (21),

$$\min(\alpha \times E_{consumption} + \beta \times T_{trip}) \quad (21)$$

where α and β are weighting coefficients for the energy consumption and trip duration. The $E_{consumption}$ is determined by external and internal vehicle losses as described in (12) – (19), which are dependent on the specific vehicle speed profile of the trip. The optimization occurs for a driving segment consisting of a start increasing from zero speed and an end point where speed again returns to zero. Thus, a full trip may consist of many driving segments, where each driving segment is optimized. This concept is shown in Figure 3-4, where the trip is broken down into two driving segments, where the stop point (which could be, for example, a stop sign) is the division between the two driving segments.

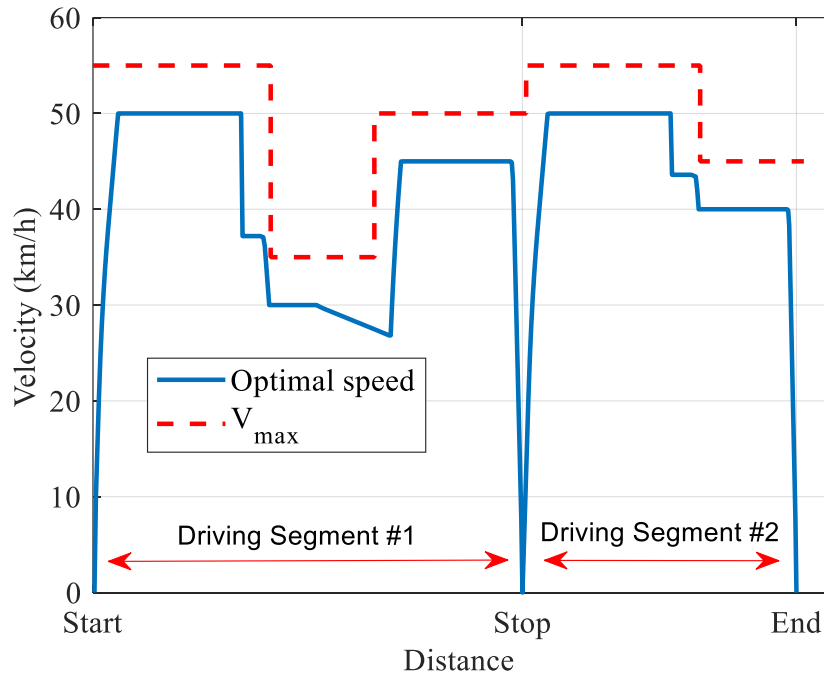


Figure 3-4 Illustration of proposed method for optimization

One main difficulty in modeling the vehicle internal losses accurately is dealing with the motor and inverter efficiency, η_{motinv} , which can vary greatly across different operating points (Figure 3-3). For example, [29] shows that in order to have a high accuracy motor loss approximation, the constant torque region must be modeled independently from the constant power region, where the first part requires 11 terms of torque and speed, up to τ^4 and ω^4 , and the second part needs 15 terms of the combinations of τ and ω , which becomes very complex. For a more tractable approach, the following options exist: ignore motor/inverter losses, approximate a constant efficiency, approximate efficiency using a simple polynomial, or use the detailed two-dimensional look-up table obtained experimentally. Using the actual look-up table gives the highest accuracy by far, but is not possible in a convex problem formulation. For example, Figure 3-5 shows the Bolt EV

motor efficiency data fitted to a second order polynomial approximation using MATLAB's curve fitting toolbox and Figure 3-6 shows the corresponding error across the map.

A convex problem formulation is desired, as these are generally fast and easy to solve, and assure global optimality suitable for real-time implementation [10]. However, this formulation is incompatible with the most accurate representation of motor/inverter efficiency, an experimentally-derived look-up table. Thus, this work proposes the use of successive convex programming, as illustrated in Figure 3-7. At the beginning of the algorithm, an initial guess is generated for the velocity and torque of all the segments (v_a , τ_a). The optimization is then performed in successive loops using more and more precise motor/inverter efficiency data from the look-up table until the velocity profile converges.

In order to address the challenge of generating the initial values for v_a and τ_a , a two-level MPC structure is proposed, consisting of high-level MPC and low-level MPC. The high-level controller generates the overall speed trajectory over the trip using a constant motor/inverter efficiency for the whole driving segment. Then, the low-level controller uses

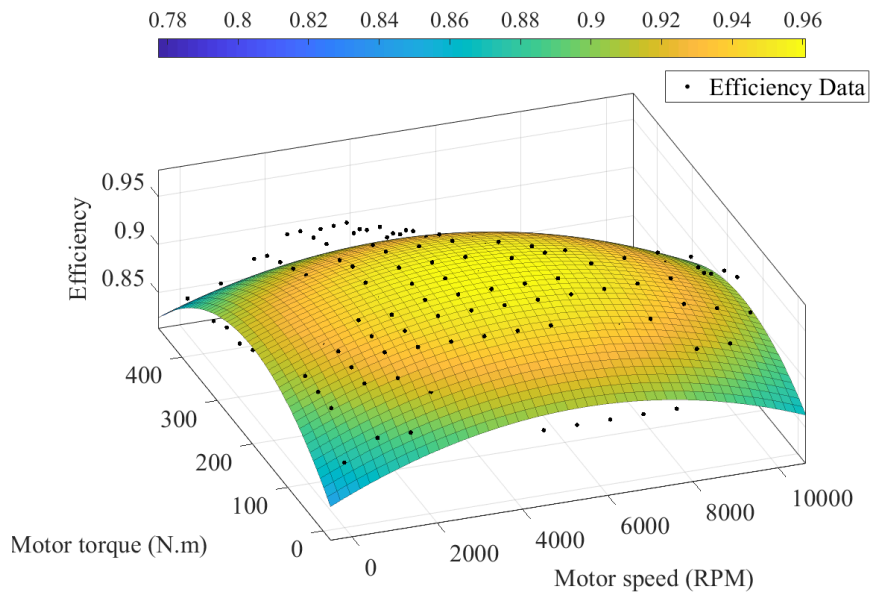


Figure 3-5 Efficiency data vs fitted second order approximation from Chevy Bolt EV [12]

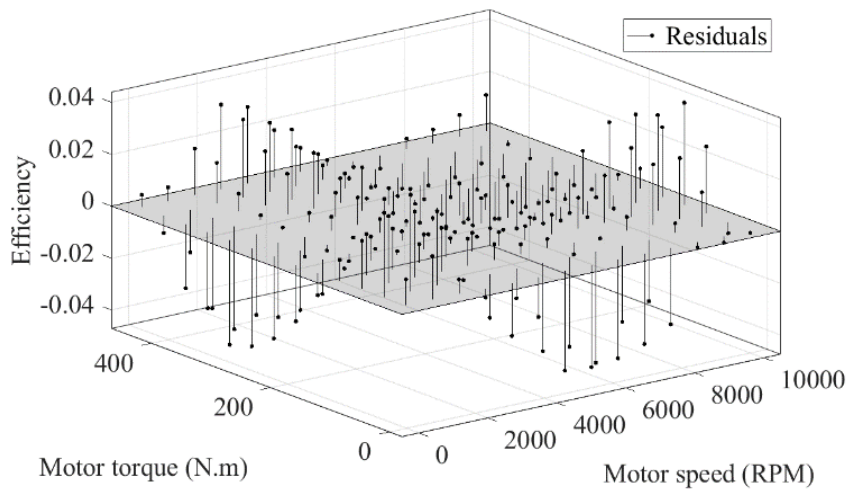


Figure 3-6 Error between efficiency data and fitted polynomial from Chevy Bolt EV [12]

the data coming from the high-level controller as the initial values (first guess) and then tries to generate better results for the smaller portion of the road ahead using the

mentioned successive approach. For the high-level MPC, the tunable parameter is the number of segments, and the length of each segment changes as the vehicle proceeds, but for the low-level MPC, there are two parameters to choose: length of the window ahead and number of segments. Figure 3-8 illustrates this control platform, where the trip requirements and road data are used as input for the high-level MPC. V_{d_high} and τ_{d_high} are the desired speed and torque generated by the high-level MPC, which are used as inputs for the low-level MPC. Then V_{d_low} and τ_{d_low} are produced by the low-level MPC and are sent to the autonomous vehicle as the desired trajectory. The actual measured values for time, velocity, and distance are used as feedback for the high-level MPC (t_{mes} , v_{mes} , X_{mes}).

The optimization problem in (22) is once solved in the high-level MPC for the whole trip using the constant motor/inverter efficiency, then the velocity and torque data

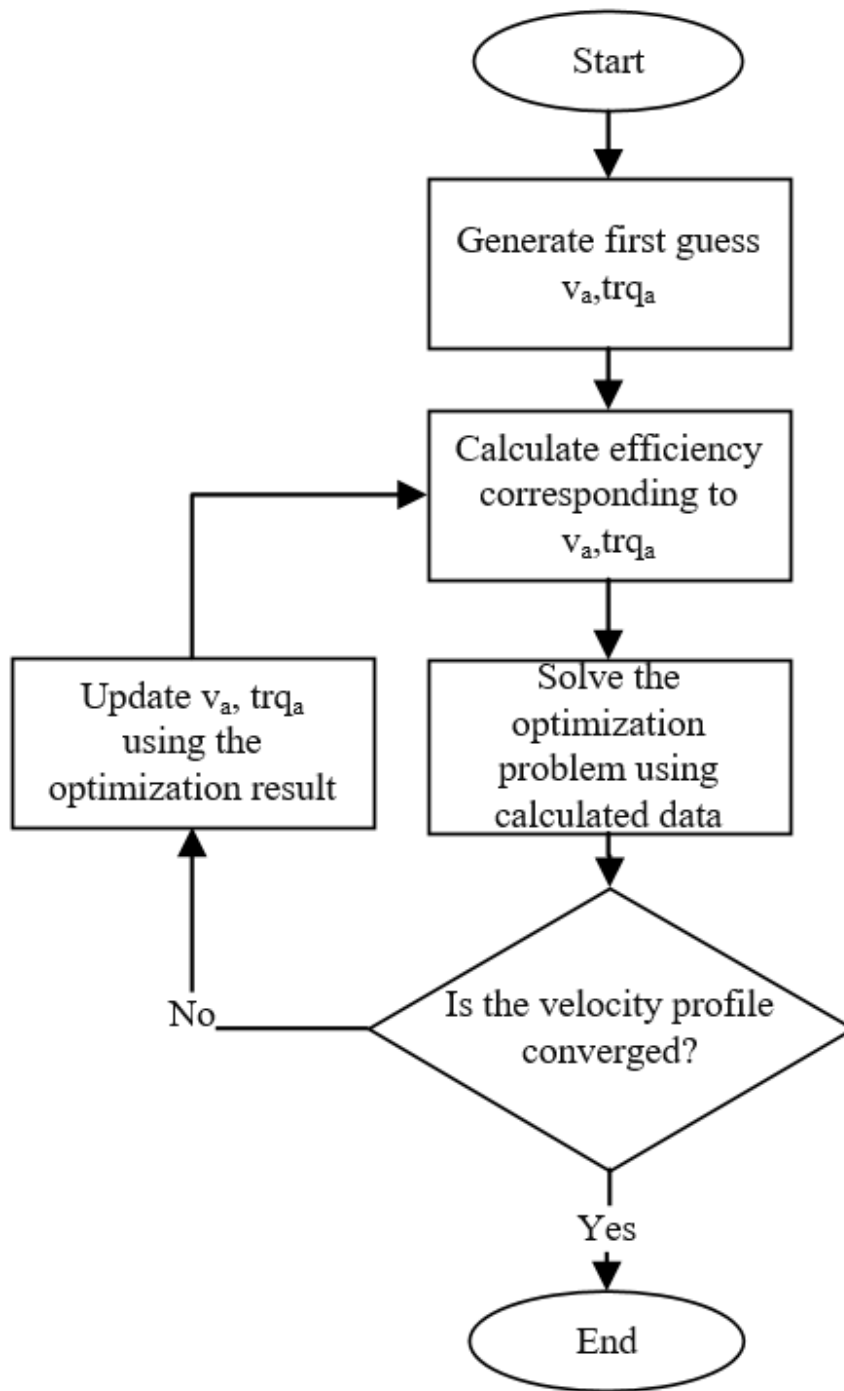


Figure 3-7 Flowchart of the successive convex optimization approach

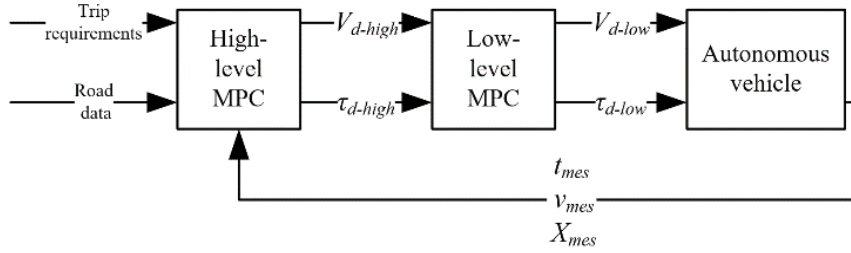


Figure 3-8 Proposed two-level control platform

for the next portion of the road (e.g. 100m ahead) is extracted from the results of the high-level MPC and is fed to the low-level MPC as the initial value. The low-level MPC solves (22) for that portion of the road using the detailed motor/inverter efficiency map in a successive manner. The new values for velocity and torque are compared to the values from the last iteration; if the data is converged the process is done, if not, the next iteration is started.

The optimization problem is shown in (22), where the objective function represents the energy consumption over the whole planned horizon. Δx^T is the transposed vector of distance of segments. Trip time is shown by t_N , and a term is added to penalize fluctuation in the speed profile with the weight of ζ . It is shown in (22) that the time constraint is added to the objective function in terms of energy using accessory usage described in (19).

Velocity at each segment is limited between small non-zero value ε (to prevent non-singularity), and V_{lim} which is the upper boundary velocity (22a). Initial and ending velocity (V_{start} and V_{end}) for each horizon of planning is pre-defined (22b). Time at the start of planning is shown with t_I and it is set to be equal to T_{start} (22c). Arrival time is set to be in an acceptable interval of duration illustrated as T_{end_min} , and T_{end_max} (22d). Time at the end of each segment is calculated as shown in (3), but the formulation is not generally

convex (dividing a convex function by another convex function is not necessarily convex) so an arbitrary variable, ρ_v , is added to maintain the convex format of the optimization. The concept of using ρ_v in a second order cone format is proposed in [22] and it is shown that it is effectively a relaxed version of $\rho_v=1/v$ (22e, 22f). The "second-order cone" arises from the constraint, which is equivalent to requiring the Euclidian norm to lie in the affine function [23]. The motor torque is divided into positive torque and original torque (22g). The reason for this classification is that only positive torque actually uses energy to overcome losses or accelerate. The more detailed format of velocity calculation which was shown in (7) is shown in (22i). These losses are also considered in the objective function. The regenerative braking energy is considered, as the τ variable can have negative values, which representing the reverse flow of energy during regenerative braking.

The main differences between the formulations used in this work compared to [22] are: the addition of the constraint for limiting to comfortable acceleration and deceleration rates, the low-level/high-level MPC to allow for the successive use of the detailed motor/inverter efficiency map, the consideration of accessory power losses, and that the objective function in this study accounts for the actual energy usage instead of an energy-like objective.

The entire formulation of (22) is a convex SOCP (Second-order cone programming) form. Thus, solvers with the capability of working with conic optimization problems can be used to find the solution. The CVX solver is one of these capable solvers which can be integrated into both MATLAB and C [30][31].

$$\begin{aligned}
\min \quad & \left\{ \alpha \left(\begin{aligned} & \left[\begin{aligned} & |\text{loss}_{final\ drive}| + |\text{loss}_{MotorInverter}| \\ & F_{aero} + F_{roll} + F_{grade} + \text{loss}_{Battery} + \\ & |v_{i+1} - v_i| \times \zeta \end{aligned} \right] \\ & + \Delta t^T \times P_{accessory} \end{aligned} \right) \right\} \quad (22) \\
s.t. \quad & \varepsilon \leq v_i \leq V_{lim} \quad (22a) \\
& v_1 = V_{start} \quad v_N = V_{end} \quad (22b) \\
& t_1 = T_{start} \quad (22c) \\
& T_{end_min} \leq t_N \leq T_{end_max} \quad (22d) \\
& t_{i+1} = t_i + \Delta x_i \rho_{v,i} \quad (22e) \\
& \left\| \begin{aligned} & 2 \\ & v_i - \rho_{v,i} \end{aligned} \right\| \leq v_i + \rho_{v,i} \quad (22f) \\
& 0 \leq \tau_{pos} \quad \tau_{mot} \leq \tau_{pos} \quad (22g) \\
& \tau_{min} \leq \tau_{mot} \leq \tau_{max} \quad (22h) \\
& v_{i+1} = v_i + \begin{bmatrix} F_{driveshaft} - \\ [F_{aero} + F_{roll} + F_{grade}] \end{bmatrix} \Delta x_i / m v_i \quad (22i)
\end{aligned}$$

To preserve the real-time performance of the suggested algorithm, two conditions should be considered: 1) if the velocity profile is converged, and 2) if the allocated acceptable time of the algorithm is spent. Whichever of these conditions holds, the algorithm will stop going through the next loop and will generate the current result for the speed trajectory as the final result. If the convergence doesn't happen in the specified time, a sub-optimal solution would be chosen that is feasible and maintains the controllability of the vehicle optimal solution would be chosen that is feasible and maintains the controllability of the vehicle.

3.3 Vehicle Modeling

The dynamic model for the Tesla Models S with 85kWh battery was created in MATLAB/Simulink using logged driving data in the Toronto, Canada area, as shown in Figure 3-9. In this model, a PI feedback loop represents the driver behavior; the logged

speed data from the drive cycle feeds into the loop as the reference speed, and the driver requests a motor/brake torque considering the current simulated speed to follow the speed profile as closely as possible. In the controller block, the controller generates the motor torque demand subject to limitations of the vehicle components. In the plant model, the next simulated vehicle speed, $v_{chas}(t+1)$, is calculated using the force applied to the wheels and resisting forces, as shown in (23).

$$v_{chas}(t+1) = v_{chas}(t) + \left(\frac{1}{m} \int_t^{t+1} \left(F_{out_wh} - \frac{1}{2} \rho A C_d v_{chas}^2(t) \right) dt \right) \quad (23)$$

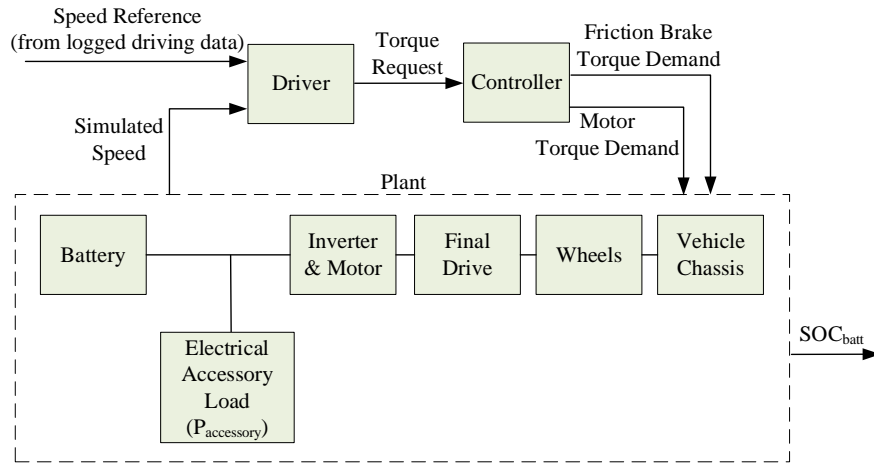


Figure 3-9 Block diagram of vehicle model

In (23), m is the vehicle mass in kg, ρ is the air density, A is the vehicle frontal area in m^2 , and C_d is the coefficient of drag. The force out of the wheel, F_{out_wh} , is calculated backward considering rolling losses, final drive losses, and motor/inverter losses to generate the battery current. Then the corresponding next battery SOC value, $SOC(t+1)$ is calculated using (24).

$$SOC(t+1) = SOC(t) + \frac{1}{C_{batt}} \int_t^{t+1} -I_b dt \quad (24)$$

The vehicle parameters are shown in Table 3-1. Three logged drive cycles for the Model S are used to validate the accuracy of the model. The objective of creating this model is to compare energy use between the optimal speed trajectory (results of the proposed algorithm) and the real-world speed profile using this model. Logged speed data and simulated speed data for three drive cycles (T1, T2, T3) for the Model S are shown in Figure 3-10.

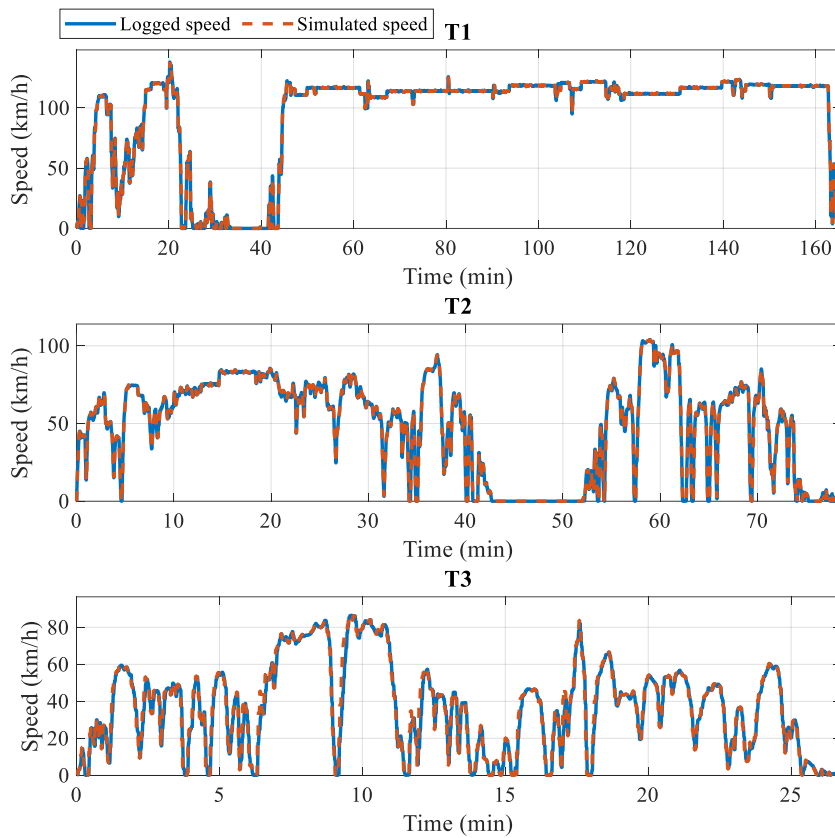


Figure 3-10 Logged vs simulated drive cycle data of a Tesla Model S

The comparison between the simulated vehicle energy consumption to the logged energy consumption for the shown cycles are illustrated in Table 3-2. Less than 3.3% difference between the simulated and the logged energy consumption shows an acceptable accuracy considering there are some unknowns in the logged data. There are 4 main potential sources of error. Firstly, mass was not logged during the drive cycles. The simulated vehicle uses curb mass + driver, but if the real vehicle had multiple passengers and/or cargo during the drive, this would change the energy use slightly. Accessory power usage is also not specifically logged in the dataset. Estimates are made using battery current during times that the vehicle is stopped, but these may be erroneous during driving times, especially long driving times like in T1. Thirdly, wind is unknown during the logged driving, though wind speed is set to zero in the vehicle model for validation. Fourthly, logged GPS altitude is used to estimate grade, but there is some inherent noise and error in this data. The GPS altitude data has been filtered and fed into the model to approximate road grade. Despite these unknowns from the logged data, the model is still able to have very accurate energy use across three unique drive cycles of significant driving time.

Table 3-1 Baseline values of Tesla Model S vehicle parameters

Mass m_c (kg)	C_d	Frontal Area (m^2)	Battery Size (kWh)	Wheel Radius (mm)
2108	0.24	2.43	85	352

Table 3-2 Vehicle Model Energy Usage Validation

Vehicle Model	Cycle	Logged Energy (kWh/cycle)	Simulated Energy (kWh/cycle)	Error (%)
Tesla Model S	T1	22.95	23.17	0.97
	T2	21.29	21.99	3.30
	T3	41.16	40.40	-1.85

3.4 Simulation Results

The proposed convex optimization problems are solved using CVX software inside MATLAB using the Mosek solver. To show the effect of considering a detailed efficiency map, a comparison between optimization results of two cases, one with constant motor inverter efficiency (90%) and one with a detailed efficiency map, is conducted. Figure 3-11 shows the results of this study. The selected route's distance is 300m, where the control horizon of the high-level MPC and low-level MPC are both 50 segments, where the size of each segment, ΔX , is 4 m for the low-level MPC. This is the number of the segments that the route ahead is discretized into.

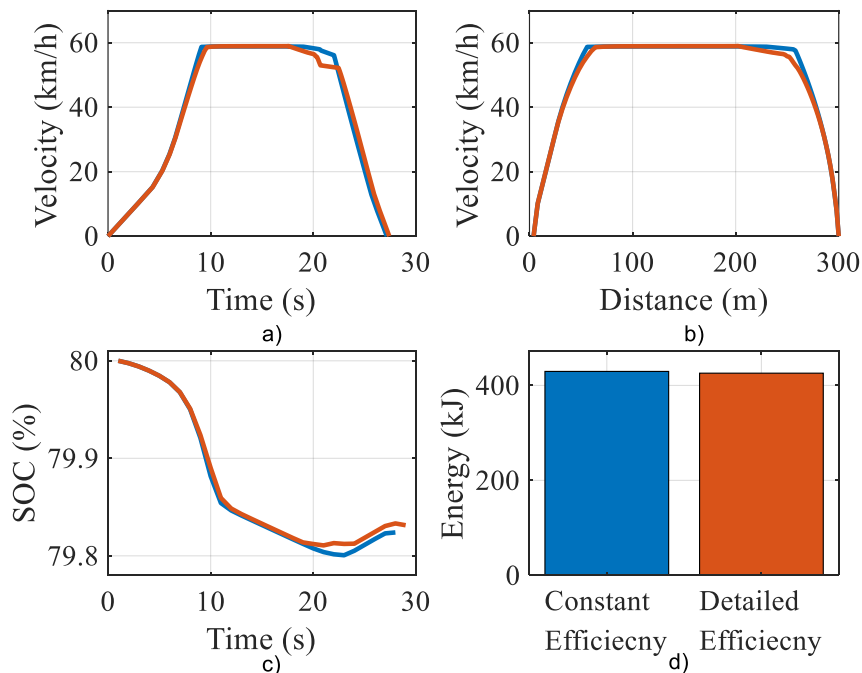


Figure 3-11 a) Time-speed profile b) Distance-speed profile c) Time-SOC d) Energy consumption of the Tesla model S with constant efficiency

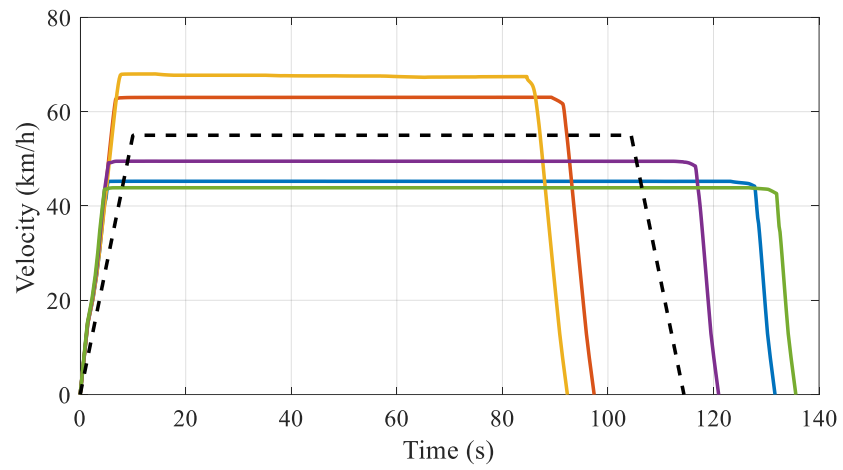
Using a detailed efficiency map for this study case will result in 0.88% energy saving comparing to constant efficiency over the 300m trip. The fact that efficiency changes in different speed and torque levels can be used by the solver to generate a more detailed answer which results in a better performance in terms of the energy for the vehicle.

3.4.1 Energy Focused Optimization

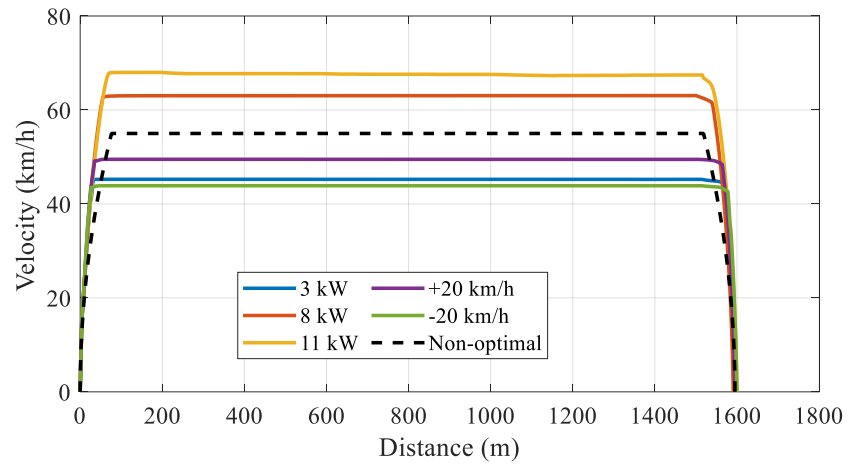
In order to show how the optimal speed profile changes for different conditions, a study of five different cases for the Tesla Model S is conducted: three different accessory power levels (3kW, 8kW, and 11kW), and two different wind speeds (+20 km/h, and -20 km/h). Figure 3-12 illustrates the resulting speed profiles versus time and distance respectively. The maximum allowed speed is set to 70 km/h over a 1600 m route. In order to focus on energy consumption, β is set to 0 in these simulations. As shown in Figure 3-12, when the driving condition changes, the optimal speed profile changes as well. The optimal speed profile tries to go faster when there is high accessory usage. For the cases with different wind speeds, when the speed blows in the same direction as the vehicle drives (+20km/h), the algorithm chooses a higher optimal speed compared to when the wind is resisting (-20 km/h). To show the effectiveness of the optimal profiles, a non-optimal arbitrary speed profile is added to Figure 3-12 (shown using dashed black line) for comparison, consisting of constant acceleration from 0 to 55 km/h in 10 seconds, deceleration from 55 to 0 km/h in 10 seconds, and a 55 km/h cruising speed. The comparison between the energy usages of the optimal and non-optimal driving profiles for the different cases is shown Table 3-3. For all the cases, the optimal speed trajectories calculated using the proposed algorithm result in less energy usage compared to the non-

optimal arbitrary speed profile. It is clear that the accessory power use makes a significant impact on the energy-optimal speed profile; in this case, an 8 kW accessory load gives an optimal speed profile coincidentally close to the arbitrary speed, so only about 1% of energy is saved. However, if accessory load is 3 kW or 11 kW, the optimal speed profile changes significantly, and 3-4% of energy can be saved.

A study on a real-world logged drive cycle of the Tesla Model S is also conducted. In this case, the traveled distance is 585 meters in 74 seconds. Three different accessory usage 3kW, 8kW, and 11kW are studied. For the goal of the simulations, some default values are selected for different parameters. The wind speed is set to 0 km/h, the road grade is equal to 0%, and the vehicle curb mass used. In Figure 3-13, Figure 3-14, and Figure 3-15, the simulation results for the resulting optimal speed trajectory and the real-world speed profile at the 3 kW, 8 kW and 11 kW accessory usage in the time domain and spatial domain is shown. These figures also contain the corresponding used energy as well as the simulated battery SOC.



a)



b)

Figure 3-12 a) Time-speed profile b) Distance-speed profile for five different cases

Table 3-3 Study cases for different cases

	Non-optimal Profile Energy Usage (kJ)	Optimal Profile Energy Usage (kJ)	Energy Saved (%)
3kW accessory usage	1039.8	998.7	3.95
8kW accessory usage	1614.8	1599.4	0.95
11kW accessory usage	1959.8	1900.6	3.02
+20 km/h Wind speed	956.9	932.5	2.55
-20 km/h Wind speed	1158	1104.3	4.63

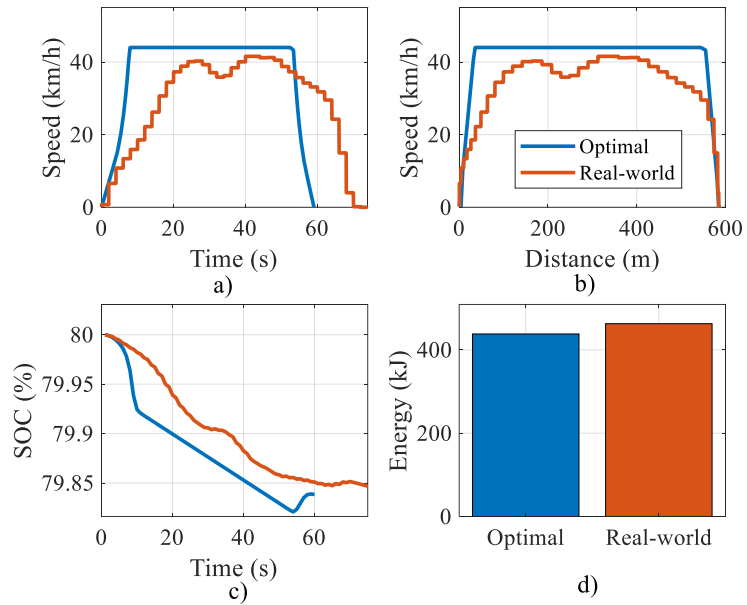


Figure 3-13 a) Time-speed profile b) Distance-speed profile c) Time-SOC d) Energy consumption of the Tesla model S at 3 kW accessory usage

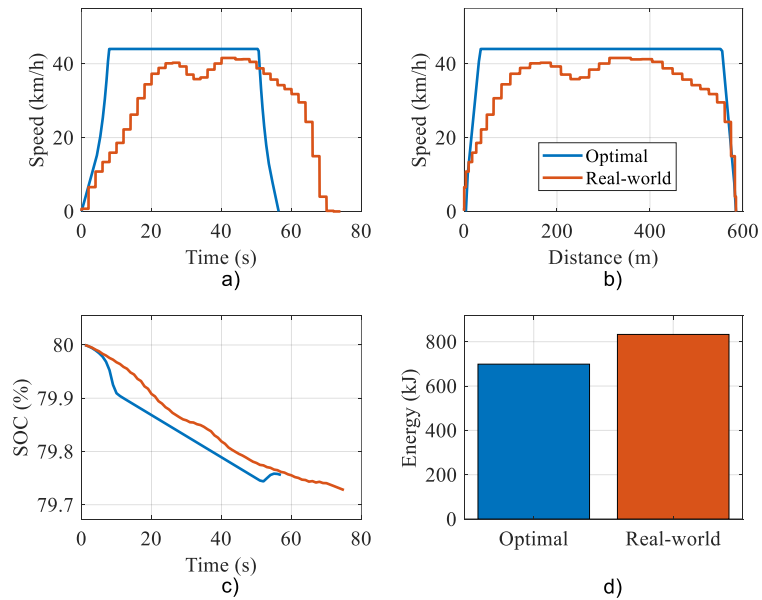


Figure 3-14 a) Time-speed profile b) Distance-speed profile c) Time-SOC d) Energy consumption of the Tesla model S at 8 kW accessory usage

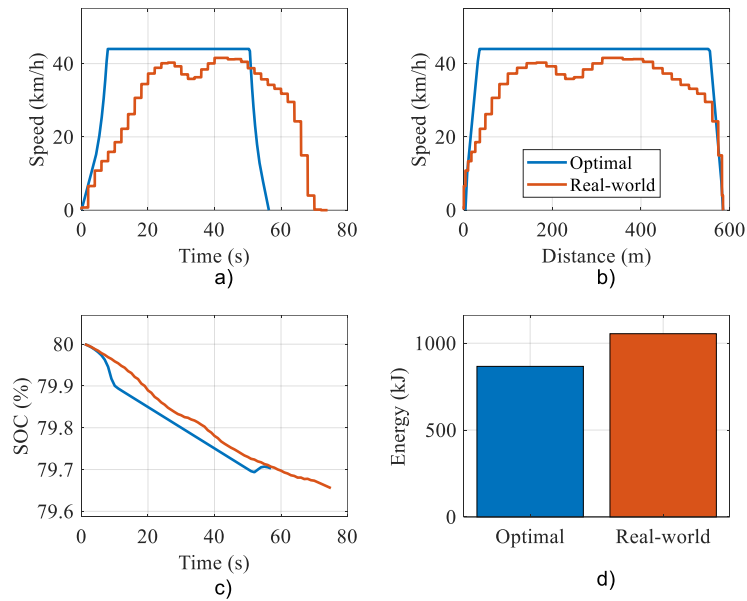


Figure 3-15 a) Time-speed profile b) Distance-speed profile c) Time-SOC d) Energy consumption of the Tesla model S at 11 kW accessory usage

The results show that 9.66%, 16.09%, and 17.83% energy savings result from the vehicle following the optimal speed trajectory compared to the logged real world drive cycle, for the 3 kW, 8 kW, and 11 kW accessory power levels, respectively. For these specific cases, the optimal speed profiles are almost identical, but this is because a speed limit of 45 km/h has been applied to stay close to the real-world driving constraints. If this upper limit were raised higher, the results would be more different, and specifically, the 11 kW case would choose an even higher optimal speed to make the trip have a shorter travel time.

Considering the studied cases, it is shown that optimal speed is not always the lowest or the highest allowed speed, and it can change significantly with the given condition.

Table 3-4 Simulated energy use of cases over 585m trip

	Real-world Driving Energy (kJ)	Optimal Driving Energy (kJ)	Saved Energy (%)
3kW accessory usage	462.8	418.1	9.66
8kW accessory usage	832.8	698.8	16.09
11kW accessory usage	1055	866.8	17.83
+10 km/h Wind speed	453.2	405.5	10.52
-10 km/h Wind speed	475.6	433.8	8.78
+5% road grade	1192	1153	3.27
-5% road grade	-165.2	-200.7	21.48
-2% road grade	190.07	135.21	28.86
+2% road grade	756.85	716.96	5.27
-8% road grade	-521.65	-582.54	11.67
+8% road grade	1627.30	1574.20	3.26
+5 km/h Wind speed	457.63	414.48	9.42
-5 km/h Wind speed	468.81	422.10	9.96
+ 20km/h Wind speed	446.85	401.07	10.24
- 20km/h Wind speed	491.54	447.14	9.03
+ 30km/h Wind speed	443.65	400.15	9.80
- 30km/h Wind speed	510.61	467.82	8.38

Further, it is shown that a more gradual acceleration is not always best, as for high accessory power usage, optimal energy use is obtained by minimizing trip time. The results for 17 different cases are summarized in Table 3-4, where the accessory power is set to 3 kW unless otherwise noted. These cases are selected to demonstrate different external and internal conditions (e.g. windy weather or a ramp). These results show that the amount of saved energy can change dramatically in different cases. The real-world energy usage shown in Table 3-4 is obtained from running the Simulink Tesla Model S vehicle model

on the real-world drive cycle, so that simulation-based energy values are used for both cases (real speed profile and optimal speed profile) for a fair comparison.

3.4.2 Time and Mixed Time-Energy Optimization

The proposed algorithm can also be used to generate a purely time-optimal drive cycle or a mixed time-energy optimal drive cycle. Two cases are simulated for investigation: 3kW and 8kW accessory usage over a 1500m route, where other parameters such as wind speed and grade are set to zero. For each scenario, three different optimization objectives are considered: energy-focused ($\alpha=1, \beta=0$), time-focused ($\alpha=0, \beta=1$), and mixed time-energy ($\alpha=1, \beta=1000$). The maximum allowed speed is set to 70 km/h. Figure 3-16 summarizes the energy use and trip duration for these scenarios, and Figure 3-17 shows the resulting optimal velocity profiles with respect to time and distance. For the 3kW accessory load, the energy-focused case uses the lowest energy at 942 kJ and has the longest trip duration at 124 seconds. The time-focused result has the same velocity profile for both accessory power levels since it will maximize speed wherever possible, and uses 21.5% more energy than the energy-focused result for the 3kW case. However, for the 3kW accessory load, the mixed time-energy result is very favorable as it has only increased energy use by 1.1% (compared to the energy-focused result) but has shortened the trip duration to 99 seconds. The 8kW results follow a similar pattern, where the mixed time-energy result strikes a balance between time and energy as expected. However, the energy and time differences between the 3 results for 8kW are much smaller than for the 3kW results, because with higher accessory load, energy use and time are not “competing” as much, meaning higher speed is better for both energy and time. For example, at 8kW, the

energy- focused result gives 1511 kJ energy usage for a 92 second trip, and the time- focused result increases energy use by 3.8% and reduces the trip duration to 85 seconds. Overall, the optimization of energy use and trip duration is highly dependent on the instantaneous values of vehicle parameters considered in the proposed algorithm, such as accessory power usage, wind, and grade.

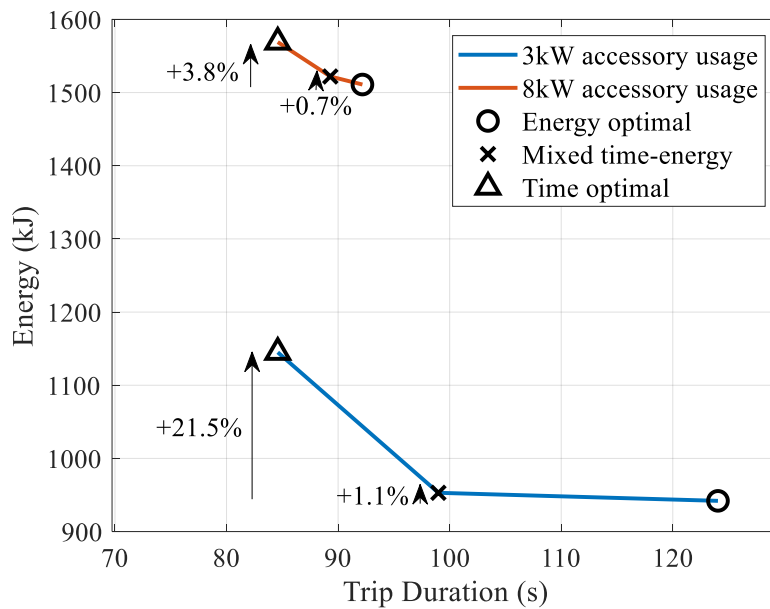


Figure 3-16 Energy consumption vs. trip duration for two different cases with three different optimization objectives (Energy optimal, Time optimal, Mixed time-energy)

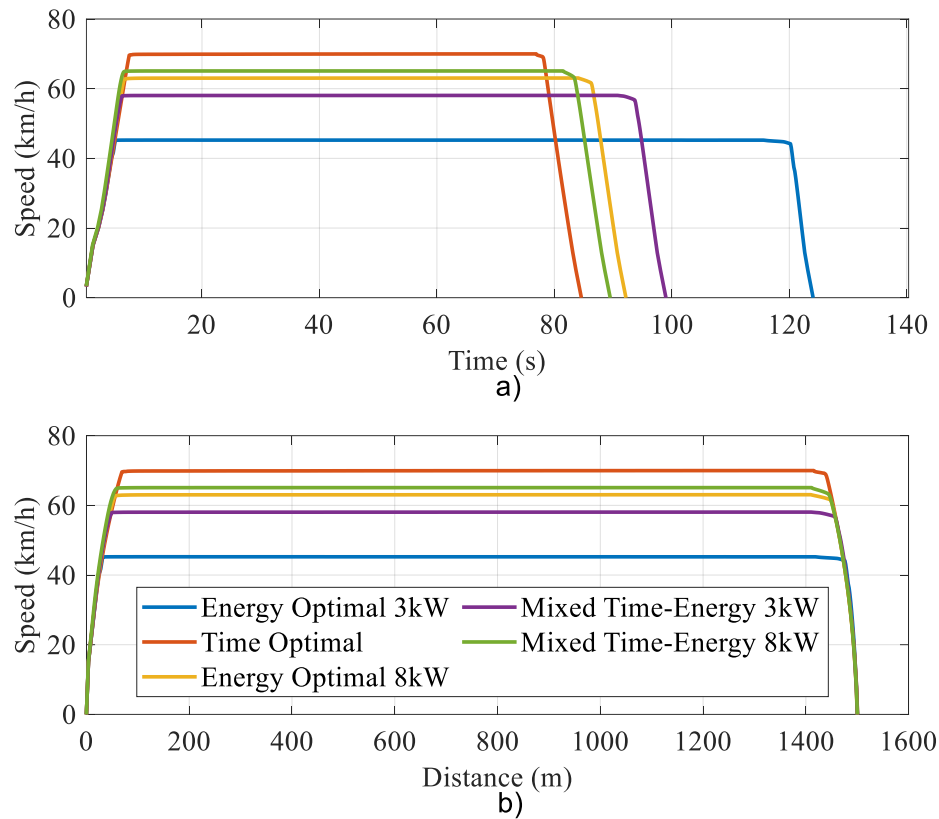


Figure 3-17 Speed profiles for two different cases with three different optimization objectives (Energy focused, Time focused, Mixed Time-Energy) a) speed vs time b) speed vs distance

3.4.3 Computational Effort

Figure 3-18 shows a comparison between the execution time and optimal energy usage for different segmentation sizes for a drive of 585m with 3kW accessory power. The MPC algorithm is run with different segment choices to create various optimal velocity profiles. Then the Simulink vehicle model is run on each velocity profile to calculate the energy usage (y-axis in Figure 3-18). The presented simulation results are performed using a Dell laptop computer with Windows 10 environment, core i7 1.8 GHz CPU and 16 GB RAM. Even though implementation of this suggested algorithm on a microcontroller will

have less computational power compared to a laptop with multiple cores, it is a well-known fact that coding in lower-level coding languages such as C++ will make code a lot faster. The time values on the x-axis are the times for each iteration of the low-level MPC. The segment size in the high-level MPC changes as the vehicle proceeds, so is not a constant number, but it discretizes the remainder of the trip into the selected number of segments. ΔX is the length of the low-level MPC segments. By increasing the number of segments (smaller distance segments), the accuracy of the model excels, but the execution time will also get larger. Also, the results show that the segment size of the low-level MPC is the most important to minimize, as it has a large effect on the vehicle energy consumption, whereas the choice of number of high-level segments has little effect on the energy consumption results. Considering the results in Figure 3-18, the trade-off between optimal energy and execution time is noticeable and should be weighed carefully based on the availability of vehicle on-board computing resources.

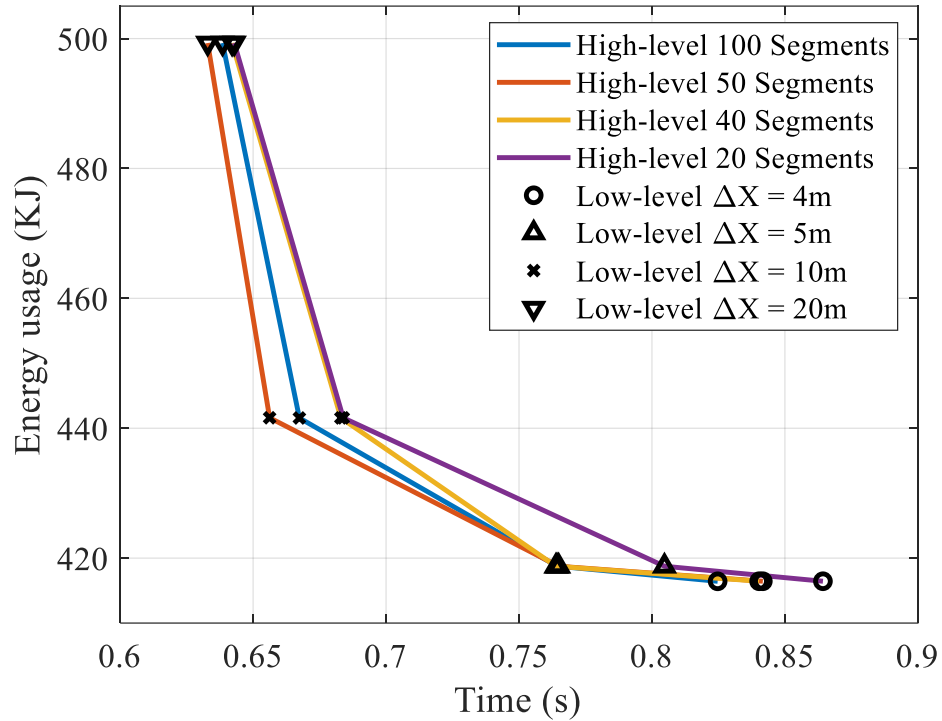


Figure 3-18 Execution time vs. vehicle energy usage for different horizon length

3.5 Conclusion

This chapter presents a novel two-level MPC trajectory planning framework to solve the energy-optimal speed profile planning problem. A convex formulation is developed which performs successive optimizations to allow for the use of detailed motor/inverter efficiency maps. A comparison between using detailed efficiency maps versus using constant efficiency shows an energy savings of 0.88% over a 300m driving segment. A Tesla Model S vehicle is modeled and validated to real world data. The model is used to drive optimal and non-optimal speed profiles to quantify energy savings. Compared to an arbitrary constant-speed profile, the optimal profile saves between 0.95% and 4.63% of energy over a 1.6km driving segment. It is found that considering the high

accessory losses of autonomous vehicles is critical for finding the optimal speed trajectory. Compared to a more variable real-world logged drive cycle, the optimal profile saves between 3.26% and 28.86% of energy. The trade-off between execution time and optimality of results is also investigated.

3.6 Chapter 3 References

- [1] J. A. Baxter, D. A. Merced, D. J. Costinett, L. M. Tolbert and B. Ozpineci, "Review of electrical architectures and power requirements for automated vehicles," *IEEE Transportation Electrification Conference and Expo (ITEC)*, Long Beach, CA, pp. 944-949, 2018.
- [2] A. Cela et al., "Energy optimal real-time navigation system," *IEEE Intelligent Transportation Systems Magazine*, vol. 6, no. 3, pp. 66-79, Fall 2014.
- [3] M. Wang, L. Zhang, Z. Wang, Y. Sai and Y. Chu, "A real-time dynamic trajectory planning for autonomous driving vehicles," *2019 3rd Conference on Vehicle Control and Intelligence (CVCI)*, Hefei, China, 2019, pp. 1-6.
- [4] K. P. Divakarla, A. Emadi, and S. Razavi, "A cognitive advanced driver assistance systems (ADAS) architecture for autonomous-capable electrified vehicles," *IEEE Transactions on Transportation Electrification*, vol. 5, no. 1, pp. 48-58, March 2019.
- [5] P. Michel, D. Karbowski, and A. Rousseau, "Impact of connectivity and automation on vehicle energy use," *SAE Technical Paper Series*, No. 2016-01-0152, May 2016.
- [6] V. Larsson, L. Johannesson Mårdh, B. Egardt and S. Karlsson, "Commuter route optimized energy management of hybrid electric vehicles," *IEEE Transactions on Intelligent Transportation Systems*, vol. 15, no. 3, pp. 1145-1154, June 2014.
- [7] G. Ma, M. Ghasemi and X. Song, "Integrated powertrain energy management and vehicle coordination for multiple connected hybrid electric vehicles," *IEEE Transactions on Vehicular Technology*, vol. 67, no. 4, pp. 2893-2899, April 2018.
- [8] L. Guo, B. Gao, Y. Gao and H. Chen, "Optimal energy management for HEVs in eco-driving applications using bi-level MPC," *IEEE Transactions on Intelligent Transportation Systems*, vol. 18, no. 8, pp. 2153-2162, Aug. 2017.
- [9] C. Flores, V. Milanés, J. Perez, D. Gonzalez, and F. Nashashibi, "Optimal energy consumption algorithm based on speed reference generation for urban electric vehicles," *IEEE Intelligent Vehicles Symposium (IV)*, pp. 730-735, 2015.
- [10] Y. Ikezawa, H. Fujimoto, D. Kawano, Y. Goto, and M. Tsuchimoto, "Bench test of minimum time autonomous driving for electric vehicle based on optimization of velocity profile considering energy constraint," *IECON 2015 - 41st Annual Conference of the IEEE Industrial Electronics Society*, 2015.
- [11] H. Yoshida, H. Fujimoto, D. Kawano, Y. Goto, and M. Tsuchimoto, "Range extension autonomous driving for electric vehicles based on optimal velocity trajectory and driving braking force distribution considering road gradient information," *IECON 2015 - 41st Annual Conference of the IEEE Industrial Electronics Society*, 2015.
- [12] A. Meshginqalam and J. Bauman, "An onboard real-time-implementable framework for calculating the optimal cruising speed of electric autonomous vehicles," *2019 IEEE Transportation Electrification Conference and Expo (ITEC)*, Detroit, MI, USA, 2019, pp. 1-6, doi: 10.1109/ITEC.2019.8790538.
- [13] K. Kim, H. Lee, C. Song, C. Kang and S. W. Cha, "Optimization of speed trajectory for eco-driving considering road characteristics," *2018 IEEE Vehicle Power and Propulsion Conference (VPPC)*, Chicago, IL, 2018, pp. 1-5.

- [14] E. Ozatay et al., "Cloud-based velocity profile optimization for everyday driving: a dynamic-programming-based solution," *IEEE Transactions on Intelligent Transportation Systems*, vol. 15, no. 6, pp. 2491-2505, Dec. 2014.
- [15] S. Akhegaonkar, L. Nouvelière, S. Glaser and F. Holzmann, "Smart and green ACC: energy and safety optimization strategies for EVs," in *IEEE Transactions on Systems, Man, and Cybernetics: Systems*, vol. 48, no. 1, pp. 142-153, Jan. 2018, doi: 10.1109/TSMC.2016.2600273.
- [16] P. Themann, J. Bock, and L. Eckstein, "Optimisation of energy efficiency based on average driving behaviour and driver's preferences for automated driving," *IET Intell. Transport Syst.*, vol. 9, no. 1, pp. 50–58, 2015.
- [17] W. ShangGuan, X. Yan, B. Cai and J. Wang, "Multiobjective optimization for train speed trajectory in CTCS high-speed railway with hybrid evolutionary algorithm," *IEEE Transactions on Intelligent Transportation Systems*, vol. 16, no. 4, pp. 2215-2225, Aug. 2015.
- [18] J. Han, A. Sciarretta, L. L. Ojeda, G. De Nunzio and L. Thibault, "Safe- and eco-driving control for connected and automated electric vehicles using analytical state-constrained optimal solution," in *IEEE Transactions on Intelligent Vehicles*, vol. 3, no. 2, pp. 163-172, June 2018.
- [19] M. Held, O. Flärdh and J. Mårtensson, "Optimal speed control of a heavy-duty vehicle in urban driving," *IEEE Trans. on Intelligent Transportation Systems*, vol. 20, no. 4, pp. 1562-1573, April 2019.
- [20] Y. Shao and Z. Sun, "Eco-approach with traffic prediction and experimental validation for connected and autonomous vehicles," in *IEEE Transactions on Intelligent Transportation Systems*, Feb. 2020.
- [21] M. A. S. Kamal, M. Mukai, J. Murata, and T. Kawabe, "Model predictive control of vehicles on urban roads for improved fuel economy," *IEEE Trans. Control Syst. Technol.*, vol. 21, no. 3, pp. 831–841, May 2013.
- [22] D. Yazhensky, M. Rashid and S. Sirouspour, "An on-line optimal controller for a commuter train," in *IEEE Transactions on Intelligent Transportation Systems*, vol. 20, no. 3, pp. 1112-1125, March 2019.
- [23] S. Boyd and L. Vandenberghe, *Convex Optimization*. Cambridge: Cambridge University Press, 2004.
- [24] J.-B. Hiriart-Urruty and C. Lemaréchal, *Convex Analysis and Minimization Algorithms I: Fundamentals*, vol. 305. Berlin, Germany: Springer, 2013.
- [25] MOSEK ApS. The MOSEK optimization toolbox for MATLAB manual. Version 8.0 . 2019 [Online]. Available: <http://docs.mosek.com/7.0/pythonapi/index.html>
- [26] National Weather Service, Oceanic and Atmospheric Administration, <https://www.weather.gov/documentation/services-web-api>
- [27] Burrell, Timothy A, Campbell, Steven L, Coomer, Chester, Ayers, Curtis William, Wereszczak, Andrew A, Cunningham, Joseph Philip, Marlino, Laura D, Seiber, Larry Eugene, and Lin, Hua-Tay. Evaluation of the 2010 Toyota Prius Hybrid Synergy Drive System. United States: N. p., 2011. Web. doi:10.2172/1007833.

- [28] A. A. Malikopoulos, S. Hong, B. B. Park, J. Lee and S. Ryu, "Optimal control for speed harmonization of automated vehicles," *IEEE Transactions on Intelligent Transportation Systems*, vol. 20, no. 7, pp. 2405-2417, July 2019.
- [29] A. Mahmoudi, W. L. Soong, G. Pellegrino and E. Armando, "Loss function modeling of efficiency maps of electrical machines," *IEEE Transactions on Industry Applications*, vol. 53, no. 5, pp. 4221-4231, April 2017.
- [30] Michael Grant and Stephen Boyd. CVX: Matlab software for disciplined convex programming, version 2.0 beta. <http://cvxr.com/cvx>, September 2013.
- [31] Michael Grant and Stephen Boyd. *Graph implementations for nonsmooth convex programs, Recent Advances in Learning and Control (a tribute to M. Vidyasagar)*, V. Blondel, S. Boyd, and H. Kimura, editors, pages 95-110, Lecture Notes in Control and Information Sciences, Springer, 2008. http://stanford.edu/~boyd/graph_dcp.html

Chapter 4

4. Integrated Convex Speed Planning and Energy Management for Autonomous Fuel Cell Hybrid Electric Vehicles

4.1 Introduction

Fuel cell hybrid electric vehicles (FCHEVs) have the potential to play a critical role in transitioning to a clean and sustainable transportation system. Though battery electric vehicles (BEVs) have a higher powertrain efficiency, BEVs face challenges such as limited range and long charging times [1]. Though fast-charging can somewhat alleviate these challenges, it also increases battery degradation [2] and adds logistical challenges such as finding available fast-charging stations and waiting to charge. FCHEVs have zero harmful tailpipe emissions, offer fast refueling times, and have potentially longer ranges with high-density on-board hydrogen storage [1]. Thus, a flexible and sustainable future transportation paradigm will likely utilize both vehicle types, BEVs for shorter commutes, and FCHEVs for longer distance driving and new mobility concepts with high amounts of driving like ride-sharing and autonomous taxis [3].

Autonomous driving offers further advantages with the goals of collision avoidance, passenger convenience, and mobility for groups that have driving challenges, such as the elderly and disabled [4]. However, autonomous driving technology, mainly sensors and computational hardware, increases a vehicle's accessory power load. Though exact values of this increase are not well-published and will vary vehicle-to-vehicle, [5] estimates that a few kilowatts of continuous power may be required for fully autonomous vehicles. Thus, in order to realize the safety and convenience of autonomous vehicles within a clean and sustainable transportation paradigm, special care must be focused on reducing autonomous vehicle energy use wherever possible. Fortunately, autonomous driving inherently offers two unique options for energy use reduction at the vehicle level: (i) determination of

optimal second-by-second speed trajectories to minimize internal and external vehicle losses [6] – [8], and (ii) optimization of hybrid energy management strategies given future knowledge of the trip [9], [10]. At the fleet level, fully connected autonomous vehicles can further reduce energy use through ridesharing [11], improved traffic flow at intersections [12], [13], and platooning [14].

This chapter focuses on the vehicle-level minimization of energy use for an autonomous FCHEV. There is growing interest in autonomous FCHEVs, as shown by Hyundai’s recent testing of an autonomous FCHEV on a 190 km high-speed trip from Seoul to Pyeongchang [15]. Furthermore, [3] conducts research on autonomous ride-hailing fleets to compare using FCHEVs or BEVs, and shows that smaller fleet sizes of FCHEVs can be used due to lower refuel times and longer ranges. Reference [3] concludes that, despite higher initial costs, FCHEV fleets can be economically competitive with BEVs [3]. Reference [16] studies an integrated motion and powertrain joint optimization for autonomous FCHEVs using model predictive control (MPC), but solving the nonlinear problem takes a high computation time, making it unsuitable for real-time use. Linear approximations are then used in [16] to simplify the calculations, but these simplifications reduce the optimality of the solution. Furthermore, [16] does not generate the optimal speed profile, and component efficiency maps are simplified into second order and linear models.

Much prior research has focused on vehicle energy minimization of autonomous vehicles of any type by optimization of the speed trajectory. Reference [17] divides the trip into road segments with constant grade and generates optimal speeds for each segment but only considers external vehicle losses. Yet the internal vehicle losses such as inverter loss, motor

mechanical loss, battery loss, and accessory loss are essential components of the total energy consumed by a vehicle, and are not considered in [17] – [19]. To achieve a globally optimal speed profile, it is common to use dynamic programming (DP) [20] – [23]. However, DP is computationally expensive and is thus not ideal for real-time applications. On the other hand, convex optimization is a practical alternative since it is fast to run; however, to develop a convex formulation, many simplifications are often made which can reduce the accuracy of the result. For example, [24] and [25] use a convex formulation in a MPC platform, but only consider simple external vehicle losses. The authors' previous research [7], [8] presents a framework for solving the optimal speed planning problem for autonomous BEVs using convex optimization, while considering detailed internal and external vehicle losses.

Much research has also focused on the energy management strategy (EMS) of FCHEVs. Since a fuel cell-powered vehicle must have an energy storage system (usually a battery) to accept regenerative braking energy and provide fast bursts of power during acceleration, an EMS is required to determine the instantaneous power flows from the fuel cell and battery during driving. There are two main categories of EMSs: rule-based and optimization-based. Although rule-based control strategies are simple and robust, they do not guarantee optimality in terms of minimizing fuel use. Optimization-based methods include DP [26], non-linear optimization [27], convex optimization [28] – [36], and equivalent consumption minimization strategy [37]. Convex optimization involves formulating a problem with convex equations so that a maxima or minima can be easily found. The convex optimization approach is attractive for real-time EMS problems because

after the convex formulation is complete, convex problems are often easier and faster to solve compared to non-convex problems [38]. However, [28] – [36] use convex optimization to address the EMS problem, and do not consider the additional challenge of optimizing the speed trajectory with the EMS.

A further evolution of hybrid vehicle EMSs is to use the predicted future velocity to help improve EMS decisions [39] – [41]. In [39] and [40], the EMS problem is solved using the MPC approach, and in [41], it is solved using convex programming. Reference [42] goes further to propose a speed planning algorithm that is activated when a fuel cell bus is 100 m from an intersection, so that the speed planning outcome can improve the energy use through the intersection, where the EMS is solved in real-time using MPC. In [43], the co-optimization of the speed trajectory and power management for a FCHEV is studied using Pontryagin's Minimum Principle to reduce the computational burden of DP. The possible actions for DP are limited to full acceleration, full regenerative braking, full brake, coasting, and cruising, so the full range of vehicle motion is not considered, and thus the results do not represent a true optimum. For example, it is well-accepted that slower accelerations can be more efficient than full throttle accelerations. Furthermore, simplifications such as setting the inverter/motor efficiency to a constant value and the DC/DC converter efficiency to 100% further erode the accuracy of the results. Still, [43] shows the benefits of the co-optimization approach over a sequential optimization (speed planning then EMS optimization), especially for aggressive or hilly driving. However, the long execution time of the co-optimization approach in [43] is not implementable in real-time, and the presented alternative real-time sequential method can have up to 24% worse energy use.

Conversely, this study contributes to autonomous FCHEV research by proposing energy use minimization through optimal speed planning and energy management using convex optimization, which is not found in the prior literature. The convex formulation allows the algorithm to run in real-time, and detailed loss modeling is used to ensure a highly accurate result. Thus, the first novel contribution of this work is the proposed successive method, where convex optimization is first used to generate the optimal speed trajectory, then convex optimization is used to solve the EMS problem using the optimal speed trajectory. The second novel contribution of this work is the proposed integrated method, which uses the knowledge of the EMS (instantaneous fuel cell power) to affect the optimal speed trajectory, such that the speed planning and EMS problems are solved in an integrated way using convex optimization. The only prior work that attempted a similar integrated optimization approach for speed planning and EMS for a FCHEV is [43]; however, it excludes important loss details and since it uses DP, it has to limit the motor torque options to a few unrealistic levels to make computation feasible, yet it still has a long execution time that is not realistic for real-time implementation. Thus, the proposed successive and integrated methods in this chapter are the first to (i) optimize speed planning then EMS for a FCHEV using fast convex optimization suitable for real-time use (successive method), and (ii) optimize speed planning and the EMS in an integrated way for a FCHEV using fast convex optimization suitable for real-time use (integrated method).

The rest of this chapter is organized as follows. Section 4.2 describes the convex problem modeling and formulation, including the use of experimental data to create and validate the fuel cell and battery models. Section 4.3 provides the convex simulation results, including

a comparison to arbitrary short drive cycles, a sensitivity analysis of varying the vehicle electrical accessory load, analysis of results on long real-world drive cycles, and a computation time analysis. Section 4.4 presents a DP formulation to be used as benchmark and compares the proposed convex methods to the DP results. Finally, Section V concludes the chapter.

4.2 Convex Problem Modeling and Formulation

4.2.1 General Overview

Figure 4-1 shows the general concepts of the proposed successive and integrated optimization methods, where P_d is the vehicle power demand and η_{FC} is the fuel cell (FC) system efficiency. Since the FC system efficiency depends on its output power, selecting how to allocate power between the battery and FC will affect the system's overall efficiency, which will affect the optimal speed decision, as shown in Figure 4-1(b) for the integrated method. For both methods, the proposed real-time framework is that the optimization algorithm plans the velocity for the window ahead, and as the vehicle proceeds, it periodically provides feedback signals such as position (distance), velocity, accessory power level, time spent so far, grade, etc. The proposed method uses these feedback signals to rerun the optimization algorithm and update the speed trajectory according to the new input data. For example, the computational effort analysis in Section III-E uses a 1000 m look-ahead window.

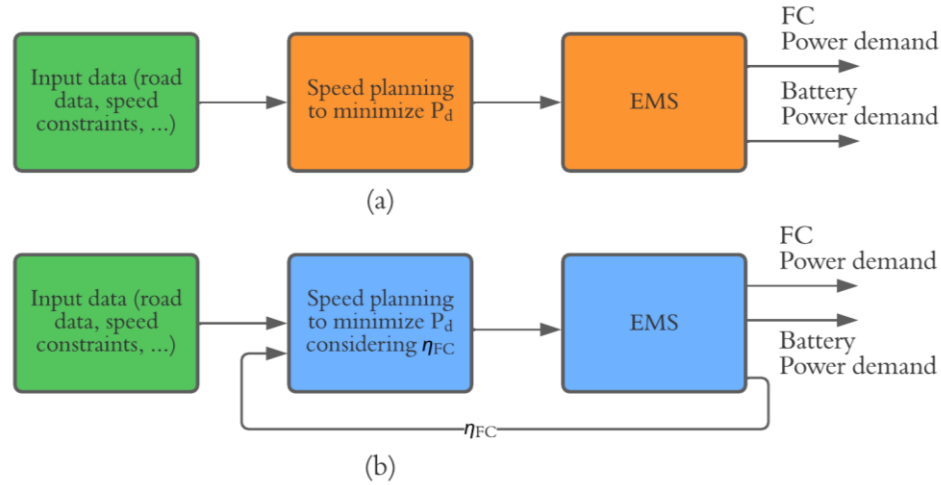


Figure 4-1 a) Successive optimization method b) Integrated optimization method using η_{FC} feedback

The general form of the convex optimization formulation is shown in (1), where $f(x)$ is the objective function, $g_i(x)$ is the i^{th} equality constraint, and $h_j(x)$ is the j^{th} inequality constraint. If all these functions are convex, the optimization problem becomes a convex optimization problem. The goal is to formulate vehicle dynamics, physical limitations, and all the major vehicle losses as convex constraint functions and the energy consumption as the convex objective function.

$$\begin{aligned}
 & \min_x f(x) \\
 & s.t. \\
 & \begin{cases} g_i(x) = 0 & i = 1, \dots, m \\ h_j(x) \leq 0 & j = 1, \dots, n \end{cases}
 \end{aligned} \tag{1}$$

Figure 4-2 shows a block diagram of the target study vehicle, the 2017 Toyota Mirai [44]. The FC system consists of different subsystems, including the fuel cell stack, compressor, pumps, and DC/DC converter. The main source of the energy in this vehicle is the fuel cell stack (114 kW peak power [44]) and the energy storage system is a nickel metal-hydride battery (1.6 kWh [44]).

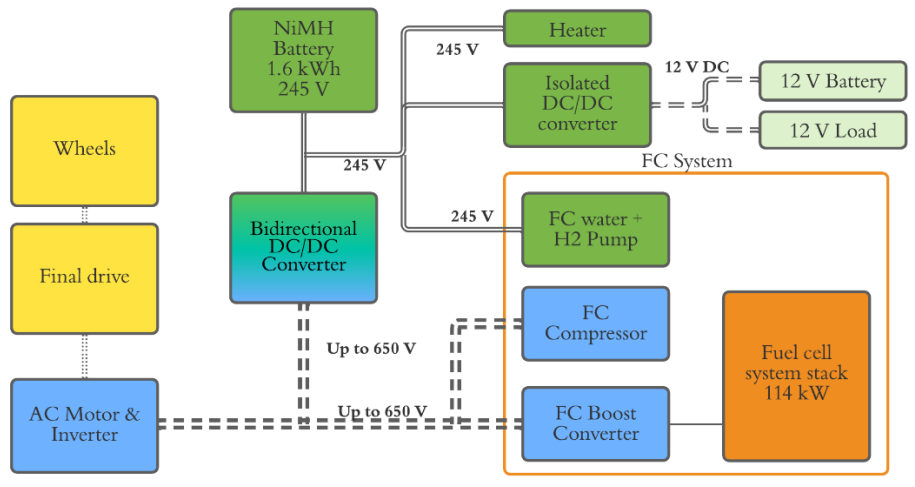


Figure 4-2 Toyota Mirai 2017 block diagram

4.2.2 Convex Vehicle Model

This research formulates vehicle dynamics in a discrete position domain point-mass system. The principal for the formulations comes from the kinematics in (2)-(3). In these formulations, Δx_i is the traveled distance (m) in the i^{th} segment, Δt_i is the amount of time (s) required to travel Δx_i , and v_i is the speed (m/s) in that segment. Time at the next step can be calculated using time at the current step plus the amount of time required to travel that segment, as shown in (4).

$$\Delta x_i = v_i \times \Delta t_i \quad (2)$$

$$\Delta t_i = \Delta x_i / v_i \quad (3)$$

$$t_{i+1} = t_i + \Delta x_i / v_i \quad (4)$$

As Newton's law of motion expresses, there is a relationship between the applied net force and acceleration, as shown in (5), where ΣF is the net applied force (N), m is the vehicle mass (kg), and a is the acceleration (m/s^2). Assuming constant force is applied

within each segment results in a constant acceleration in each segment, and thus the change of speed of the next segment can be found using (6) - (8).

$$\sum F = ma \quad (5)$$

$$\Delta v = a \times \Delta t \quad (6)$$

$$v_{i+1} = v_i + a_i \times \Delta t_i \quad (7)$$

$$v_{i+1} = v_i + \frac{(\sum F_i / m) \times \Delta x_i}{v_i} \quad (8)$$

The net applied force for a segment is calculated using applied electrical motor torque and external resisting force in (9). External resisting forces against the vehicle are presented in (10)-(12). Aerodynamic drag, F_{aero} , is shown in (10) where ρ_{air} is the air density (1.225 kg/m³), A is the vehicle effective frontal area (m²), C_d is the drag coefficient, v_{chass} is the chassis speed (m/s), and v_w is the tangential wind speed (m/s). Equation (11) shows the rolling resistance force, F_{roll} , where m is vehicle mass (kg), g is the gravitational constant (9.81 m/s²), θ is the road grade in radians, and μ_1 and μ_2 are rolling resistance coefficients. Equation (12) shows the grade resisting force, F_{grade} . The force at the output of the final drive, F_{out_fd} , is shown in (13), where τ_{mot} is the motor torque, f_d is the final drive ratio, r_{wh} is the wheel radius (m) and η_{fd} is the final drive efficiency. Based on the sign of the applied motor torque, the corresponding formula should be used, so that energy losses occur across the final drive whether the vehicle is in propelling mode (τ_{mot} positive) or

regenerative braking mode (τ_{mot} negative). In this formulation, a constant final drive efficiency (0.97) for η_{fd} is used.

$$\sum F_i = F_{out_fd,i} - [F_{aero,i} + F_{roll,i} + F_{grade,i}] \quad (9)$$

$$F_{aero} = \frac{1}{2} \rho_{air} A C_d (v_{chass} - v_w)^2 \quad (10)$$

$$F_{roll} = mg \cos \theta (\mu_1 + \mu_2 v_{chass}) \quad (11)$$

$$F_{grade} = mg \sin \theta \quad (12)$$

$$\begin{cases} F_{out_fd} = \frac{\tau_{mot} f_d \eta_{fd}}{r_{wh}} & \tau_{mot} > 0 \\ F_{out_fd} = \frac{\tau_{mot} f_d}{\eta_{fd} r_{wh}} & \tau_{mot} < 0 \end{cases} \quad (13)$$

The relationship between vehicle speed, motor rotational speed (ω_{mot} in rad/s), and wheel speed (ω_{wh} in rad/s) is shown in (14) and (15).

$$v_{chass} = \frac{\omega_{mot} r_{wh}}{f_d} \quad (14)$$

$$\omega_{wh} = \frac{\omega_{mot}}{f_d} \quad (15)$$

The FC system is complicated and can be modeled in various ways. For example, multiphase models are very complex and highly accurate [45-46]. However, since the goal of this study is to run a fast online convex optimization process to generate optimal speed trajectories and an optimal EMS, a simpler approach is taken by assuming the FC system operates at its optimal conditions. In this case, using a FC system efficiency map to describe

the relationship between FC output electrical power and hydrogen consumption is sufficient, especially considering much prior literature on this topic uses a second-order approximation of this efficiency map [1], [16], [28], [29], [32], [39]. The FC system efficiency includes all relevant losses, such as water and H₂ pumps, compressor, boost converter, and FC stack. This FC efficiency is a function of FC output power, as shown in Figure 4-3. This map is extracted from experimental tests by Argonne National Laboratory [44] on the FC in the Toyota Mirai. In [44], both FC stack efficiency (peak is 66%) and FC system efficiency (peak is 63.7%) are shown, and these analyses are based on steady state speed tests. The FC system efficiency curve from [44] is used to model the FC in this study, as shown in Figure 4-3.

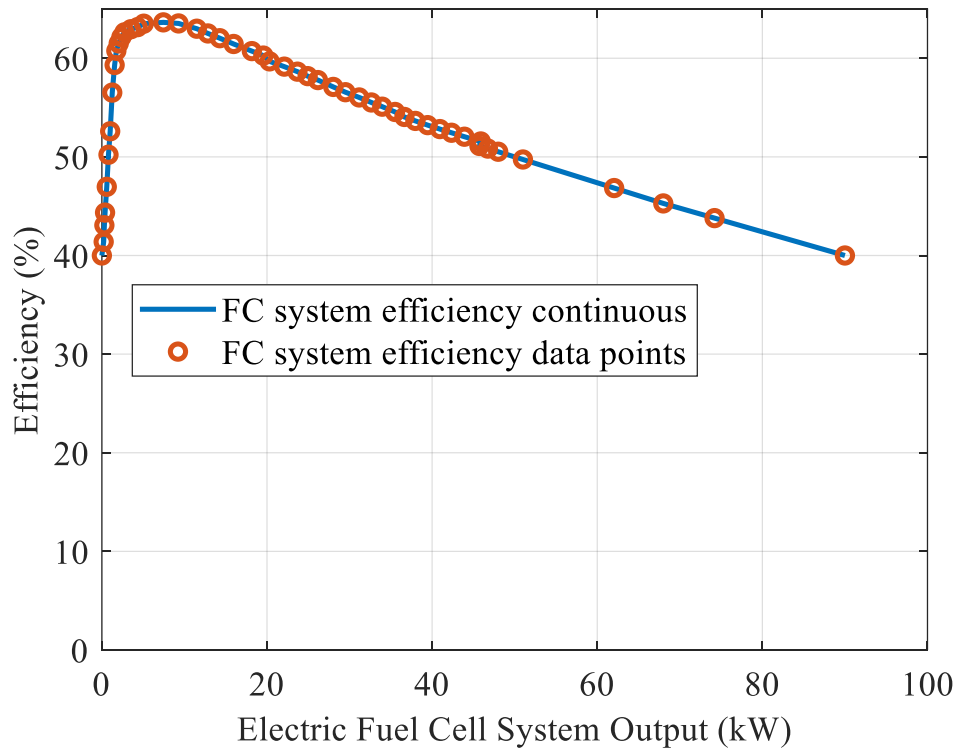


Figure 4-3 FC system efficiency as a function of FC output power, as extracted from [43]

To verify the accuracy of the FC system efficiency map in Figure 4-3, experimentally logged data (by Argonne National Laboratory) from three drive cycles of the Toyota Mirai are used [47]. This publicly available dataset includes FC output power and H₂ flow rate. To validate the extracted FC system efficiency map, the experimentally logged FC power data is fed into the model and the resulting simulated H₂ flow rate is read as the output. This simulated H₂ flow rate is then compared with the experimentally logged H₂ flow rate, and the results are shown in Figure 4-4 for Test ID 61712033. Table 4-1 summarizes the validation results for three test drive cycles and shows that using the FC system efficiency map in Figure 4-3 gives reasonable accuracy compared to the experimental data, with the cumulative error less than 2.4% and the RMSE less than 3.3%.

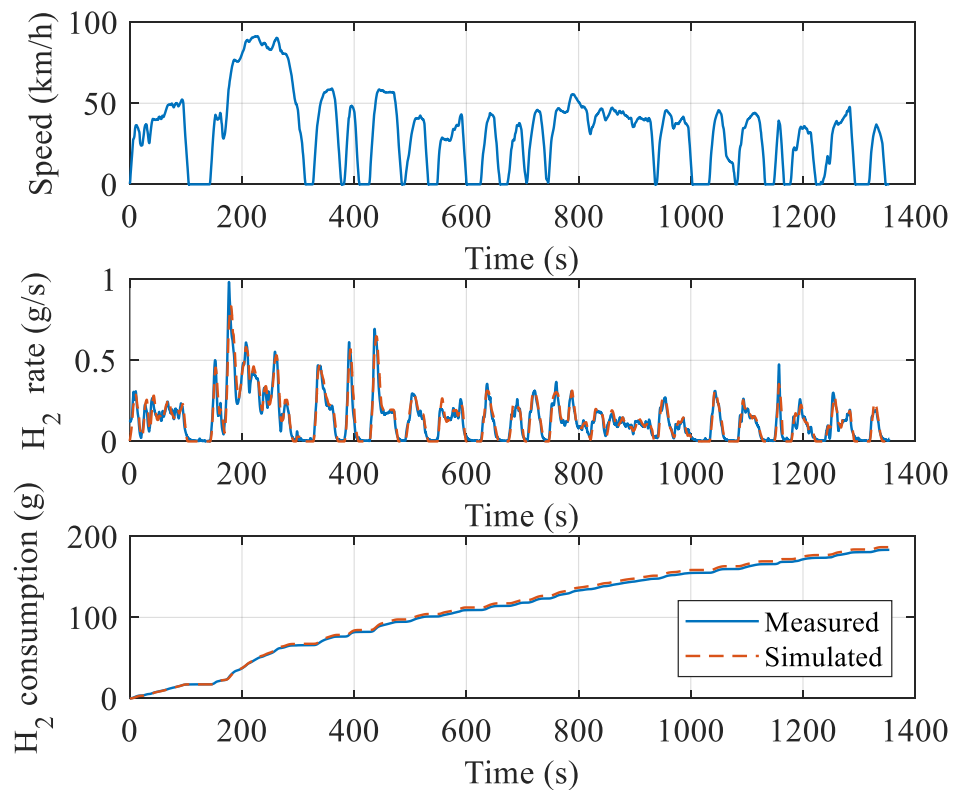


Figure 4-4 UDDS test cycle for fuel cell system validation (Test ID 61712033)

Table 4-1 Validation of Fuel Cell Model

Data Test ID	Simulated H ₂ Consumption (g)	Logged H ₂ Consumption (g)	Error in Cumulative H ₂ Consumption (%)	RMSE H ₂ Consumption (%)
61712033	186.66	183.37	1.79	1.81
61712034	1154.37	1182.63	-2.39	3.27
61712037	306.56	307.14	-0.19	1.87

The battery is modeled as a voltage source, V_{oc} , in series with internal resistance, R_b . Equation (16) shows how terminal voltage V_{term} is calculated where I_b is the battery current and is considered positive when the battery is discharging. The open circuit voltage, V_{oc} , is a function of the battery state-of-charge (SOC), and the logged data extracted from the tests provided in [47] are used to generate a linear approximation of V_{oc} over SOC. This linear approximation is shown in (17), where ($V_0=155.8$, $\zeta=2.252$). The value for R_b is also estimated using the experimentally logged data (0.6899Ω). Battery output power, P_b , is calculated using (18) and the amount of power loss in the battery P_{loss_batt} is expressed in (19). The battery SOC calculation is shown in (20), where C_{Ah} is the battery capacity in Amp-hours.

$$V_{term} = V_{oc} - R_b I_b \quad (16)$$

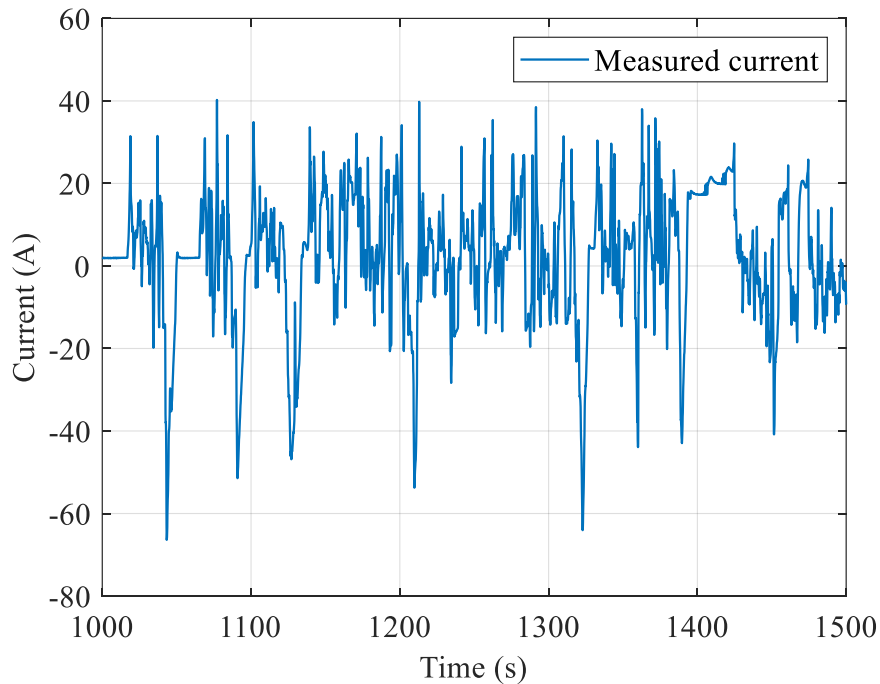
$$V_{oc} = V_0 + \zeta \times SOC \quad (17)$$

$$P_{batt} = V_{term} I_b \quad (18)$$

$$P_{loss_batt} = R_b I_b^2 \quad (19)$$

$$SOC_{i+1} = SOC_i + \frac{1}{3600 \times C_{Ah}} \int_{t_i}^{t_{i+1}} I_b(t) dt \quad (20)$$

To validate the parameter choices of the battery modeling, a Simulink-based simulation is developed to study the battery behavior. In this simulation, logged current data (from Toyota Mirai Test ID-61712034, a UDDS cycle) [44] is sent into the battery model as the input, and the battery terminal voltage and battery SOC are the outputs. Figure 4-5(a) shows the input current, and Figure 4-5(b) and (c) show the comparison between the simulated results and the logged data of battery voltage and SOC respectively. Table 4-2 shows the results for validation of the battery model over three different logged cycles from [47]. The results show a close correlation (less than 5% RMSE and close to one for correlation coefficients) between the logged and simulated battery data, which validates the battery modeling parameters used.



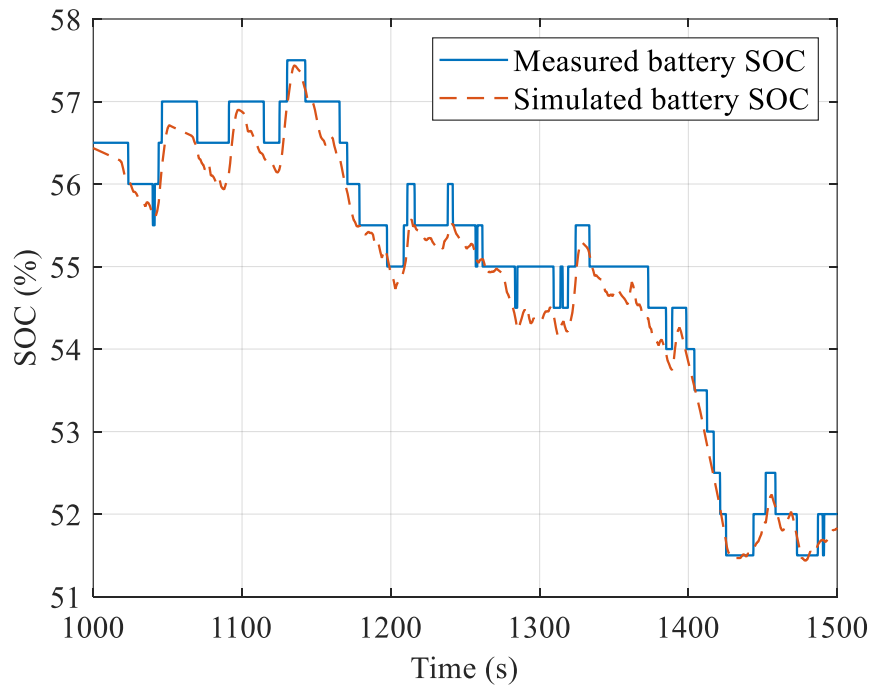
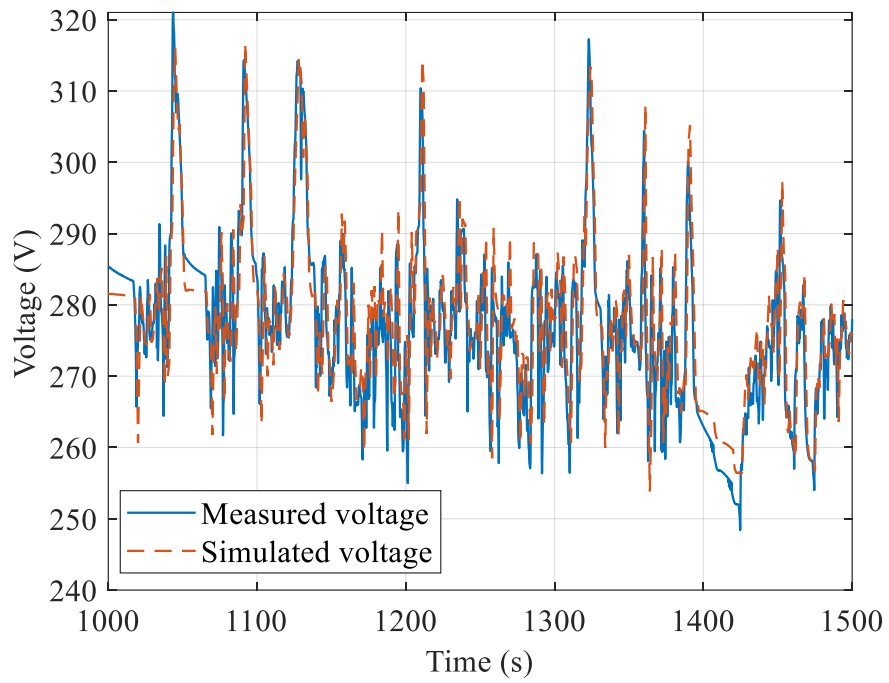


Figure 4-5 Battery model validation a) battery input current b) battery terminal voltage c) battery SOC

Table 4-2 Validation of Battery Model

Data Test ID	RMSE Voltage (%)	RMSE SOC (%)	Correlation Voltage	Correlation SOC
61712033	2.57	0.67	0.9397	0.9914
61712034	1.31	0.66	0.9560	0.9861
61712037	4.05	1.35	0.9834	0.9985

It is crucial to consider the physical limitations of the vehicle, such as the maximum motor torque available, as this will limit the vehicle's acceleration. Maximum available electric motor torque depends on the speed of the electric motor, as shown in Figure 4-6 (blue curve in the efficiency map). The maximum torque curve can be approximated using a minimum function over a second-order polynomial in combination with a constant value (21). This second-order approximation is shown in Figure 4-6 using the black dashed curve.

$$|\tau_{mot}| \leq \min_{\tau}(\tau_{max}, a_2 v_{chass}^2 + a_1 v_{chass} + a_0) \quad (21)$$

Figure 4-6 shows the efficiency map for a combined permanent magnet (PM) electric motor and inverter. This map is generated based on the Toyota Prius motor inverter efficiency map provided in [48] by the U.S. Department of Energy. Since specific Mirai motor efficiency data is not available, and both the Mirai and Prius use PM motors, the Prius map has been scaled to meet the specifications of the Toyota Mirai electric motor.

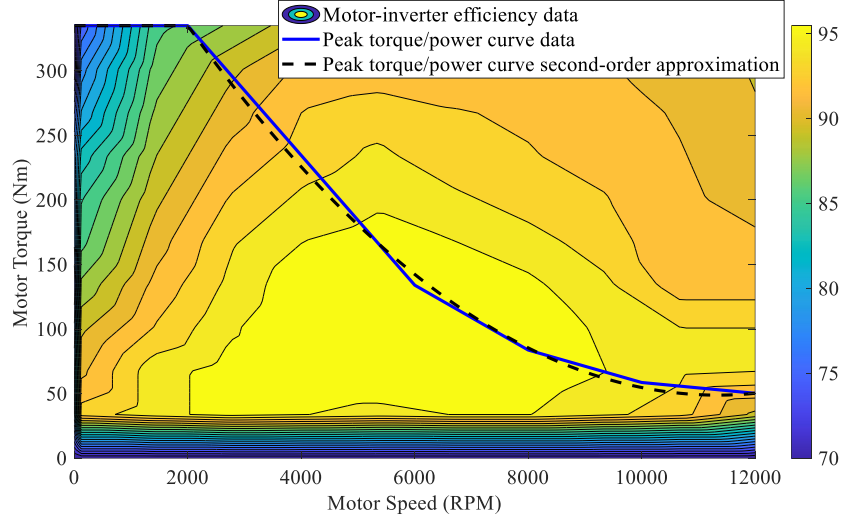


Figure 4-6 Combined PM motor and inverter efficiency map based on [48]

Loss in the combined motor-inverter is expressed in (22), where η_{motinv} is the motor-inverter efficiency. As shown in Figure 4-6, the motor-inverter efficiency is a function of motor speed and torque, and this dependency is implemented using a 2-dimensional look-up table. This 2-D look-up table is utilized every iteration after solving the convex problem using calculated speed and torque characteristics and the value for the motor-inverter efficiency is updated. Equation (23) shows the final drive loss. Since motor torque can have both negative and positive values (braking and accelerating), the loss is always positive. Table 4-3 lists parameter values for the Toyota Mirai that are used in the convex vehicle model and the simulation results in Section III and IV.

$$P_{Motor\ Inverter\ Loss} = \left| \frac{\tau_{mot} f_d (1 - \eta_{motinv})}{r_{wh}} \times v_{chass,i} \right| \quad (22)$$

$$P_{Final\ Drive\ Loss} = \left| \frac{\tau_{mot} f_d (1 - \eta_{fd})}{r_{wh}} \times v_{chass,i} \right| \quad (23)$$

Table 4-3 Vehicle Specifications based on Toyota Mirai

Parameter	Value	Unit
Vehicle mass (m)	1940	Kg
Frontal area (A)	2.38	m ²
Rolling resistance (μ_l)	0.008	-
Aerodynamic drag coefficient (C_d)	0.29	-
Wheel radius (r_{wh})	0.371	m
Final drive ratio (f_d)	3.478	-
Maximum FC output power (P_{FCmax})	113	kW
Maximum battery output power ($P_{battmax}$)	25	kW

Using the preceding loss equations, Figure 4-7 shows an example of how considering the FC efficiency can affect the optimal speed selection, and thus gives motivation for why it should be considered in optimal speed planning (the proposed integrated method). Figure 4-7 shows two ways of calculating the energy consumption of a vehicle model using the Toyota Mirai parameters and travelling at constant speeds over a 5 km trip with 3 kW accessory power. The assumption in this example is that all vehicle demand power comes from the FC stack. One way to calculate energy consumption is to consider the power out of the FC, which is needed to power the traction and accessory needs. Often, this is the power/energy that is attempted to be minimized in other studies that generate optimal speed profiles [16], [42], [43]. In Figure 4-7 (top), the blue line represents this energy for different constant speed options, and the optimal speed is found to be 54 km/h. However, if the hydrogen energy input to the FC is considered instead by dividing FC power by the FC efficiency at that operating point, the red dashed line is obtained for energy consumption, and the optimal speed for energy minimization is found to be 52 km/h. This simple example illustrates the concept used in the proposed integrated optimization method: since the FC

efficiency can affect the optimal speed selection, it should be considered in optimal speed planning.

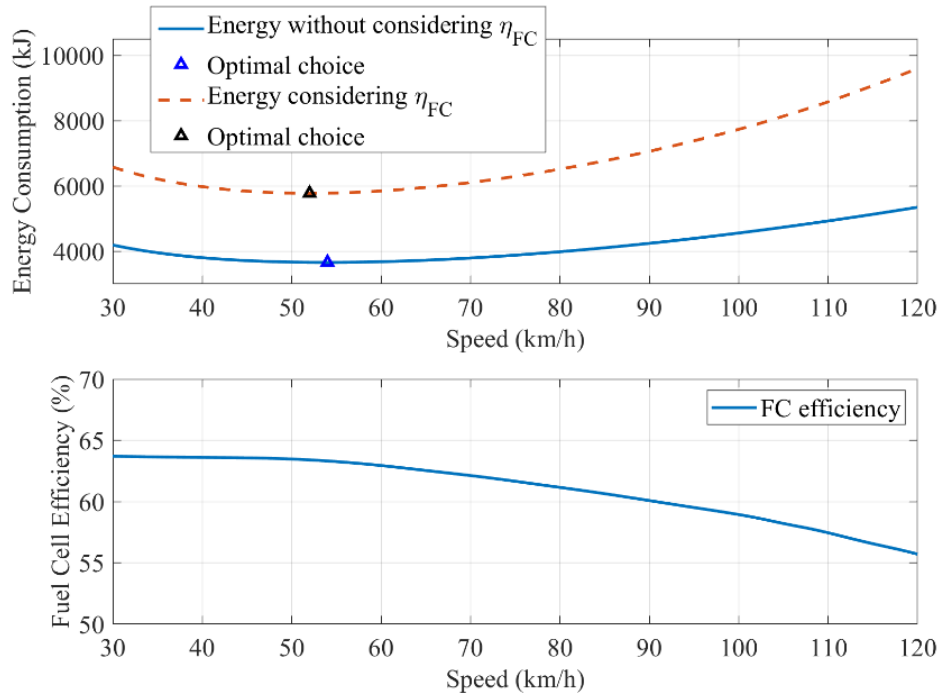


Figure 4-7 . Effect of fuel cell efficiency on energy consumption and optimal speed selection.

4.2.3 Convex Optimization Formulation

In this study, the optimization process has two interconnected parts. The first optimization problem focuses on finding the optimal speed trajectory for the given trip. The second optimization problem aims to perform optimal energy management between the fuel cell and battery. The proposed successive optimization method will be described first, and the proposed integrated method will be described afterwards. As shown in (1), the objective and constraint functions are formulated as convex functions. The objective function of the optimal speed planning problem is set to minimize hydrogen consumption

while maintaining a smooth speed trajectory and short arrival time, using the idea that all vehicle power will ultimately come from the fuel cell. Equation (24) shows this objective function, where α is the energy weight coefficient, P_d is the demand power vector, β is the trip duration weighting coefficient, T_{end} is the arrival time, and k_{speed} is the speed smoothness coefficient.

$$Objective_1 = \alpha \times [P_d^T \Delta t] + \beta \times T_{end} + k_{speed} \times \sum (v_{chass,i+1} - v_{chass,i}) \quad (24)$$

Equation (25) shows that velocity at segment $i+1$ is calculated using velocity at segment i and acceleration as a result of applied electric motor force and resistive forces. To make this function convex, an iterative method is used which is discussed in detail in [7], and variables with \sim mean this value is used from the last iteration.

$$v_{chass,i+1} = v_{chass,i} + \left(\begin{array}{l} \left[\frac{F_{out_fd}}{m} \right] - \left[(g \times \cos(\theta_i)) \times (\mu_1 + \mu_2 \times v_{chass,i}) \right] - \\ \left[g \times \sin(\theta_i) \right] - \left[\frac{1}{2} \times \frac{\rho_{air} \times A \times C_d \times (\tilde{v}_{chass,i} - v_{wind,i})^2}{m} \right] \end{array} \right) \times \left(\frac{\Delta x_i}{\tilde{v}_{chass,i}} \right) \quad (25)$$

To calculate the time at each segment, the expression is shown in (4). It is crucial to set an acceptable limit for the arrival time to make the optimal speed meet the expected criteria, and this constraint is shown in (26), where T_{min} and T_{max} are the minimum and maximum of the acceptable arrival times.

$$T_{\min} \leq T_{end} \leq T_{\max} \quad (26)$$

Since the method uses calculated time sample values from the last iteration, the variable T_{end} for the current iteration is calculated directly in the current iteration. To achieve this goal, an additional variable is added to the optimization formulation, as explained in [49]: the parameter σ_i effectively approximates $1/v_i$ as shown in (27), and using this parameter, T_{end} can be explained in a convex way as shown in (28). ($\|\bullet\|$ is notation used for Euclidean norm (norm-2) for example $\|x\| = \sqrt{x_1^2 + x_2^2 + \dots}$)

$$\left\| \frac{2}{v_i - \sigma_i} \right\| \leq v_i + \sigma_i \quad (27)$$

$$T_{end} = \sum_i \Delta x_i \times \sigma_i \quad (28)$$

Demand power at each segment is calculated in (29), where P_{acc} is the accessory power at each segment, representing the power needed for the control unit of an autonomous vehicle, HVAC system, and other accessories of the vehicle. In (29), ψ^+ represents the positive values of motor torque, τ_{mot} , so that by minimizing over ψ^+ , τ_{mot} will effectively be minimized. Equation (30) shows the constraints on ψ^+ . Overall, (29) sums up the losses in the vehicle, where the first term represents the power needed to overcome external losses (such as rolling and aerodynamic losses), the second term represents losses of the electrical accessories, the third term represents the final drive losses, the fourth term represents the motor and inverter losses, and the fifth term represents the battery losses.

$$P_{d,i}^+ = \frac{\psi_i^+ \times \tilde{v}_{chass,i} \times f_d}{r_{wh}} + P_{acc,i} + \left| \frac{\tau_{mot} f_d (1 - \eta_{fd})}{r_{wh}} \times \tilde{v}_{chass,i} \right| + \left| \frac{\tau_{mot} f_d (1 - \eta_{motinv})}{r_{wh}} \times \tilde{v}_{chass,i} \right| + R_b I_b^2 \quad (29)$$

$$\tau_{mot} \leq \psi^+ \quad , \quad 0 \leq \psi^+ \quad (30)$$

In addition to these constraints, some initial value assignments should be set in the formulation: velocity at the start of the section and time at the start of the section. In this chapter, a section is defined as a part of the trip that speed planning is performed for, where the initial speed is known (either starting from a stationary position or the calculated end velocity of the last section) and the end velocity can be known (where the vehicle needs to meet a certain velocity, or needs to stop at a stop sign, or is chosen by the optimization algorithm to be in the acceptable range). Equations (31) and (32) express these constraints, where $V_{initial}$ is the initial velocity at the start of the section, and $T_{initial}$ is the start time of that section.

$$v_{chass,1} = V_{initial} \quad (31)$$

$$t_1 = T_{initial} \quad (32)$$

Considering these constraints, the optimization formula can be constructed. Equation (33) shows the first optimization problem.

$$\begin{aligned}
& \min_{t,v,\tau} \quad (24) \\
& s.t. \quad (33) \\
& (4), (25), (26), (27), \\
& (28), (29), (30), (31), (32)
\end{aligned}$$

Solving (33) results in the optimal time and speed vectors which are used as the inputs for the second optimization problem of the proposed successive method. Using (29), demand power of the generated optimal time and speed vector is calculated. The second optimization objective (34) is to find the best energy management algorithm to use the least amount of H₂ while maintaining battery SOC in an acceptable range throughout the trip, and ensuring the final SOC is equal to the initial SOC, so the strategy is charge sustaining. Since the strategy is charge sustaining over each trip, the objective function can seek only to minimize hydrogen use and does not need to consider net changes in the battery energy, similar to the approach used in [32], [34].

$$Objective_2 = \frac{1}{\rho_{H_2}} \times \left(\left[\begin{array}{c} \left(\frac{P_{FC}}{\eta_{FC}} \right)^T \\ \Delta t_{calc} \end{array} \right] \right) \quad (34)$$

In (34), ρ_{H_2} is the hydrogen energy density, P_{FC} is the output power of the FC system, and Δt_{calc} is generated using the calculated time vector from the first optimization problem. Total demand power at the DC bus, P_d , must be provided by the available energy sources, as shown in (35), where P_{brake} is the friction braking power, P_{batt+} is the positive battery power at the battery terminals (battery discharge), P_{batt-} is the negative battery power

at the battery terminals (battery charge), and $\eta_{converter}$ is the battery DC/DC converter efficiency.

$$P_d = P_{FC} + P_{batt^+} \times \eta_{converter} + \frac{P_{batt^-}}{\eta_{converter}} + P_{brake} \quad (35)$$

FC output power should always be between zero and its maximum output power since the FC cannot accept negative power. Positive and negative battery output powers should also stay in the feasible range and brake power can only obtain negative values. These constraint functions are shown in (36)-(39).

$$0 \leq P_{FC} \leq P_{FCmax} \quad (36)$$

$$0 \leq P_{batt^+} \leq P_{batt^+max} \quad (37)$$

$$-P_{batt^+max} \leq P_{batt^-} \leq 0 \quad (38)$$

$$P_{brake} \leq 0 \quad (39)$$

Using (20), a discrete SOC update algorithm is used to determine the battery SOC through the trip in (40). The constraint of charge sustainability is shown in (41) and (42), where SOC_{init} is the initial value of battery SOC. To prevent any sudden changes in the output power of the FC system, its rate of increase/decrease is limited to an acceptable range using (43). The limitation of fuel cell fluctuation is used as suggested in [50]. (

$$|\Delta P_{FC}| = 80 \text{ kW/s})$$

$$SOC_{i+1} = SOC_i - \left[\left(\frac{P_{batt^+} + P_{batt^-}}{V_{oc} \times C_{Ah} \times 3600} \right) \times (t_{calc,i+1} - t_{calc,i}) \right] \quad (40)$$

$$SOC_1 = SOC_{init} \quad (41)$$

$$SOC_{end} = SOC_{init} \quad (42)$$

$$\frac{|P_{FC,i+1} - P_{FC,i}|}{(t_{calc,i+1} - t_{calc,i})} \leq \Delta P_{FC} \quad (43)$$

The second optimization problem is formulated using the equations in (44).

$$\begin{aligned} & \min_{P_{FC}, P_{batt^+}, P_{batt^-}, P_{break}} \quad (34) \\ & s.t. \quad (44) \\ & (35), (36), (37), (38), \\ & (39), (40), (41), (42), (43) \end{aligned}$$

The preceding equations and explanations constitute the proposed successive optimization method, as shown in Figure 4-1 (a). Using this framework, the following additions are proposed to create the integrated optimization method in Figure 4-1 (b). For the integrated method, using the findings of (44), the value of FC efficiency can be updated using the detailed FC efficiency map, and these new values are used to solve (33), and update calculated results for time and velocity (optimal speed trajectory). This loop will continue until either of the loop ending conditions are satisfied: (i) convergence of the speed profiles, or (ii) reaching the maximum allowed time for algorithm execution. This

algorithm sequence is shown in Figure 4-8, where the difference in the successive method is that there will be no feedback loop to update the FC system efficiency (η_{FC}).

The optimization procedure is performed over a window of prediction ahead and this window is divided into k segments. In study cases where there are no pre-defined velocity points to reach over the trip (as discussed in Sections III-A and III-B) the window size is kept constant over the trip. In cases where there are logged data and pre-defined velocity points (as discussed in Section III-C) the window is set to the distance between each two points, and its size may change throughout the trip.

To study the effects of the FC system efficiency on the optimal speed planning, the formulation in (24) is adjusted in a way to include the FC system efficiency as shown in (45). Therefore, the objective in (24) is used in the successive method when solving (33), and the objective in (45) is replaced in the integrated method when solving (33).

$$Updated\ Objective_1 = \alpha \times \left[\left(\frac{P_d}{\eta_{FC}} \right)^T \Delta t \right] + \beta \times T_{end} + k_{speed} \times \sum (v_{chass,i+1} - v_{chass,i})$$

(45)

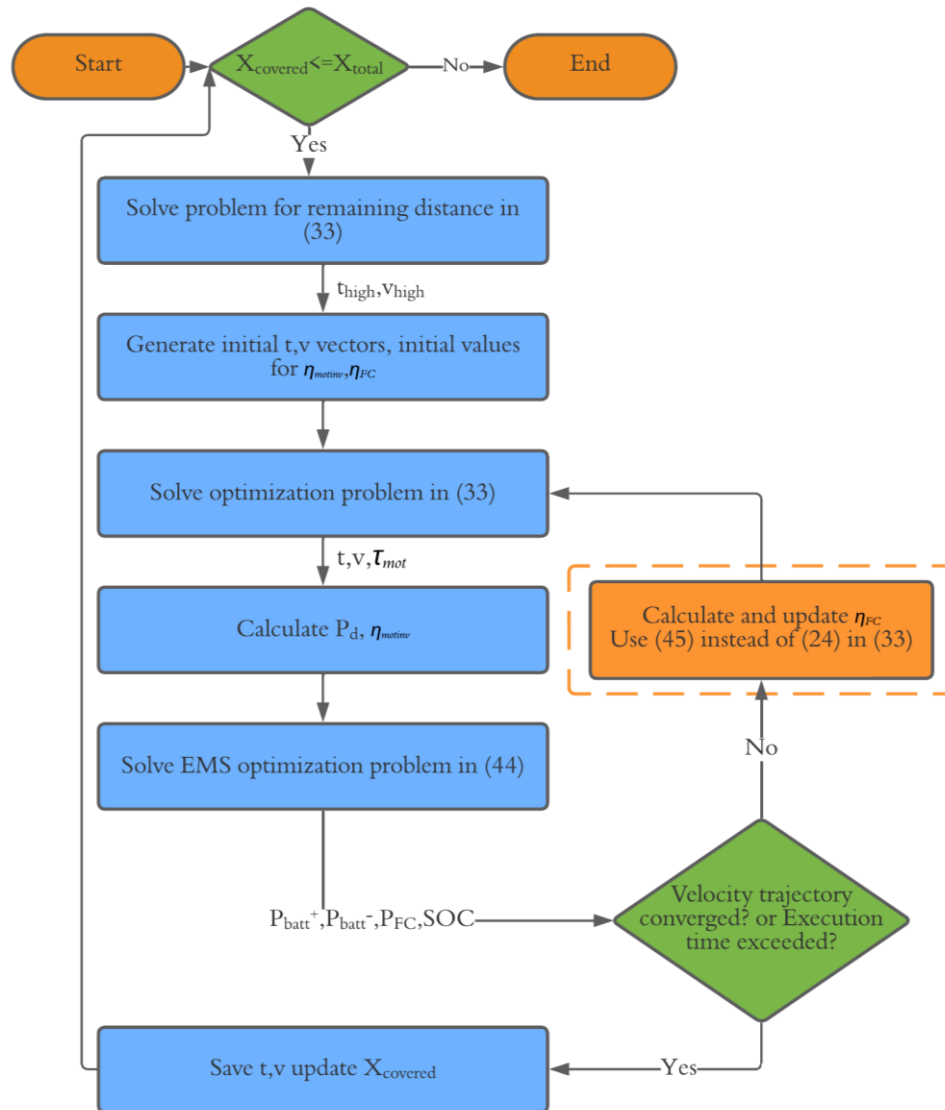


Figure 4-8 Integrated optimization algorithm flowchart (the successive method does not contain the orange-encircled part)

Section III discusses how in some cases, generated speed profiles are below average city driving velocity. To address this, a penalty factor is added to the objective function for

being away from the desired speed. The adjusted objective function is shown in (46), where V_{des} is the vector of the desired velocity over the trip.

$$Objective_I = \alpha \times \left[\left(\frac{P_d}{\eta_{FC}} \right)^T \Delta t \right] + \beta \times T_{end} + k_{speed} \times \sum (v_{chass,i+1} - v_{chass,i}) + k_{des} \times \sum |v_{chass,i} - V_{des,i}| \quad (46)$$

4.3 Convex Simulation Results and Discussion

To study the performance of the proposed algorithms, optimization problems are formulated and solved using CVX software inside MATLAB using SeDuMi solver [51-53].

4.3.1 Short Test Cycle Results

To study the effect of considering the FC efficiency in the objective function, three cases are tested using different methods: the integrated method, the successive method, and an arbitrary method. These trips are set to travel two different distances (1000 m and 1500 m) with a maximum speed of 60 km/h. Also, these trips start from a zero speed (stationary condition) and end at zero speed. The resulting 1000 m optimal speed trajectory is shown in Figure 4-9. Both convex-successive and convex-integrated methods have a notably different profile shape compared to an arbitrary trip with mostly constant speed, as they accelerate to a higher speed at the start of the trip and decelerate slowly for most of the trip. Compared to the successive method, the effect of the integrated method can be

seen in the generated speed profile, where using the feedback of FC system efficiency means this method tries to lower the speed at the top speed area to minimize the FC power demand to allow the FC to operate at a higher efficiency. Table 4-4 summarizes the findings for H₂ consumption, showing improvement in the hydrogen consumption of the proposed methods compared to an arbitrary speed profile with optimized EMS. Both methods (integrated and successive) have notable advantages over the arbitrary speed profile in terms of H₂ consumption (more than 10% over all trips). Furthermore, the integrated method shows an advantage over the successive method of 0.27% to 2.37%. Since the successive method is still performing optimization, the improvement of the integrated method is not expected to be large but is still relevant and useful given the fact that it is simple to implement.

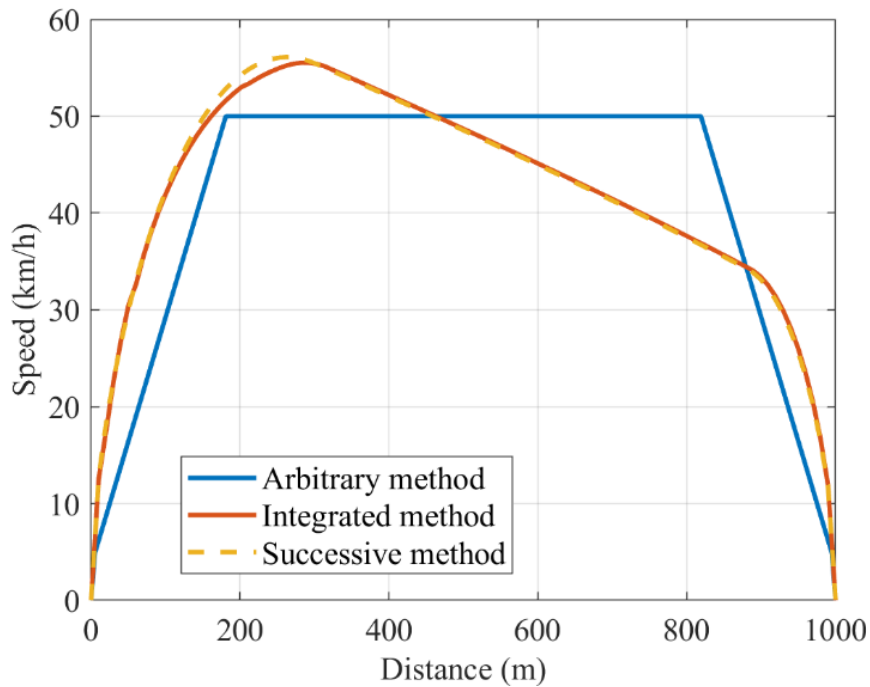


Figure 4-9 Comparison of arbitrary speed profile with optimal results from successive and integrated methods

Table 4-4 Optimization Results for Short Test Cycles

Trip (m)	Distance	Method	H ₂ Consumption (g)	Advantage of Integrated Method (%)
1000		Arbitrary	8.37	14.65
		Successive	7.32	0.27
		Integrated	7.30	-
1500		Arbitrary	14.89	10.70
		Successive	13.77	2.37
		Integrated	13.45	-

4.3.2 Electric Accessory Sensitivity Analysis

Since the vehicle electrical accessory loads can vary widely over the day or over the year, mainly due to changing heating and air conditioning needs, it is useful to investigate how the proposed optimization framework performs at different accessory load levels. This section performs a sensitivity analysis on the proposed formulations using values of $P_{acc} =$

1 kW, 2.5 kW, 5 kW, and 8 kW. The optimal speed trajectory results are shown in Figure 4-10 for the 1000 m trip. These results show that for both the successive and integrated methods, a higher P_{acc} leads to higher optimal speeds since a longer travel time will result in higher energy consumption at higher P_{acc} – thus the optimization process tries to speed up the trip, though all trips are completed within the upper limit allowed, T_{end} . Thus, a higher P_{acc} value acts as a higher coefficient for arrival time in (24). Comparing the successive and integrated speed curves for the same P_{acc} value shows that the integrated method reduces speed (and hence fuel cell power) at some peak speed areas due to the feedback of FC efficiency, which lowers FC power at otherwise high power points to increase FC efficiency. Table 4-5 summarizes the hydrogen consumption for each speed trajectory in Figure 4-10. Compared to the arbitrary speed trajectory, the integrated method reduces hydrogen use by 10% to 21%. Compared to the successive method, the integrated method reduces hydrogen use by about 0.2% to 0.7%.

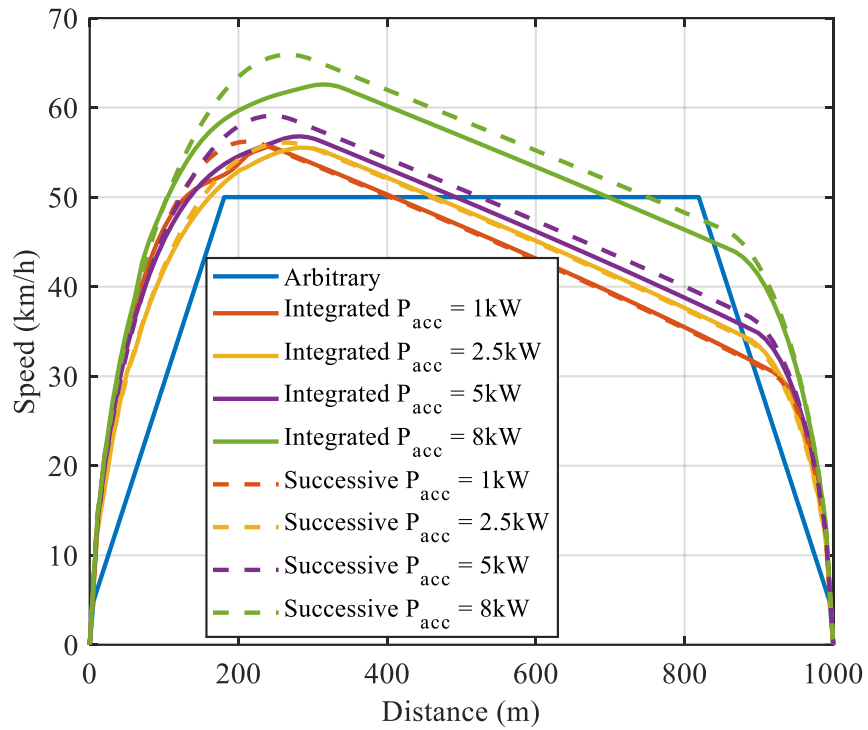


Figure 4-10 Sensitivity analysis optimal speed trajectories for different values of electric accessory power

Table 4-5 Optimization Results for Sensitivity Analysis of P_{acc}

P_{acc} (kW)	Method	H ₂ Consumption (g)	Advantage of Integrated Method (%)
1	Arbitrary	5.98	10.12
	Successive	5.47	0.73
	Integrated	5.43	-
2.5	Arbitrary	8.37	14.65
	Successive	7.32	0.27
	Integrated	7.30	-
5	Arbitrary	12.21	16.06
	Successive	10.54	0.19
	Integrated	10.52	-
8	Arbitrary	17.04	21.62
	Successive	14.06	0.35
	Integrated	14.01	-

4.3.3 Logged Driving Cycle Results

To show the effect of optimal speed planning on hydrogen consumption, three different driving scenarios are studied. This experimentally logged data is selected from publicly available data from Argonne National Laboratory, and is generated using dynamometer testing of a 2017 Toyota Mirai [47]. These trips are selected in a way to start and end in a stationary condition ($v_{start} = 0$), cover different distances, and reach various top speeds to cover distinct driving situations (city or highway). The accessory power in these simulations is set to 2.5 kW, reflecting a moderate heating or air conditioning load. To make this comparison more realistic, sample points through the trip are selected to make the optimal speed trajectory go through the same velocity points. In real-time driving, these points represent known future points in the road due to changes in speed limit or the need to slow down to perform a turn. These sample points are added to the optimization problem as constraints and the algorithm runs for each portion between these sample points and finds the optimal speed trajectory in between them. In all the case studies presented below, the integrated method is used since it yields the most advantageous results, based on Section III-A. In these simulation studies, the H₂ consumption advantage is only the result of optimal speed planning since the same EMS (optimization problem in (44)) is performed for the real-world logged driving cycle as well, for a fair comparison. Results for these investigations are illustrated in Figs. 11 to 13 for the three selected driving scenarios.

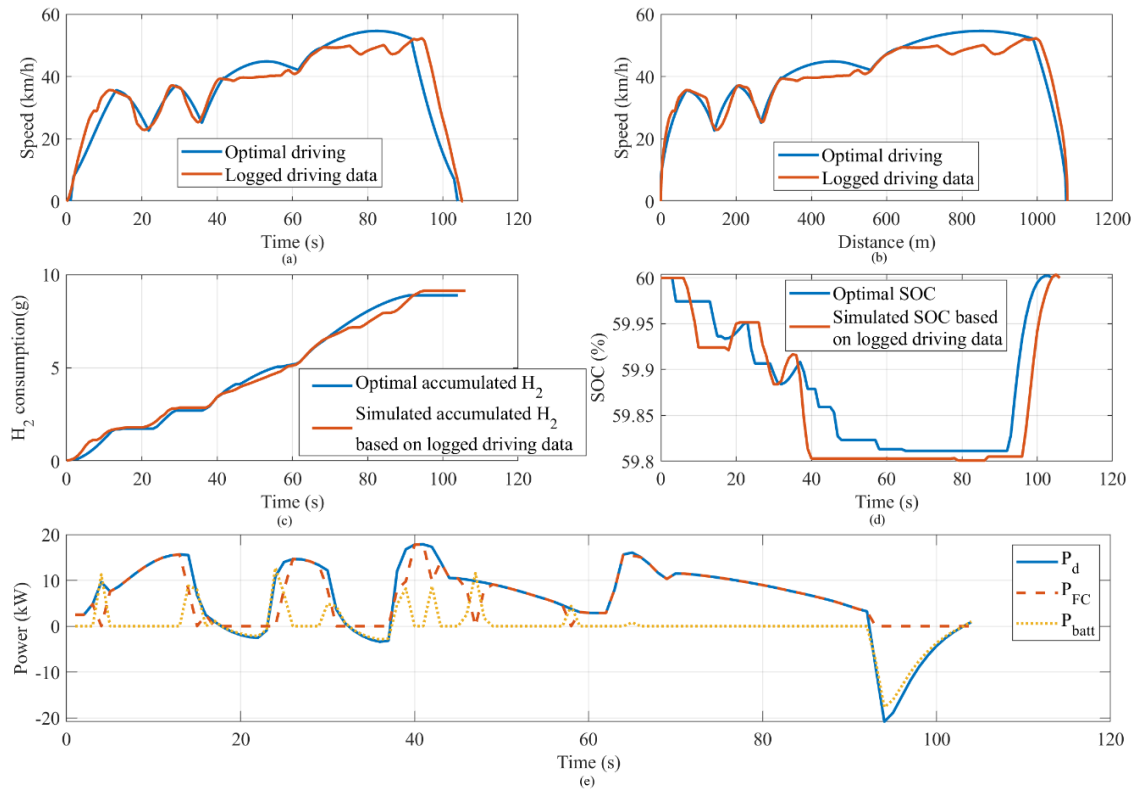


Figure 4-11 Optimal vs logged driving for Trip 1: a) time-speed trajectory b) distance-speed trajectory c) cumulative H₂ consumption d) time-SOC curve e) optimal power split based on optimal speed planning

Figure 4-11 shows a comparison between optimal and logged driving speeds for a 1080 m trip with a maximum speed of 53 km/h, which represents typical city driving. The optimal speed trajectory meets the high and low velocity points through the trip at the same distance points of the real-world driving, but between these points, the algorithm is free to choose the speed trajectory. The speed profile is smooth between the fixed velocity points and avoids frequent acceleration and deceleration. This smoothness of the speed profile also affects the SOC curve and decreases its fluctuations. Figure 4-11 also shows that the EMS is working properly in charge-sustaining mode as the battery SOC at the end of the

trip is equal to its initial value, 60%. Interestingly, the optimal speed path is able to finish the trip in shorter time than the logged trip, as shown in Figure 4-11 (a). The optimal H₂ advantage on this trip is 2.82% compared to logged driving, where both the optimal and logged speeds use the optimal EMS.

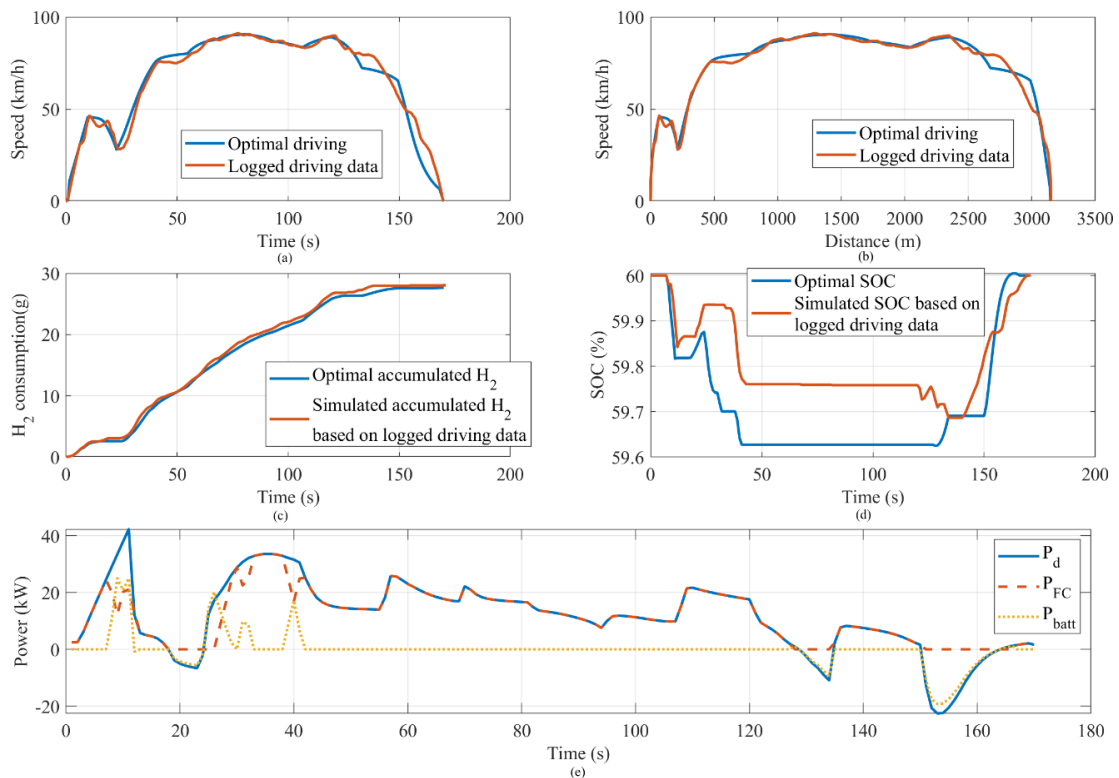


Figure 4-12 . Optimal vs logged driving for Trip 2: a) time-speed trajectory b) distance-speed trajectory c) cumulative H₂ consumption d) time-SOC curve e) optimal power split based on optimal speed planning

Figure 4-12 shows the simulation results of a 3152 m trip with a top speed of 92 km/h, which is a combination of city and highway driving. The optimal speed trajectory is smooth and reaches the predefined velocity points. In the power management process (Figure 4-12 (e)), it is shown that the optimal EMS algorithm tries to recharge the battery

as much as possible during the braking and uses this power in the acceleration events, and the EMS maintains the SOC at the end of the trip. The amount of decrease in H₂ consumption of the optimal speed profile for this trip is 1.43%.

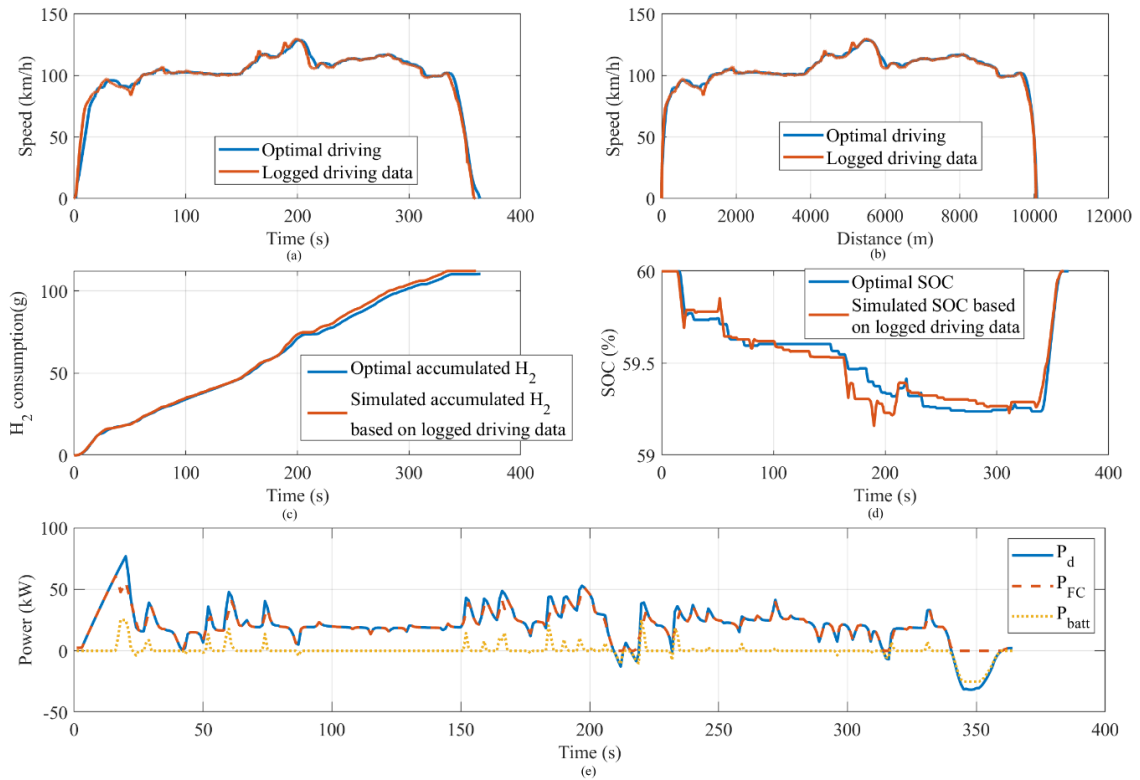


Figure 4-13 Optimal vs logged driving for Trip 3: a) time-speed trajectory b) distance-speed trajectory c) cumulative H₂ consumption d) time-SOC curve e) optimal power split based on optimal speed planning

Figure 4-13 shows the simulation results for a long trip of about 10 km, where the vehicle mostly maintains a high speed above 95 km/h and reaches the top speed of 130 km/h. The optimal speed trajectory eliminates most of the fluctuations of real-world driving. Since the speed profile does not contain many braking sections, chances to save

regenerative power are limited. Similar to the other scenarios, the charge is sustained over the trip and the ending SOC is equal to the initial SOC. Optimal speed for this trip provides 1.90% improvement in H₂ consumption. Table 4-6 summarizes the reduction in H₂ consumption for these cases for only optimizing the speed profile using the integrated method (since the optimal EMS split is used for all simulations in these cases).

Table 4-6 Summary of Results for Optimal speed vs logged speed (both using optimal EMS)

	Trip distance (m)	Optimal Speed H ₂ Consumption (g)	Logged Speed (non-optimal) H ₂ Consumption (g)	H ₂ Consumption Reduction (%)
Trip 1	1080	8.88	9.13	2.82
Trip 2	3152	27.65	28.05	1.43
Trip 3	10200	109.99	112.05	1.90

4.3.4 Road Speed Limit Changes

In some cases, the optimal speed trajectory may have maximum speeds lower than the speed limit on a road section. To address this issue, (46) can be used to add a penalty factor for being away from a desired speed. The results of the algorithm with the new objective function (46) are shown in Figure 4-14. For this study, the desired speed limits over the trip are specified in (47) and are shown in Figure 4-14 with a red dashed line. By using this algorithm, the optimal speed tries to reach the desired velocities through the trip and chooses the optimal profiles for the transition. The desired speed can be selected for different parts of the path considering the traffic rules and maximum allowed speed.

$$\left\{ \begin{array}{ll} & 0 \leq X < 200 \\ V_{des} = 50 \text{ km/h} & 1400 \leq X \leq 1600 \\ & 200 \leq X < 600 \\ V_{des} = 70 \text{ km/h} & 1200 \leq X < 1400 \\ & 600 \leq X < 1200 \\ V_{des} = 85 \text{ km/h} & \end{array} \right. \quad (47)$$

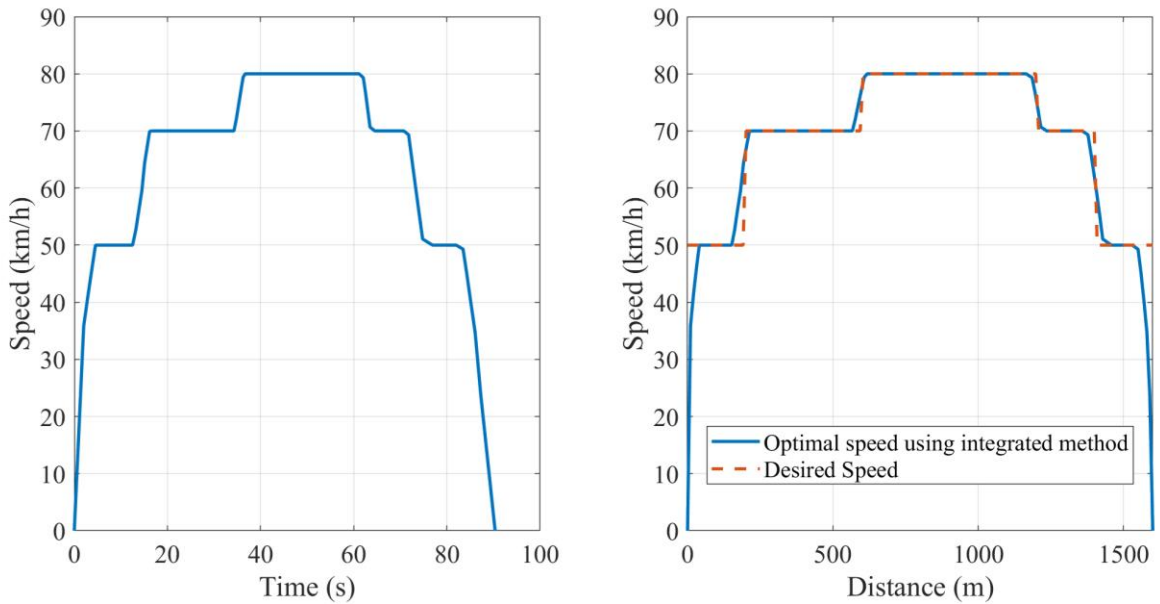


Figure 4-14 Optimal speed trajectory with addition of desired velocity to the objective by (a) time, and (b) distance

4.3.5 Computational Effort Analysis

Figure 4-15 shows the trade-off between each iteration time and H_2 consumption (a reflection of optimality), using different numbers of segments to divide up a given trip. Values on the y-axis represent the amount of time spent on solving the optimization problem using Mosek [54] solver integrated in the CVX software in MATLAB, and the x-

axis shows the H₂ usage during the simulated test case. These simulations are run on a Dell laptop computer with core i7 2.8 GHz CPU and 16 RAM. This study considers a 1km road with a constant 2.5 kW accessory power throughout the trip. As the number of segments in an optimization window increases, the optimal H₂ consumption decreases as expected due to higher accuracy, but the execution time increases, which is the inevitable cost for getting more precise results. Regardless, these results show that excellent optimality can be achieved in short simulation times that are suitable for on-board real-time implementation. Though multiple iterations may be used for each trip (four are used in the DP comparison), the total run-time can still remain well below one second. Even though implementation of this suggested algorithm on a microcontroller will have less computational power compared to a laptop with multiple cores, it is a well-known fact that coding in lower-level coding languages such as C++ will make code a lot faster.

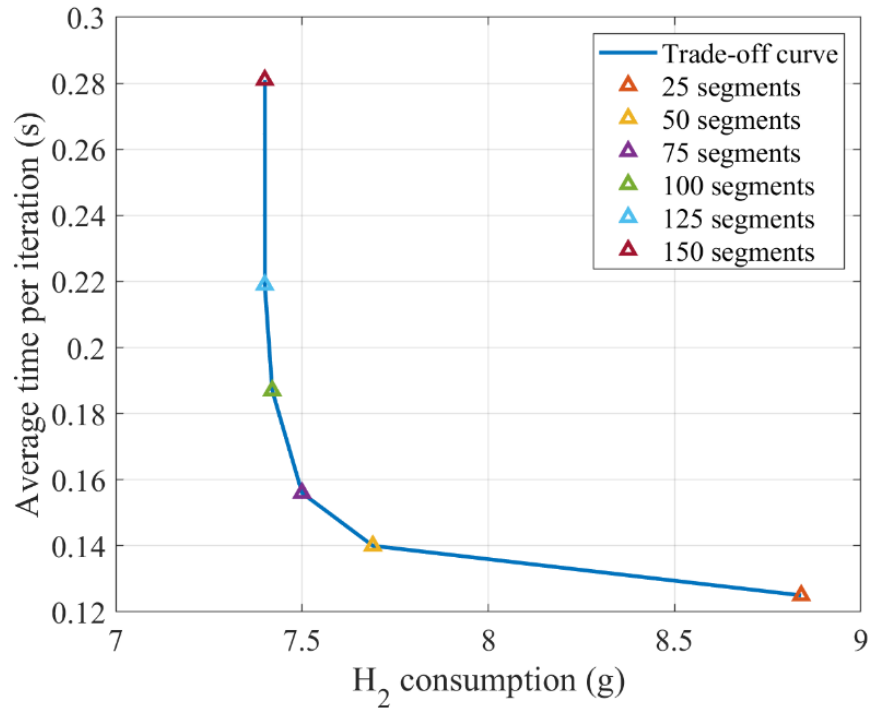


Figure 4-15 Optimal speed trajectory with addition of desired velocity to the objective

4.4 Convex Comparison to Dynamic programming

In this section, the results of the proposed convex formulations are compared to results from dynamic programming, which is often used as an optimization benchmark [43]. Dynamic programming (DP) aims to find the optimal solution by determining the optimal decision at each time step considering the current state of the system [55]. The main drawback to DP is the high computation time, which often renders it unsuitable for real-time implementation. For example, [43] allows only 5 options of motor torque for each segment to try to deal with DP's curse of dimensionality, yet these few torque options cannot cover all possible optimal vehicle motions, so the result is sub-optimal. Thus, for DP, the accuracy of the optimal solution is highly dependent on the precision of the problem

formulation and the discretization of optimization variables. Therefore, there is a clear tradeoff in DP formulations of run-time versus accuracy. Due to this curse of dimensionality, using DP to solve both the speed planning and EMS problem in an integrated way is infeasible with standard computing resources if a high discretization of motor torque options is desired. Reference [43] attempts this process but must use only 5 torque options, leading to a non-optimal result and a very high runtime. Thus, in order to obtain a more truly optimal speed profile to compare to the convex solution, this chapter uses DP to find the optimal speed profile only using 135 motor torque options, leading to a torque discretization of 5 Nm. Then, the optimal EMS is found for the determined speed profile using the convex formulation given in (44).

4.4.1 Dynamic Programming Formulation

The general concept of DP can be described as assuming a sequence of terminal functions T_1, T_2, \dots, T_n where γ is an argument representing the state of the system at time $i \in [1 \dots n]$. The value of $T_n(\gamma)$ is the value at the last time sample in state γ . The value obtained by T_i in earlier time samples $i = 1, 2, \dots, n-1$ is calculated backwards using a recursive method (Bellman equation) [55]. For $i = 2, \dots, n$ the terminal value of T_{i-1} at any state γ is calculated using the value of T_i (cost to reach T_i from T_n) and the cost of the decision at time $i-1$ based on the current state and decision. This process is done until the final value for T_1 at the initial state of the system is found, which is the optimal value of the optimal policy. Then by tracking back the calculations that have already been done, the optimal path (decision) is recovered.

The problem of optimal speed planning for FCHEVs using DP is studied in prior literature [43]. The DP formulation in this chapter follows the method presented in [43]. The state vector γ has two variables (time and vehicle speed) and the input, u , has a single variable (motor force, F_{mot}). The optimal speed planning problem over a given trip distance is found using (48), which is solved using *dpm* (a generic DP MATLAB function) [56].

$$J = \int_0^{x_f} F_{mot} \eta_{motinv}(F_{mot}, \gamma_2) dx \quad (48a)$$

$$\gamma = [\gamma_1, \gamma_2]' = [t, v_{chas}]' \quad (48b)$$

$$u = [u_1] = [F_{mot}] \quad (48c)$$

$$\dot{\gamma}_1 = \frac{1}{\gamma_2} \quad (48d)$$

$$\dot{\gamma}_2 = \frac{u_1 - F_{resisting}}{m\gamma_2} \quad (48e)$$

$$\gamma_1(0) = 0 \quad \gamma_2(0) = v_0 \quad (48f)$$

$$\gamma_1(x_f) = t_f \quad \gamma_2(t_f) = v_f \quad (48g)$$

In (48a), J is the cost function to be minimized which represents energy, η_{motinv} is the motor efficiency which is a function of motor force (torque converted to force) and speed. Equations (48d) and (48e) show how the transition between states is happening, where $F_{resisting}$ is the sum of resisting forces; since all equations are in the distance domain, the derivatives are also with respect to distance. In (48f) and (48g) the initial and final values for the state variables are shown where v_0 is the initial speed, v_f is the final speed, and t_f is

the final time. Attempts to solve this DP problem have confirmed that discretizing motor torque into more segments achieves better results in terms of energy consumption. The discretization used to solve this problem is: $\Delta x = 10$ m, $\Delta t = 1$ s, $\Delta v = 1$ m/s, and $\Delta \tau = 5$ Nm. The resulting optimal speed trajectory of the DP problem (t and v) is fed into the convex EMS problem (44) to allow a fair comparison between the DP and convex method for optimal speed planning.

4.4.2 Dynamic Programming Results

Two scenarios are analyzed: trips of 1000 m and 1500 m with a maximum speed limit of 100 km/h. The DP method takes 64.8 and 110.3 seconds to determine the solution for the two study cases, respectively. The optimal speed trajectories for DP, convex-integrated, and convex-successive methods are shown in Figure 4-16. The convex speed trajectories have a similar shape to that of DP but have a slower acceleration and reach a higher peak speed. As found previously, the integrated method reduces speed near the peak compared to the successive method to avoid the lower efficiency regions of fuel cell operation. Table 4-7 compares the equivalent hydrogen consumptions of these three speed trajectories. Since the same EMS method (44) is used to generate the optimal energy allocation, the difference in the equivalent hydrogen consumption is only the result of the speed profile differences. The results show that the proposed convex-integrated method performs within 1% of the DP method, and the convex-successive method performs within 2.6% of the DP method. However, the convex methods have a much lower computational burden and thus a faster calculation time (0.748s and 0.873s for four iterations, respectively), meaning they can be run in real-time.

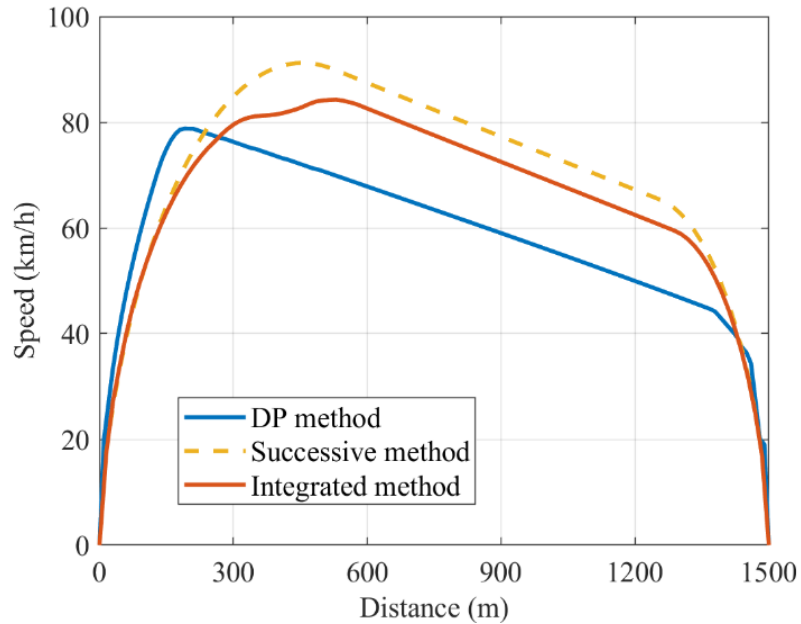


Figure 4-16 Comparison between three speed trajectories generated using the integrated method, successive method, and DP method

Table 4-7 Equivalent Hydrogen Consumption Comparison for DP Method

Trip (m)	Distance (m)	Method	H ₂ Consumption (g)	Advantage of DP Method (%)
1000		DP	7.24	-
		Successive	7.32	1.10
		Integrated	7.30	0.82
1500		DP	13.42	-
		Successive	13.77	2.60
		Integrated	13.45	0.22

4.5 Conclusions and Future Work

This chapter presents novel successive and integrated convex speed planning and energy management algorithms to solve the minimum hydrogen consumption problem for autonomous FCHEVs. For the proposed convex formulations, an iterative method is used to utilize the detailed FC system and motor-inverter efficiency maps in the objective

functions. The component models are carefully created and validated according to experimentally logged data from the Toyota Mirai. The simulation results show that the proposed integrated method, which considers FC system efficiency in the optimization objective function for speed planning, leads to 0.19% to 2.37% less hydrogen consumption compared to the successive method on short drive cycles with varying accessory loads. On the same test cycles, the integrated method uses 10.12% to 21.62% less hydrogen than an arbitrary constant-speed profile. Furthermore, when considering real-world logged drive cycles, the proposed integrated method reduces hydrogen use by 1.43% to 2.82% just through speed optimization, since an optimal EMS is used for both cases. A computational effort analysis shows that the proposed algorithms are suitable for real-time implementation on autonomous FCHEVs, since each calculation iteration takes between 0.13 s and 0.28 s on standard computing resources, depending on the selection of number of segments in each window. Finally, a detailed comparison to a DP benchmark formulation, which cannot run in real-time, shows that the proposed integrated convex method results in hydrogen use within 1% of the optimal DP result. Future work will focus on adding the consideration of other vehicles on the road (i.e., fleet-level optimization) and will try to determine its influence on optimal speed planning.

4.6 Chapter 4 References

- [1] H. B. Jensen, E. Schaltz, P. S. Koustrup, S. J. Andreasen and S. K. Kaer, "Evaluation of Fuel-Cell Range Extender Impact on Hybrid Electrical Vehicle Performance," in *IEEE Transactions on Vehicular Technology*, vol. 62, no. 1, pp. 50-60, Jan. 2013, doi: 10.1109/TVT.2012.2218840.
- [2] C. -H. Chung, S. Jangra, Q. Lai and X. Lin, "Optimization of Electric Vehicle Charging for Battery Maintenance and Degradation Management," in *IEEE Transactions on Transportation Electrification*, vol. 6, no. 3, pp. 958-969, Sept. 2020, doi: 10.1109/TTE.2020.3000181.
- [3] J. K. Kenny, S. Breske, en N. R. Singstock, "Hydrogen-powered vehicles for autonomous ride-hailing fleets", *International Journal of Hydrogen Energy*, 2022.
- [4] S. A. Bagloee, M. Tavana, M. Asadi, en T. Oliver, "Autonomous vehicles: challenges, opportunities, and future implications for transportation policies", *Journal of Modern Transportation*, vol 24, no 4, bll 284–303, Des 2016.
- [5] J. A. Baxter, D. A. Merced, D. J. Costinett, L. M. Tolbert, and B. Ozpineci, "Review of electrical architectures and power requirements for automated vehicles," in *Proc. IEEE Transp. Electrific. Conf. Expo (ITEC)*, Long Beach, CA, USA, Jun. 2018, pp. 944–949
- [6] A. Meshginqalam and J. Bauman, "An Onboard Real-Time-Implementable Framework for Calculating the Optimal Cruising Speed of Electric Autonomous Vehicles," 2019 *IEEE Transportation Electrification Conference and Expo (ITEC)*, 2019, pp. 1-6, doi: 10.1109/ITEC.2019.8790538.
- [7] A. Meshginqalam and J. Bauman, "Two-Level MPC Speed Profile Optimization of Autonomous Electric Vehicles Considering Detailed Internal and External Losses," in *IEEE Access*, vol. 8, pp. 206559-206570, 2020, doi: 10.1109/ACCESS.2020.3038050.
- [8] A. Meshginqalam and J. Bauman, "Investigation of Critical Parameters for Selecting Energy-Optimal Cruising Speed Using a Low-Computation Framework," in *IEEE Transactions on Industry Applications*, vol. 57, no. 3, pp. 2825-2837, May-June 2021, doi: 10.1109/TIA.2021.3057037.
- [9] V. Larsson, L. Johannesson Mårdh, B. Egardt, and S. Karlsson, "Commuter route optimized energy management of hybrid electric vehicles," *IEEE Trans. Intell. Transp. Syst.*, vol. 15, no. 3, pp. 1145–1154, Jun. 2014.
- [10] G. Ma, M. Ghasemi, and X. Song, "Integrated powertrain energy management and vehicle coordination for multiple connected hybrid electric vehicles," *IEEE Trans. Veh. Technol.*, vol. 67, no. 4, pp. 2893–2899, Apr. 2018.
- [11] L. Tate, S. Hochgreb, J. Hall, and M. Bassett, "Energy efficiency of autonomous car powertrain," *SAE Warrendale, PA, USA, Tech. Paper*, 2018-01-1092, Mar. 2018.
- [12] S. I. Guler, M. Menendez, and L. Meier, "Using connected vehicle technology to improve the efficiency of intersections," *Transp. Res. Part C: Emerg. Technol.*, vol. 46, pp. 121–131, 2014.

- [13] G. Bucsan et al., “Mobility analysis of electric autonomous vehicle networks driven by energy-efficient rerouting,” in Proc. IEEE 85th Veh. Technol. Conf., 2017, pp. 1–5
- [14] V. Turri, B. Besselink, and K. H. Johansson, “Cooperative look-ahead control for fuel-efficient and safe heavy-duty vehicle platooning,” IEEE Trans. Control Syst. Technol., vol. 25, no. 1, pp. 12–28, Jan. 2017
- [15] N. Fearn, “Hyundai tests First Autonomous Fuel Cell Cars,” Internet of Business, 05-Feb-2018. [Online]. Available: <https://internetofbusiness.com/hyundai-tests-autonomous-fuel-cell-cars/>. [Accessed: 05-Jan-2022].
- [16] H. Zheng, J. Wu, W. Wu and Y. Wang, "Integrated Motion and Powertrain Predictive Control of Intelligent Fuel Cell/Battery Hybrid Vehicles," in IEEE Transactions on Industrial Informatics, vol. 16, no. 5, pp. 3397-3406, May 2020, doi: 10.1109/TII.2019.2956209.
- [17] C. Flores, V. Milanés, J. Pérez, D. González, and F. Nashashibi, “Optimal energy consumption algorithm based on speed reference generation for urban electric vehicles,” in Proc. IEEE Intell. Vehicles Symp. (IV), Jun. 2015, pp. 730–735
- [18] Y. Ikezawa, H. Fujimoto, D. Kawano, Y. Goto, and M. Tsuchimoto, “Bench test of minimum time autonomous driving for electric vehicle based on optimization of velocity profile considering energy constraint,” in Proc. 41st Annu. Conf. IEEE Ind. Electron. Soc. (IECON), Nov. 2015, pp. 004609–004614.
- [19] H. Yoshida, H. Fujimoto, D. Kawano, Y. Goto, and M. Tsuchimoto, “Range extension autonomous driving for electric vehicles based on optimal velocity trajectory and driving braking force distribution considering road gradient information,” in Proc. 41st Annu. Conf. IEEE Ind. Electron. Soc. (IECON), Nov. 2015, pp. 004754–004759.
- [20] K. Kim, H. Lee, C. Song, C. Kang, and S. W. Cha, “Optimization of speed trajectory for eco-driving considering road characteristics,” in Proc. IEEE Vehicle Power Propuls. Conf. (VPPC), Chicago, IL, USA, Aug. 2018, pp. 1–5.
- [21] E. Ozatay, S. Onori, J. Wollaeger, U. Ozguner, G. Rizzoni, D. Filev, J. Micheline, and S. Di Cairano, “Cloud-based velocity profile optimization for everyday driving: A Dynamic-Programming-Based solution,” IEEE Trans. Intell. Transp. Syst., vol. 15, no. 6, pp. 2491–2505, Dec. 2014.
- [22] S. Akhegaonkar, L. Nouveliere, S. Glaser, and F. Holzmann, “Smart and green ACC: Energy and safety optimization strategies for EVs,” IEEE Trans. Syst., Man, Cybern. Syst., vol. 48, no. 1, pp. 142–153, Jan. 2018, doi: 10.1109/TSMC.2016.2600273.
- [23] P. Themann, L. Eckstein, and J. Bock, “Optimisation of energy efficiency based on average driving behaviour and driver’s preferences for automated driving,” IET Intell. Transp. Syst., vol. 9, no. 1, pp. 50–58, Feb. 2015.
- [24] Y. Shao and Z. Sun, “Eco-approach with traffic prediction and experimental validation for connected and autonomous vehicles,” IEEE Trans. Intell. Transp. Syst., early access, Feb. 13, 2020, doi: 10.1109/TITS.2020.2972198.
- [25] M. A. S. Kamal, M. Mukai, J. Murata, and T. Kawabe, “Model predictive control of vehicles on urban roads for improved fuel economy,” IEEE Trans. Control Syst. Technol., vol. 21, no. 3, pp. 831–841, May 2013.

- [26] X. Meng, Q. Li, G. Zhang and W. Chen, "Efficient Multidimensional Dynamic Programming-Based Energy Management Strategy for Global Composite Operating Cost Minimization for Fuel Cell Trams," in *IEEE Transactions on Transportation Electrification*, vol. 8, no. 2, pp. 1807-1818, June 2022, doi: 10.1109/TTE.2021.3120425.
- [27] Y. Zhang, C. Zhang, Z. Huang, L. Xu, Z. Liu and M. Liu, "Real-Time Energy Management Strategy for Fuel Cell Range Extender Vehicles Based on Nonlinear Control," in *IEEE Transactions on Transportation Electrification*, vol. 5, no. 4, pp. 1294-1305, Dec. 2019, doi: 10.1109/TTE.2019.2958038.
- [28] X. Hu, N. Murgovski, L. M. Johannesson and B. Egardt, "Optimal Dimensioning and Power Management of a Fuel Cell/Battery Hybrid Bus via Convex Programming," in *IEEE/ASME Transactions on Mechatronics*, vol. 20, no. 1, pp. 457-468, Feb. 2015, doi: 10.1109/TMECH.2014.2336264.
- [29] M. Pourabdollah, B. Egardt, N. Murgovski and A. Grauers, "Convex Optimization Methods for Powertrain Sizing of Electrified Vehicles by Using Different Levels of Modeling Details," in *IEEE Transactions on Vehicular Technology*, vol. 67, no. 3, pp. 1881-1893, March 2018, doi: 10.1109/TVT.2017.2767201.
- [30] S. Hou, J. Gao, Y. Zhang, M. Chen, J. Shi, and H. Chen, "A comparison study of battery size optimization and an energy management strategy for fchevs based on dynamic programming and convex programming," *International Journal of Hydrogen Energy*, vol. 45, no. 41, pp. 21858–21872, 2020.
- [31] X. Wu, X. Hu, X. Yin, L. Li, Z. Zeng, and V. Pickert, "Convex programming energy management and components sizing of a plug-in Fuel Cell Urban Logistics Vehicle," *Journal of Power Sources*, vol. 423, pp. 358–366, 2019.
- [32] X. Wu, P. Jiang, Z. Fan and J. Fu, "Optimal Power Distribution of Fuel Cell Electric Trucks via Convex Programming," 2021 IEEE 16th Conference on Industrial Electronics and Applications (ICIEA), 2021, pp. 408-411, doi: 10.1109/ICIEA51954.2021.9516199.
- [33] X. Lin, Z. Wang, S. Zeng, W. Huang, and X. Li, "Real-time optimization strategy by using sequence quadratic programming with multivariate nonlinear regression for a fuel cell electric vehicle," *International Journal of Hydrogen Energy*, vol. 46, no. 24, pp. 13240–13251, 2021.
- [34] X. Wu, X. Hu, X. Yin, Y. Peng, and V. Pickert, "Convex programming improved online power management in a range extended fuel cell electric truck," *Journal of Power Sources*, vol. 476, p. 228642, 2020.
- [35] A. Khalatbarisoltani, M. Kandidayeni, L. Boulon and X. Hu, "Power Allocation Strategy Based on Decentralized Convex Optimization in Modular Fuel Cell Systems for Vehicular Applications," in *IEEE Transactions on Vehicular Technology*, vol. 69, no. 12, pp. 14563-14574, Dec. 2020, doi: 10.1109/TVT.2020.3028089.
- [36] H. F. Gharibeh, A. S. Yazdankhah, M. R. Azizian and M. Farrokhifar, "Online Energy Management Strategy for Fuel Cell Hybrid Electric Vehicles With Installed PV on Roof," in *IEEE Transactions on Industry Applications*, vol. 57, no. 3, pp. 2859-2869, May-June 2021, doi: 10.1109/TIA.2021.3061323.

- [37] A. Sciarretta and L. Guzzella, "Control of hybrid electric vehicles," in *IEEE Control Systems Magazine*, vol. 27, no. 2, pp. 60-70, April 2007, doi: 10.1109/MCS.2007.338280.
- [38] S. P. Boyd and L. Vandenberghe, *Convex optimization*. Cambridge: Cambridge University Press, 2018.
- [39] D. Shen, C. Lim, P. Shi and P. Bujlo, "Energy Management of Fuel Cell Hybrid Vehicle Based on Partially Observable Markov Decision Process," in *IEEE Transactions on Control Systems Technology*, vol. 28, no. 2, pp. 318-330, March 2020, doi: 10.1109/TCST.2018.2878173.
- [40] Y. Zhou, A. Ravey, and M.-C. Péra, "Multi-objective energy management for fuel cell electric vehicles using online-learning enhanced Markov Speed Predictor," *Energy Conversion and Management*, vol. 213, p. 112821, 2020.
- [41] S. Quan, Y.-X. Wang, X. Xiao, H. He, and F. Sun, "Real-time energy management for fuel cell electric vehicle using speed prediction-based model predictive control considering performance degradation," *Applied Energy*, vol. 304, p. 117845, 2021.
- [42] G. Jinquan, H. Hongwen, L. Jianwei, and L. Qingwu, "Real-time energy management of fuel cell hybrid electric buses: Fuel cell engines friendly intersection speed planning," *Energy*, vol. 226, p. 120440, 2021.
- [43] Y. Kim, M. Figueroa-Santos, N. Prakash, S. Baek, J. B. Siegel, and D. M. Rizzo, "Co-optimization of speed trajectory and power management for a fuel-cell/battery electric vehicle", *Applied Energy*, vol 260, bl 114254, 2020.
- [44] H. Lohse-Busch, K. Stutenberg, M. Duoba, S. Iliev, *Technology Assessment of A Fuel Cell Vehicle: 2017 Toyota Mirai*, Argonne National Laboratory, 2018.
- [45] Z. Gong et al., "A 1 + 1-D Multiphase Proton Exchange Membrane Fuel Cell Model for Real-Time Simulation," in *IEEE Transactions on Transportation Electrification*, vol. 8, no. 2, pp. 2928-2944, June 2022, doi: 10.1109/TTE.2021.3115794.
- [46] G. Zhang, L. Fan, J. Sun, and K. Jiao, 'A 3D model of PEMFC considering detailed multiphase flow and anisotropic transport properties', *International Journal of Heat and Mass Transfer*, τ. 115, σσ. 714–724, 2017.
- [47] Energy Systems D3 2016 Toyota Mirai. [Online]. Available: <https://www.anl.gov/es/energy-systems-d3-2016-toyota-mirai>. [Accessed: 11-Mar-2022].
- [48] T. A. C. Burrell, S. L. Coomer, C. Ayers, C. W. Wereszczak, A. A. Cunningham, J. P. Marlino, L. D. Seiber, L. Eugene, and L. Hua-Tay, *Evaluation of the 2010 Toyota Prius Hybrid Synergy Drive System*. Washington, DC, USA: U.S. Department of Energy, 2011, doi: 10.2172/1007833.
- [49] D. Yazhemy, M. Rashid and S. Sirouspour, "An On-Line Optimal Controller for a Commuter Train," in *IEEE Transactions on Intelligent Transportation Systems*, vol. 20, no. 3, pp. 1112-1125, March 2019, doi: 10.1109/TITS.2018.2846480.
- [50] Q. Li et al., "A State Machine Control Based on Equivalent Consumption Minimization for Fuel Cell/ Supercapacitor Hybrid Tramway," in *IEEE Transactions on Transportation Electrification*, vol. 5, no. 2, pp. 552-564, June 2019, doi: 10.1109/TTE.2019.2915689.

- [51] J. F. Sturm, “Using SeDuMi 1.02, a MATLAB toolbox for optimization over symmetric cones”, *Optimization methods and software*, vol 11, no 1–4, bll 625–653, 1999.
- [52] M. Grant en S. Boyd, “CVX: Matlab Software for Disciplined Convex Programming, version 2.1”, Mrt-2014. [Online]. Available at: <http://cvxr.com/cvx>.
- [53] M. Grant en S. Boyd, “Graph implementations for nonsmooth convex programs”, in *Recent Advances in Learning and Control*, V. Blondel, S. Boyd, en H. Kimura, Reds Springer-Verlag Limited, 2008, bll 95–110.
- [54] M. ApS, “The MOSEK optimization toolbox for MATLAB manual. Version 9.0”, 2019.
- [55] R. E. Bellman, *The Theory of Dynamic Programming*. Santa Monica, CA: RAND Corporation, 1954.
- [56] O. Sundstrom and L. Guzzella, "A generic dynamic programming Matlab function," *2009 IEEE Control Applications, (CCA) & Intelligent Control, (ISIC)*, 2009, pp. 1625-1630, doi: 10.1109/CCA.2009.5281131.

Chapter 5

5. Conclusions and Future Work

5.1 Summary

This research has shown that both external (environmental) conditions and internal vehicle conditions should be considered in an algorithm for determining the optimal cruising speed of an electric autonomous vehicle. The simulation results show that factors such as wind speed, electrical accessory power consumption, and grade have the largest effect on the selection of optimal cruising speed, and factors such as ambient temperature, battery SOC level, and vehicle mass have smaller effects that are useful in fine-tuning the optimal speed.

A computationally efficient framework is proposed to quickly calculate the energy-optimal cruising speed and determine near-optimal transition rates when parameters change that lead to a new energy-optimal cruising speed. The proposed constant rate acceleration results in only a 0.45% higher energy use compared to the ideal offline-calculated DP speed transitions over the 2 km test case.

A convex formulation is developed which performs successive optimizations to allow for the use of detailed motor/inverter efficiency maps. A comparison between using detailed efficiency maps versus using constant efficiency shows an energy savings of 0.88% over a 300m driving segment. A Tesla Model S vehicle is modeled and validated to real world data. The model is used to drive optimal and non-optimal speed profiles to quantify energy savings. Compared to an arbitrary constant-speed profile, the optimal profile saves between 0.95% and 4.63% of energy over a 1.6 km driving segment. It is found that considering the high accessory losses of autonomous vehicles is critical for finding the optimal speed trajectory. Compared to a more variable real-world logged drive

cycle, the optimal profile saves between 3.26% and 28.86% of energy. The trade-off between execution time and optimality of results is also investigated to further justify the ability of real-time implementation.

To better investigate the optimal speed planning effect on hybrid electric vehicles, novel successive and integrated convex speed planning and energy management algorithms are proposed to solve the minimum hydrogen consumption problem for autonomous FCHEVs. For the proposed convex formulations, an iterative method is used to utilize the detailed FC system and motor-inverter efficiency maps in the objective functions. The component models are carefully created and validated according to experimentally logged data from the Toyota Mirai. The simulation results show that the proposed integrated method, which considers FC system efficiency in the optimization objective function for speed planning, leads to 0.19% to 2.37% less hydrogen consumption compared to the successive method on short drive cycles with varying accessory loads. On the same test cycles, the integrated method uses 10.12% to 21.62% less hydrogen than an arbitrary constant-speed profile. Furthermore, when considering real-world logged drive cycles, the proposed integrated method reduces hydrogen use by 1.43% to 2.82% just through speed optimization, since an optimal EMS is used for both cases. A computational effort analysis shows that the proposed algorithms are suitable for real-time implementation on autonomous FCHEVs, since each calculation iteration takes between 0.13 s and 0.28 s on standard computing resources, depending on the selection of number of segments in each window. Finally, a detailed comparison to a DP benchmark formulation, which cannot run in real-time, shows

that the proposed integrated convex method results in hydrogen use within 1% of the optimal DP result.

5.2 Recommendations for Future Work

The recommendations for future work focus on the improvement of existing algorithms as well as adding to the optimization concept. The first recommendation is to implement the suggested frameworks on control hardware such as a microcontroller to check the framework in a hardware-in-loop platform (for example RT-LAB) to further investigate its performance in real-world conditions and debug any issues. It is vital to test the algorithm for reliability-optimality under different test scenarios and compare the findings to well known methods such as rule-based methods which are very reliable but not always optimal. It is also important to check the availability of used signals in a real-world environment and modify the method if there are unavailable signals.

The second recommendation is to add the consideration of other vehicles on the road and study what should change in proposed frameworks to prepare them for a fleet-level implementation rather than a vehicle-level optimization. In a fleet-level study, there are many complex types of signals and communications such as vehicle to vehicle (V2V), vehicle to infrastructure (V2I), vehicle to pedestrian (V2P), and vehicle to network (V2N) communications. Perception of these signals as well as making decisions based on analysis of them is a complex task that should be carefully studied. In some of the previous literature on this subject, this problem is tackled using simple constraints in the code where the optimal speed planning system is only active when there is a safe distance from vehicle ahead.

The third recommendation is based on findings of the study on FCHEVs. This study can be further investigated with cases where the hybrid system includes supercapacitors (with or without batteries) to better illustrate if using more components and additional energy storage can have a sizable effect on optimal speed trajectory of an electric vehicle. Since adding energy storage and required components will increase the cost, this recommendation can be expanded to a cost feasibility study.

The last recommendation is to add uncertainty into the formulation. Many different parameters are uncertain while driving. For example, measurements of the sensors can generate noisy data, and the fact that there will be human drivers on the road adds another factor that cannot directly be measured. It would be helpful to investigate methods that can deal with uncertain systems such as reinforcement learning and evaluate its performance in a changing environment.